[redacted] COPY

[redacted]
UNCLASSIFIED

NATIONAL AERONAUTICS AND SPACE ADMINISTRATION

LAB-C01273

Space Programs Summary No. 37-39, Volume I

for the period March 1, 1966 to April 30, 1966

The Lunar Program

(Title Unclassified)

Classification Changed to
UNCLASSIFIED
JPL Letter to Authority NASA-Langley
on Nov. 4, 1970, signed by W. E. Hanson
Date: Jan. 4, 1971
By: A. Castain

JET PROPULSION LABORATORY
LIBRARY
JUL 1 1966
CALIFORNIA INSTITUTE OF TECHNOLOGY

Copy No. 477

JET PROPULSION LABORATORY
CALIFORNIA INSTITUTE OF TECHNOLOGY
PASADENA, CALIFORNIA

May 31, 1966

UNCLASSIFIED

[redacted]
GROUP 4 Downgraded at 3 year intervals;
[redacted] 12 years.

143116

[redacted]

UNCLASSIFIED
CONFIDENTIAL

Preface

The *Space Programs Summary* is a six-volume, bimonthly publication that documents the current project activities and supporting research and advanced development efforts conducted or managed by JPL for the NASA space exploration programs. The titles of all volumes of the *Space Programs Summary* are:

Vol. I. The Lunar Program (Confidential)

Vol. II. The Planetary–Interplanetary Program (Confidential)

Vol. III. The Deep Space Network (Unclassified)

Vol. IV. Supporting Research and Advanced Development (Unclassified)

Vol. V. Supporting Research and Advanced Development (Confidential)

Vol. VI. Space Exploration Programs and Space Sciences (Unclassified)

The *Space Programs Summary,* Vol. VI consists of an unclassified digest of appropriate material from Vols. I, II, and III; an original presentation of technical supporting activities, including engineering development of environmental-test facilities, and quality assurance and reliability; and a reprint of the space science instrumentation studies of Vols. I and II.

W. H. Pickering, *Director*
Jet Propulsion Laboratory

Space Programs Summary No. 37-39, Volume I

Copyright © 1966, Jet Propulsion Laboratory, California Institute of Technology

Prepared under Contract No. NAS 7-100, National Aeronautics & Space Administration

This document contains information affecting the national defense of the United States, within the meaning of the Espionage Act, 50 U.S.C., Sections 793 and 794, the transmission or revelation of which in any manner to an unauthorized person is prohibited by law.

UNCLASSIFIED
CONFIDENTIAL

UNCLASSIFIED

Contents

I. *Surveyor* Project 1
A. Introduction 1
B. System Engineering 2
C. System Analysis 6
D. Launch Vehicle Integration 18
E. System Testing 22
F. Launch Operations 28
G. Space Flight Operations 32
H. Aerospace Ground Equipment 33
I. Flight Control 36
J. Electronics 43
K. Electrical Power Supply 46
L. Propulsion 48
M. Spacecraft Vehicle and Basic Bus Mechanisms 64
N. Scientific Payload 68
O. Thermal Control 71
P. Engineering Mechanics 76
Q. Telecommunications 85

References 91

UNCLASSIFIED

UNCLASSIFIED
CONFIDENTIAL

I. *Surveyor* Project

A. Introduction

Calculated to span the gap between the *Ranger* flights and Project *Apollo*, the *Surveyor* spacecraft is designed to take the next step in lunar technology by attempting soft landings on the Moon. The first launches will be engineering test missions to demonstrate system capability up to soft landing, and limited post-landing operations. The engineering payload includes elements of redundancy, diagnostic telemetry, touchdown instrumentation, and survey TV.

Following the engineering test missions, *Surveyor's* objectives are to extend our knowledge of lunar conditions and to verify suitability of *Apollo* landing sites.

Hughes Aircraft Company, Space Systems Division, is under contract to develop and fabricate the first seven spacecraft. The launch vehicle is a combination *Atlas/Centaur*. The JPL Space Flight Operations and Deep Space Network (Mission Operations System) will be utilized for flight control and tracking. The first launch is presently anticipated for the second quarter of 1966.

The major portion of the following material relating to the *Surveyor* spacecraft system was derived from material prepared by the Hughes Aircraft Company; articles prepared by the JPL Technical Sections are identified by footnotes to the article titles. The principal model designations and vehicles discussed are defined in Table 1.

Table 1. Model and vehicle designations

Designation	Description
SC-1—7	Flight spacecraft with engineering payload
SC-8—10	Flight spacecraft with scientific payload
A-21	Model designation for spacecraft with engineering payload (SC-1—7)
A-24	Model designation for spacecraft with scientific payload (SC-8—10)
T-21	Model A-21 prototype system test spacecraft
T-2	Simplified spacecraft for evaluation of terminal descent propulsion and flight control
S-2	Test spaceframe for vibration, shock, and static structural tests
S-6, -7	Test spaceframe for vernier propulsion system tests
S-9	Structural test model
S-10	Temperature control model

UNCLASSIFIED
CONFIDENTIAL

UNCLASSIFIED CONFIDENTIAL

B. System Engineering

1. Special Test and Design Modification of Separation, Sensing, and Arming Devices

a. Special test. During combined systems testing at General Dynamics/Convair (GD/C), San Diego, California, 10 of the 12 retrorocket engine release squib simulators (277216-100) apparently were inadvertently fired. It was believed that a proper adjustment of the *Centaur* adapter ring pedestals, which requires the pedestal to stop against the separation, sensing, and arming device with a 0.030-in. shim between the pedestal and plunger tip, had been made, and that all separation, sensing, and arming device switches were, therefore, open. However, this procedure was not observed by Hughes Aircraft Company (HAC) personnel familiar with the device. An excessive adjustment force could have damaged the separation, sensing, and arming device or the pedestal, causing the switches to close; this could have caused the inadvertent firing.

To determine if the separation, sensing, and arming devices had been damaged, a switch continuity-plunger extension test was performed at Air Force Eastern Test Range (AFETR) March 14. Results of this test were compared with the results of test 37A performed February 5 and 17 (Table 2) and revealed no damage to parts. The fully retracted plunger dimension plus 0.030 in. is less than the closed dimension in all cases. Therefore, if the pedestal had been properly adjusted with the 0.030-in. shim, all switches must have been open.

Investigations are now being made in the following areas. Inspection of the *Centaur* adapter ring pedestal was made to locate any failure or deformation which could have caused the separation, sensing, and arming device plunger to extend farther than the 0.030-in. shim thickness. The pedestal separation, sensing, and arming device interface was inspected to determine the plunger extension in the mated condition. This was done with SC-1 mounted on the same *Centaur* adapter, and, with

Table 2. 37A test results dimensions measured from separation, sensing, and arming device mounting surface to tip of switch actuator

Actuator position and direction of movement	Separation, sensing, and arming devices									Expected
	13 (Leg 1), in.			14 (Leg 2), in.			15 (Leg 3), in.			
	Feb 5	Feb 17	Mar 14	Feb 5	Feb 17	Mar 14	Feb 5	Feb 17	Mar 14	
Fully retracted	0.230	0.236	0.230	0.238	0.235	0.238	0.239	0.241	0.237	<0.245
Clipped	0.270	0.263	0.260	0.270	0.262	0.271	0.263	0.266	0.266	
Fully extended	0.440	0.436	0.435	0.437	0.440	0.443	0.446	0.440	0.443	>0.448[a]
Extending										
Pin connectors—closed										
A-B	0.354	0.351	0.352	0.363	0.362	0.358	0.361	0.356	0.357	0.350/0.365
C-D	0.354	0.351	0.352	0.363	0.362	0.358	0.361	0.352	0.353	0.350/0.365
E-F	0.418	0.415	0.418	0.418	0.417	0.420	0.425	0.417	0.418	0.410/0.435
Retracting										
Pin connectors—open										
E-F	0.365	0.363	0.365	0.372	0.372	0.372	0.372	0.370	0.373	>0.285
C-D	0.304	0.309	0.304	0.322	0.320	0.320	0.317	0.313	0.315	>0.285
A-B	0.304	0.309	0.304	0.322	0.320	0.320	0.317	0.320	0.323	>0.285
Difference[b]	0.022	0.021	0.017	0.019	0.023	0.023	0.021	0.023	0.025	>0.013

[a]The fully extended pin connector dimensions are less than the expected value of 0.448 in., which is acceptable because the difference between pin connectors E-F closed and fully extended is still greater than the minimum expected dimension of 0.013 in.
[b]Difference = fully extended dimension minus closed dimension.

UNCLASSIFIED CONFIDENTIAL

UNCLASSIFIED

the pedestals lockwired in the same position; they were in at the time of combined systems test. Electrical systems study and testing were performed to determine if the fault was in the system circuit design or the result of miswiring, shorts, or noise.

b. Design modification. Analytical study and static load testing of the S-9 vehicle have disclosed that structural deflections during launch may be sufficient to damage the separation, sensing, and arming device and the *Centaur* pedestal, or to cause premature switch closing. If damage occurs, the solar panel may deploy while the spacecraft is still encapsulated. To prevent this possibility, the separation, sensing, and arming device design has been modified to provide an increase in the plunger travel from 0.105 to 0.390 in. by incorporating a spring loaded, telescoping plunger.

HAC is processing ECA 112447, which modifies the separation, sensing, and arming device according to criteria discussed with JPL. The plan is to provide flight accepted, modified control items to AFETR on April 7 for incorporation on the SC-1 spacecraft. Interface specification changes are being processed to effect installation of the modified separation, sensing, and arming device.

2. Reliability

a. System and subsystem a priori reliability. The *a priori* reliability of the A-21 *Surveyor* spacecraft for the flight and landing mission is 0.779. The *a priori* reliability estimates by subsystem are shown in Table 3. The decrease in system reliability since the previous reporting period is due to the inclusion of the thrust chamber assembly reliability estimates. These estimates were not available prior to the current reporting period.

b. Reliability estimates for SC-1 based on test data. The data-based reliability estimate for SC-1 is 0.54 for the flight and landing mission. The primary source of data for the estimate is system testing on SC-1. Flight acceptance test data or *a priori* estimates are used only when system testing does not provide data on a unit. The subsystem reliability estimates are shown in Table 4. Fig. 1 shows successive reliability estimates since April 1965, with a straight line (dashed) fitted to the data point to indicate the general trend.

Table 3. A-21 subsystem *a priori* reliability flight and landing mission

Subsystem	Reliability
Telecommunications	0.975
Vehicle mechanisms	0.986
Propulsion	0.886
Electrical power	0.957
Flight controls	0.955
System	0.779

Table 4. SC-1 subsystem reliability estimates based on test data, flight, and landing mission

Subsystem	Reliability
Telecommunications	0.894
Vehicle mechanisms	0.855
Propulsion	0.991
Electrical power	0.854
Flight controls	0.953
Spacecraft	0.616
(System interaction reliability factor)	(0.877)
Spacecraft reliability = (0.616) (0.877) = 0.54	

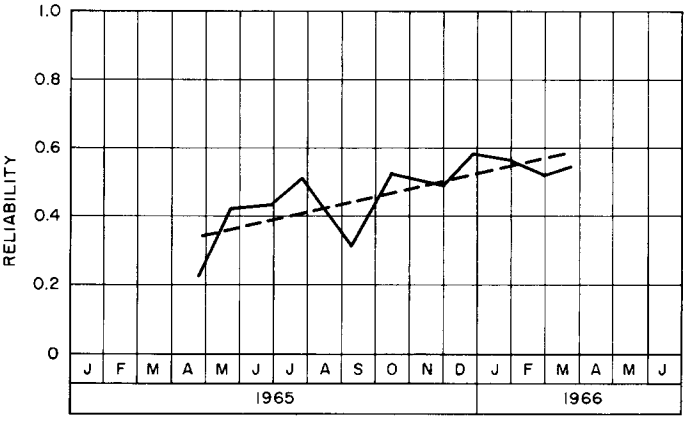

Fig. 1. SC-1 reliability

c. Mechanisms reliability. (Table 5.)

Table 5. Reliability achievement based on test results

Antenna/solar panel positioner	0.8901
Omniantenna mechanism (each)	0.9962
Separation, sensing, and arming device (each)	≈1.0
Thermal switch (each)	≈1.0

UNCLASSIFIED

UNCLASSIFIED
CONFIDENTIAL

Antenna/solar panel positioner. The solar and elevation axes of the SC-2 antenna solar panel positioner (A/SPP) (287580), Serial No. 1) failed to drive at nominal currents during flight acceptance test because of metallic galling between the bearing pins and the bore of the first stage planets of both drives. The galling was attributed to the use of soft (chromic) anodize on the pins, and to the presence of bare metal at the bores of the planet gears. The bare metal resulted from rework to remove sharp edges which had been the cause of galling and gear binding troubles.

Corrective action was applied to all gears and included changing to a harder pin material with hard (sulfuric) anodized surface, and rejecting all gears with reworked bore radii. Further action consisted of stabilization of the planetary spider against wedging loads by the addition of an outboard bearing, the use of assembly fixtures with guide pins to prevent damage during assembly, and the use of a molybdenum disulfied base dry lubricant on gear bores and shafts in place of a graphite-base lubricant.

Difficulty has been experienced with proper adjustment of lock-pin pullers, particularly with coordination of lock operation and indicator switch actuation. A major change has been made in the lock-pin puller design. The lock-pin and indicating switch have been combined into a module that can be preadjusted as a subassembly. Because of the small degree of freedom at the attachment of the pin to the pulling device, the module design provides for self-alignment as the pin seats itself in the locked position. Tools have been designed for proper adjustment and installation of the lock-pin switch modules. The new module design will be used in the antenna/solar panel positioner for SC-2.

During flight acceptance test, high temperature phase, one of the stepper motors in the SC-2 A/SPP showed a lower coil resistance than previously recorded, indicating that some turns had shorted. The motor is being carefully observed for signs of further degradation and replacement may be required.

Steps have been taken to change the wire insulation of all motor coils to an improved type. A type of insulation known as "ML" is dated 20°C higher than the Teflon insulation now used, and is claimed to have superior cold flow properties at high temperature. Consideration is also being given to limiting the duty cycle of motor operation during test such that the average coil temperature does not exceed 450°F, and to reduce the pulse length to 40 msec.

Several instances have been reported of variations in position potentiometer resistance measured as such, or as indicated by telemetry data. Investigation showed that the variances were actually caused by the variation of connector contact resistance due to atmospheric corrosion of the contact surfaces. An engineering order has been released stipulating a program for cleaning and protecting spacecraft connector contacts. The same program has been established for test equipment connector contacts.

Omniantennas. Omniantenna A has been redesigned to permit an adjustment capability which will assure that the plane is always maintained perpendicular to the base of the spacecraft. This redesign will apply to SC-1 and following spacecraft. Reinspection revealed that the orientation of omniantenna A is misaligned by 20 deg on T-21, SC-1, and SC-2. SC-1 mechanism will not be reworked to correct the misalignment, but all other deviated units will.

Separation, sensing, and arming device. A binding condition at the internal actuator arm pivot point was reported. To preclude any possible compromise in reliability, the SC-1 units have been removed and replaced with units reworked to eliminate the binding trouble.

Investigations of the interface between *Surveyor* and *Centaur* revealed that the plunger of the separation, sensing, and arming device may require as much as 0.10 in. of motion (inward deflection) owing to the acceleration of boost and vibration. A design change has been released to provide five times the former plunger travel.

Thermal switches. A shelf life test of the two type approval test thermal switches and two switches from bonded stores resulted in three switches passing the life test successfully and one of the units from bonded stores failing. Thermal contacts of the latter switch did not open until the temperature was reduced to 17°F. The nominal operating point is 50°F. An investigation to correct the contact sticking problem has been initiated.

Pin pullers. During X-ray examination of pin pullers after flight acceptance test, several shear wire deformities and partial shearing conditions were discovered. Improper handling of pin pullers after incoming inspection and prior to the X-ray examination subsequent to flight acceptance test is blamed for this damage. ECRs have been generated which recommend the provision of suitable packaging and protective devices to eliminate mishandling damage.

CONFIDENTIAL
UNCLASSIFIED

UNCLASSIFIED
CONFIDENTIAL

d. Inertial reference unit. Six trouble and failure reports (TFRs) have been closed. These were concerned with the possible incomplete fluid fill condition that became suspect in the accelerometers for the *Surveyor* inertial reference unit. Accelerometers were removed from four flight hardware inertial reference units (3, 5, 7, and 8) and returned to the vendor for rework and refill. Two additional accelerometers in *Surveyor* bonded stores were returned to the vendor for the same reasons. A bulged diaphragm condition was first noticed in the accelerometer during the teardown inspection, which followed successful completion of type approval testing. A bulged diaphragm is indicative of an outdated fill procedure which did not preclude air bubbles in the fluid. If air is present in the fluid, there is a chance that the bubbles could, at some later time, shift to the area of the moving mechanism and cause performance degradation. Replacement accelerometers for inertial reference units 3, 7, and 8 were filled by a revised procedure (adopted in mid-November 1965) which greatly reduced the possibility of air bubbles in the fluid. The position of the diaphragm which controls fluid expansion was checked by X-ray and found to be so positioned as to indicate no air in the fill fluid (within the measurement accuracy of the X-ray procedure). The replacement accelerometers were also exposed to the environments of thermal vacuum and vibration to which the inertial reference units had already been subjected, and the accelerometers were performance and X-ray checked following these environments. The replacement accelerometer for inertial reference unit 5 is not presently available and will be installed at a later date.

To further reduce the possibility of air bubbles existing in a delivered accelerometer, a new fill procedure and additional acceptance criteria have been developed by the accelerometer vendor. The procedure and additional acceptance criteria are being negotiated into the accelerometer subcontract, and will apply to the accelerometers returned to the vendor for rework and refill.

e. Materials.

Compatibility of solid propellant with vernier fluids. The compatibility of the retrorocket engine solid propellant with mono-methylhydrazine (MMH) and nitrogen tetroxide (N_2O_4) has been determined. In general, it was found that neither the liquid nor the gaseous phases of the MMH or N_2O_4 caused any significant damage to the retrorocket engine propellant.

Microstructures and lubricative compacts. Metallographic and hardness studies were made of lubricative compacts, which are a powder metal product consisting of a dry lubricant in a metallic matrix. These materials are candidates for self-lubricating components in space, particularly where sliding electric contacts are required. It was found that pressed and sintered compacts (using silver-copper as the metal and columbium selenide as the lubricant) and hot pressed silver-columbium selenide compacts retained the individual constituents of metal and lubricant. However, hot pressed compacts of iron-tantalum metal and molybdenum disulfide lubricant reacted with the graphite mold to form products that did not resemble the original lubricant.

Effect of vernier propellants on chrome plated aluminum. The comparison of thin chrome plating as applied directly to aluminum by two vendors was previously reported. The program has been completed by subjecting both platings to liquid and gaseous MMH monohydrate and MON-10. No visible deteroriation or weight change could be detected in either case.

Vacuum friction tests. Vacuum friction tests have compared Microseal 100-1 and Lubeco 905. Substrates included sulfuric acid anodized 6061-T6 and 7075-T6 aluminum, hard anodized 7075-T6 aluminum, and 416 stainless steel. Loads were 200, 500, 1000, 2000 and, in some cases, 3000 and 5000 psi. The oscillating planes friction tester was operated for 500 cycles at each load, in vacuum ranging from 10^{-8} to 10^{-9} torr. In all cases the coefficient of friction of the Lubeco 905 was considerably lower than that of the Microseal 100-1.

Polyolefin boots for space environment. The use of heat shrinkable boots for protection of electrical connectors on space vehicles has been limited in the past to rather low service temperatures, e.g., below 130°F. The limitation has been due to the presence of materials which outgas in vacuum and condense at room temperature or slightly above. The Raychem Company, at the request of HAC, has produced two formulations which appear to be completely suitable for service in hard vacuum to temperatures as high as 260°F. The formulations were identified by Raychem as 541-036 and 541-040.

New source for aluminized Mylar film. The only source for the aluminized Mylar film used on *Surveyor* has been the National Metallizing Division of the Standard Packaging Company, Trenton, New Jersey. The National Research Corporation, Cambridge, Massachusetts, has now been qualified as a second source.

Cleaning of organic thermal control paints. A program to verify methods for cleaning 3M white velvet paint

UNCLASSIFIED
CONFIDENTIAL

UNCLASSIFIED CONFIDENTIAL

has been completed. Groups of discs were both contaminated and cleaned by several methods. The change in solar absorptance and total emissivity was determined before and after exposure to ultraviolet radiation. It was found that the optical properties and ultraviolet resistance of contaminated coating could be completely restored. The use of a solvent followed by light hand-sanding appeared to be a better method than simple cleaning with iso-octane solvent or scrubbing with a water-aluminum oxide paste.

Solithane 113. A high viscosity thixotropic polyurethane compound, consisting of Solithane 113 (Thiokol Chemical Corporation) and Cab-o-Sil, a fine silica, was evaluated for use as an insulating coating on terminals and component leads. This particular composition was recommended by JPL. Tests included hardness, insulation, resistance, pot-life, storage life, viscosity, and porosity. The material was found to be satisfactory for dielectric purposes on *Surveyor* at temperatures up to at least 160°F. At the two higher test temperatures, 260 and 300°F, the insulation resistance was unacceptable.

Table 6. Performance gains

Parameters	Present design	New design
Time in minimum acceleration phase (burnout to intercept), sec	43.6	34.3
Time in maximum acceleration phase (intercept to touchdown), sec	117.4	105.1
Total time in vernier phase (burnout to touchdown), sec	161.0	139.4
Propellant consumed in minimum acceleration phase, lb	17.4	13.0
Propellant consumed in maximum acceleration phase, lb	90.2	85.0
Total vernier propellant consumed, lb	107.5	98.0
Characteristic velocity of minimum acceleration phase, ft/sec	181.0	135.0
Characteristic velocity of maximum acceleration phase, ft/sec	1027.0	961.0
Characteristic velocity of vernier phase, ft/sec	1208.0	1096.0
Reduction of time in vernier phase, sec	21.6	
Reduction of vernier propellant consumed, lb	9.5	
Reduction of vernier phase characteristic velocity, ft/sec	112	

C. System Analysis

1. Surveyor *Terminal Descent Improvements for A-24 Spacecraft*

This section presents a re-evaluation of some important design practices presently in use. Implementation of all or part of the suggested improvements should result in a significant vernier propellant saving. It is shown that a modification of the design of one breakpoint in the command descent segments, a new burnout contour design procedure, and a re-evaluation of the lunar slope/flight path allowance decreases the vernier propellant loading requirement by 9.5 lb and the RADVS and vernier operating time by 21.6 sec for the A-24 spacecraft. The specific detailed design changes recommended to implement these gains are shown in Tables 6 and 7.

The results of this study were obtained, for the most part, from use of the HAC terminal phase monte carlo program. The monte carlo results depend on the assumed error model of the *Surveyor* spacecraft. The present error model parameter values for the A-24 *Surveyor* are based on current specifications, HAC IDCs, and to a lesser extent, engineering judgment.

Table 7. Design data

Parameters	Present design[a]		Final design[b]	
	Velocity, ft/sec	Altitude, ft	Velocity, ft/sec	Altitude, ft
Burnout contour	200	22050	200	19500
	350	37150	350	32800
	500	58300	500	50000
Segments	0	0	0	0
	42	250	44	250
	88	989	93	989
	350	14570	305	10000
	651	50000	685	50000

[a]Nominal acceleration = 180 g, minimum acceleration = 0.78 g

[b]Nominal acceleration = 189 g, minimum acceleration = 0.74 g

a. Surveyor acceleration capability. One significant measure of spacecraft terminal descent performance is the spacecraft acceleration capability. In particular, an increase in spacecraft acceleration capability decreases the time in the vernier phase and decreases the vernier propellant loading requirement.

The ratio of the total maximum vernier engine thrust to maximum spacecraft weight at intercept with the command descent segments determines the maximum

UNCLASSIFIED CONFIDENTIAL

UNCLASSIFIED
CONFIDENTIAL

acceleration capability. With the present total vernier engine thrust of 312 lb, and spacecraft weight at intercept with the command descent segments at 882 lb (for an injected weight of 2500 lb), the maximum acceleration capability is 2.14 lunar g. However, when allowances are made for moment control and hardware tolerances, the maximum capability is reduced to 1.98 lunar g.

The nominal acceleration, which is used in the design of the command descent segments, differs from the maximum available acceleration by about 10%. This is due to an allowance for lunar slope/flight angle combinations which may affect the soft touchdown capability, and to RADVS and hardware tolerances. The present value of the nominal acceleration is 1.80 lunar g. The degradation of the spacecraft acceleration capability and estimates of the cost in terms of propellant and time in the vernier phase are shown in Table 8.

Table 8. Spacecraft acceleration capability degradation

Parameters	Lunar g acceleration	Change in propellant, lb	Change in time, sec
Maximum capability	2.14	—	—
Moment control allowance	−0.13	4.00	8.4
Maximum acceleration control system mechanization and hardware	−0.03	1.10	2.2
Maximum available acceleration	1.98	—	—
Lunar slope/flight path allowance	−0.10	4.00	8.9
RSS of RADVS and hardware tolerances	−0.08	3.80	8.2
Present nominal acceleration	1.80	—	—

Fig. 2 shows the decrease in vernier propellant and time in the vernier phase as a function of increased acceleration capability, as indicated in Table 6. The changes in time and propellant loading, as noted in Tables 6 and 7, are obtained from the nonlinear functions of Fig. 2. Hence, the values of the individual factors depend on the nominal point from which perturbations are made; for example, if the effect of only the slope/flight path allowance on the current design is desired, a 0.1-g perturbation on the nominal 1.8-g acceleration results in a 4.6-lb propellant saving, rather than the 4.0-lb listed in Table 8 and as shown in Fig. 2.

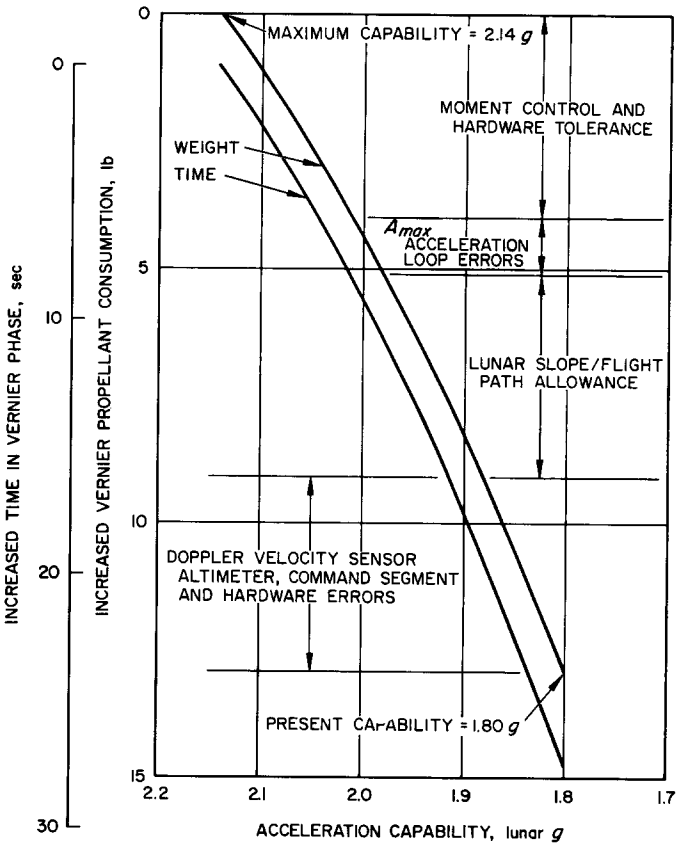

Fig. 2. Increased vernier phase propellant and time versus degradation of spacecraft acceleration capability

If it is assumed that little, if anything, can be done to improve RADVS and other hardware tolerances, and if control system mechanization errors have already been reduced to a practical minimum, two possible improvements in the spacecraft acceleration capability are available. These are in the area of moment control and lunar slope/flight path angle allowances. One obvious way to reduce the allowance for moment control would be to reduce the spacecraft CG offset allowance, if this were practical. However, since this area has already been the object of extensive engineering effort, this possibility was not investigated. The following discussion shows that a significant reduction in the lunar slope/flight path allowance may be obtained.

b. Lunar slope/flight path angle allowance. The thrust acceleration requirement is affected by the spacecraft flight path angle and the lunar slope. To accommodate adverse combinations of flight path angle and lunar slopes, an excessive acceleration requirement or allowance exists. This allowance is given as the difference

UNCLASSIFIED
CONFIDENTIAL

between the instantaneous thrust acceleration requirement and the nominal acceleration (N_n) or

$$\frac{a}{g} - N_n = \left[\cos\psi + \frac{1}{2}\sin\psi\tan(\psi - \mu) - 1\right] \tag{1}$$

where ψ is the spacecraft flight path angle and μ is the lunar slope. As an example, Eq. (1) gives for $\mu = -15$ deg and $\psi = 25$ deg an acceleration allowance of 0.08 lunar g, while for $\psi = 45$ deg the allowance is 0.34 g. The results obtained from Eq. (1) are based on a constant lunar slope whose orientation with respect to the plane of motion during the terminal descent is fixed.

Further work shows that a reasonable and less conservative requirement would be that in 99% of the cases, the spacecraft should be capable of landing on a lunar slope of 15 deg, where the orientation of the slope with respect to the plane of the trajectory is random. In this instance, the lunar slope is given by

$$\tan\mu = \tan\mu_0 \cos\theta \tag{2}$$

where μ_0 is a constant and θ describes the relation of slope to trajectory plane as a uniformly distributed random variable between 0 and 2π. It also has been shown that Eq. (3) must be satisfied to ensure that soft landing will occur 99% of the time, i.e., that the thrust acceleration demand is less than the spacecraft capability.

$$\tan\mu > \left[\frac{4N_{\max}^2 - 1 \cdot 2(N_n - 1)(1 + 2N_{\max}\cos\psi + \cos^2\psi) - 4(N_{\max}^2 - 1)\cos\psi\csc\psi}{4(N_{\max}^2 - 1)\cdot 4N_{\max}^2 - 1 - 2(N_n - 1)(2N_{\max} + \cos\psi)}\right] \tag{3}$$

where $N_{\max}$ is the maximum acceleration capability of the spacecraft.

Lunar model. Based on Ref. 1, it would appear that for baselines of 1 km, about 1% of the lunar slopes in the regional maria (M_3 or *Surveyor* target areas) are approximately 6 deg, while in the highlands or H_2 areas, the lunar slopes are 9 deg. A conservative estimate of the minimum A-24 baseline, or the terrain viewed by the range radar from intercept with the descent contour to touchdown, is about 0.5 km, assuming a minimum velocity and flight path angle of 200 ft/sec and 25 deg, respectively. In general, as the baseline decreases, the lunar slope median value increases. Therefore, since the minimum A-24 baseline is short of 1 km, and to maintain some element of conservatism, it may be assumed that the lunar slope which the *Surveyor* must be able to accommodate may be as large as the 15-deg specification requirement. The cumulative distributions of the lunar slopes presented in the JPL report suggest lunar slope density functions ranging from Uniform in the highlands to Rayleigh in the maria or target areas. This detail is pointed out because later in this summary, a uniform distribution is assumed for μ, which according to the above comment applies in the highlands, and is not typical of target areas. Thus, the choice of distribution is conservative.

The lunar slope/flight path acceleration allowance is presently computed to permit the spacecraft to accommodate burnout flight path angles up to 45 deg, and a lunar slope of 15 deg. To include the effects of gravity turn during the minimum thrust phase, the flight path angle at intercept with the descent contour should be used in the computation of the slope/flight path allowance, and not the burnout flight path angle.

Fig. 3 shows the spacecraft flight path angle at burnout and intercept with the descent contour as a function of burnout velocity for an unbraked impact angle of 45 deg. The difference between these two curves is due to the effect of gravity turn during the minimum thrust phase; i.e., the **gt** vector decreases the flight path angle. For a burnout flight path angle of 45 deg (the present design value), the flight path angle at intercept is only 17 deg.

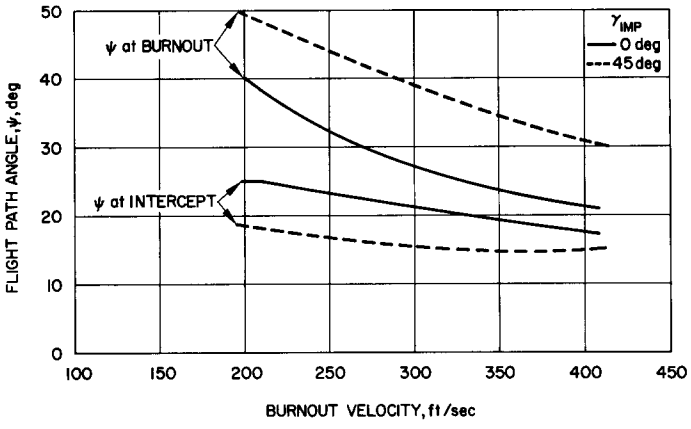

Fig. 3. Monte carlo 99% flight path angle at burnout and segment versus burnout velocity

UNCLASSIFIED
CONFIDENTIAL

Fig. 3 also shows the curve when the unbraked impact angle is 0 deg. In this case, a somewhat greater flight path angle exists at intercept with the nominal descent contour because the nominal burnout contour is closer to the descent contour (Fig. 4), and, therefore, the gravity turn effect on the flight path angle is less. For a burnout flight path angle of 40 deg, the intercept flight path angle is 25 deg. Burnout flight path angles less than 40 deg were not considered because a slope/flight path allowance, based on an unbraked impact angle of 0 deg, is a conservative choice for the A-24 spacecraft. Nonetheless, it does not appear that the intercept flight path angle would be much greater than 26 to 27 deg for a burnout angle of 45 deg.

Fig. 5 shows the acceleration margin requirements for randomly orientated lunar slopes of 15 and 9 deg, given that the intercept flight path angle is 25 deg (worst case). It should be noted that the 99% acceleration allowance or margin from Fig. 5 is less than 0.035 lunar g for a lunar slope of 15 deg. By comparison, the present design value is 0.10 g based on a lunar slope and flight path angle at burnout of 15 and 45 deg, respectively. For a lunar slope of 9 deg, the 99% requirement is 0.02 lunar g. The 99% requirement for a lunar slope uniformly distributed between 0 and 15 deg is also shown in Fig. 5 to be almost identical to the 99% requirement for a constant slope of 9 deg.

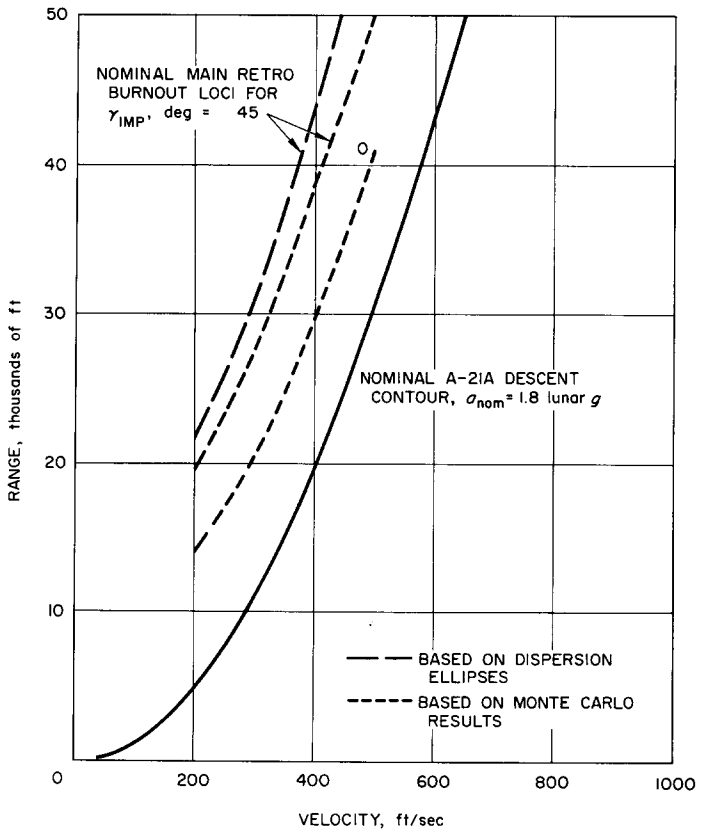

Fig. 4. Present and improved burnout contours

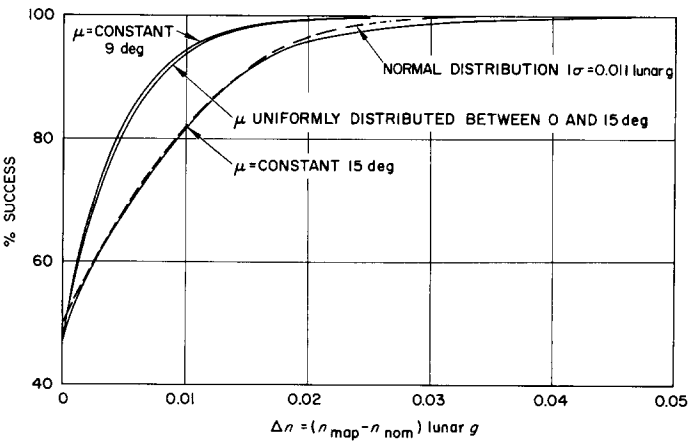

Fig. 5. Monte carlo acceleration margin for lunar slopes of 15 and 9 deg

The probability of success values of Fig. 5 are based on Eqs. (2) and (3) which are contained in the terminal descent portion of the *Surveyor* transit phase monte carlo program. All data points are based on 500 monte carlo cycles, and the quoted 99% values are equal to or greater than 99%.

Eq. (4) (Ref. 2) relates to present design practice.

$$N_n = N_{\max} - \Delta N - \left(\delta N_n^2 + \delta N_{\max}^2\right)^{1/2} \qquad (4)$$

where

δN_n = variation in N_n due to RADVS and segment errors

N_n = nominal descent acceleration

$N_{\max}$ = nominal maximum acceleration

ΔN = lunar slope/flight path allowance

$\delta N_{\max}$ = variation of $N_{\max}$ due to hardware tolerances

Eq. (4) shows that, with the exception of the lunar slope/flight path allowance which is treated as a bias, all errors or tolerances have been root-summed-squared. Fig. 5 shows that the cumulative distribution of ΔN (for $\mu = 15$ deg randomly orientated with respect to the plane of motion) does not depart greatly from a normal cumulative distribution; i.e., ΔN should be treated as a statistical event as are the other error sources. Therefore, it

UNCLASSIFIED
CONFIDENTIAL

is felt that Eq. (4) could be legitimately rewritten such that ΔN is root-sum-squared with the RADVS, segment, and hardware errors, as shown in Eq. (5).

$$N_n = N_{\max} - \sqrt{\Delta N^2 + \delta N_n^2 + \delta N_{\max}^2} \qquad (5)$$

The above analysis increases N_n by 0.09 lunar g, which would decrease the vernier propellant requirement by 3.9 lb and the vernier phase time by 8.3 sec, if only this change is made.

c. Command descent segments. The spacecraft maximum acceleration phase trajectory is commanded to follow a line segment profile which is inscribed in the design parabola described by

$$R = R_b + \frac{(V + V_\epsilon)}{2(N_n - 1)G_m} \qquad (6)$$

where R_b is the slant range bias, and V_ϵ is the static velocity tracking error (Ref. 2). As pointed out in Ref. 2, all command descent segment end points, with the exception of the one at $R = 0$, $V = 0$, are chosen to lie in this design parabola (Fig. 6). Both end points of segments 3 and 4 are fixed by hardware and RADVS considerations. The upper end point of segment 1 and the lower end point of segment 2 are also fixed by RADVS considerations. However, the lower end point of segment 1, or breakpoint for segments 1 and 2, is not fixed by any such consideration. The present design practice is to pick this breakpoint for a best fit of the descent parabola in the region of low burnout velocities.

It is felt that the best fit to the descent parabola should be that breakpoint which gives the minimum vernier phase propellant consumption. Therefore, the initial approach taken was to examine the vernier phase propellant consumption as a function of decreased slant range of the breakpoint between segments 1 and 2 along the nominal descent parabola. It was observed that the decrease in vernier propellant consumption during the maximum acceleration phase was negligible and increased for a decrease in range of about 2500 ft; i.e., the initial breakpoint was more or less optimum with respect to propellant consumption in the maximum acceleration phase. However, the vernier propellant consumption during the minimum acceleration phase decreased rather rapidly for decreasing range values along the nominal descent contour. These results (Fig. 7) show that the maximum decrease in the vernier phase propellant consumption occurs at about −5500 ft. In short, there is a tradeoff between propellant consumption in the minimum and maximum acceleration phases, and the decrease in propellant consumption is relatively constant over the −4000 to −7000-ft range.

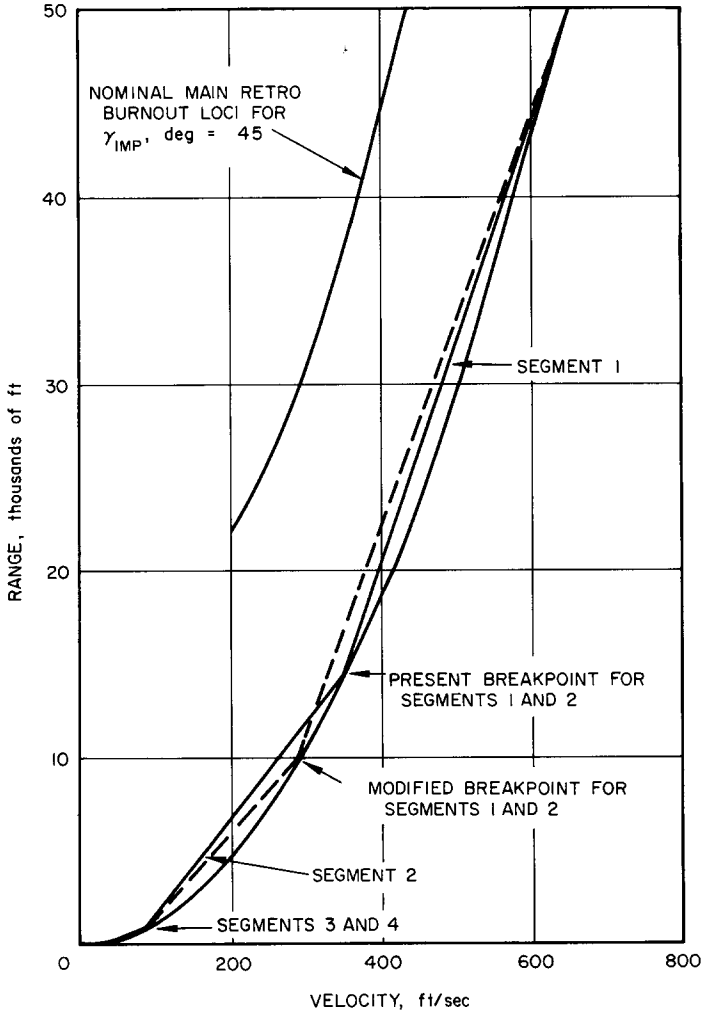

Fig. 6. Segment fits of descent contour for present and improved breakpoint

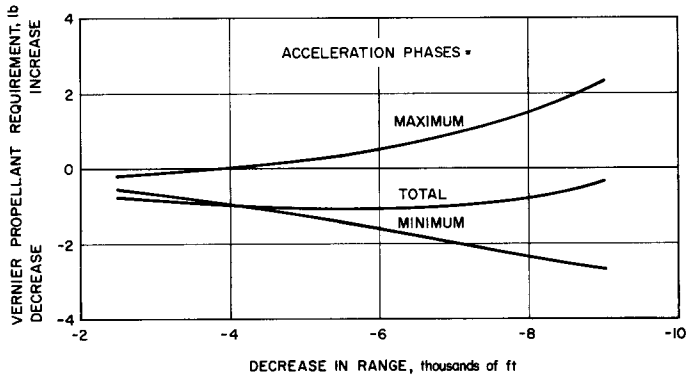

Fig. 7. Change in vernier propellant requirement as function of decreased breakpoint range

UNCLASSIFIED
CONFIDENTIAL

The change in the characteristic velocities of the maximum and minimum acceleration phases as a function of decreased breakpoint range are shown in Fig. 8. Based on the results shown in this figure, the present design value of the breakpoint range of 14,570 ft was changed to 10,000 ft, the logic being that a value of −4570 ft left the initial maximum acceleration phase characteristic velocity essentially unchanged, but at the same time, the gain in the minimum acceleration phase was very nearly a maximum. It was mentioned above that with respect to the maximum acceleration phase the current design was optimum.

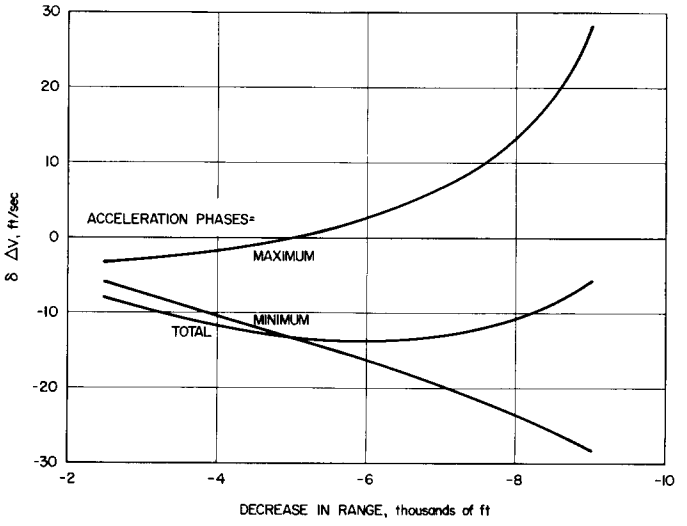

Fig. 8. Characteristic velocity as function of decreased breakpoint range

The foregoing analysis was based on the A-24 maximum vernier propellant case; i.e., an unbraked impact velocity of 2849 m/sec, an unbraked impact angle of 45 deg, and a maximum midcourse maneuver of 50 m/sec, which gives a burnout velocity of 368 ft/sec. However, the effect of the new breakpoint on vernier propellant consumption was also evaluated at 300 and 400 ft/sec (Table 9), suggesting that the new breakpoint renders better results at lower burnout velocities. In any case, it would appear that for a 2500-lb A-24 the new breakpoint saves from 1 to 1.5 lb of vernier propellant and from 2 to 3 sec of vernier phase time.

d. Burnout contour. The nominal burnout contour is presently defined in terms of the locus of 99% burnout dispersion ellipses. These ellipses are obtained by mapping preretrorocket- and retrorocket-error sources into errors in velocity, range, and flight path angle at main retrorocket burnout. The present procedure assumes that

Table 9. Breakpoint study results

Parameters	Burnout velocity, ft/sec		
	300	368	400
Change in minimum acceleration phase time, sec	− 5.20	− 3.60	− 3.00
Change in maximum acceleration phase time, sec	1.80	1.00	0.80
Total change in vernier phase time, sec	− 3.40	− 2.60	− 2.20
Change in minimum acceleration phase propellant consumption, lb	− 2.06	− 1.42	− 1.19
Change in maximum acceleration phase propellant consumption, lb	0.60	0.32	0.26
Total change in vernier phase propellant consumption, lb	− 1.46	− 1.10	− 0.93
Change in minimum acceleration phase characteristic velocity, ft/sec	−21.63	−14.91	-12.44
Change in maximum acceleration phase characteristic velocity, ft/sec	3.55	1.06	0.71
Total change in vernier phase characteristic velocity, ft/sec	−18.08	−13.85	−11.73

partial derivatives of burnout velocity, range, and flight path angle with respect to the error sources are essentially constant; i.e., linear transformation methods are valid in mapping error sources into burnout conditions. The end product of this type of analysis is a covariance matrix of burnout velocity, range, and flight path angle. An orthogonal transformation of the covariance matrix of burnout errors renders the 99% dispersion ellipses whose semi-axes are defined as 3-σ range along the velocity vector at burnout and 3-σ velocity at burnout.

The design of the burnout contours is somewhat conservative for trajectories with unbraked impact angles approaching 45 deg because the transformations from many error sources into burnout parameters are nonlinear. In other words, many of the actual distributions of *Surveyor* burnout parameters are not well described by the normal distribution assumed in the present definition of the burnout ellipses. An additional element of

CONFIDENTIAL
UNCLASSIFIED

UNCLASSIFIED

conservatism in the present burnout contour design is that the locus of the dispersion ellipses is biased away from the descent contour, such that given the worst case dispersions in burnout velocity and range (the point on a dispersion ellipse adjacent to the descent contour), enough time is left to allow for the alignment of the spacecraft roll axis to the velocity vector prior to intercept with the command descent segments.

Problems such as nonlinearity in the partial derivatives can be circumvented, and the question of degree of conservatism which should be considered in the design of the burnout contour can be assessed directly with the aid of the HAC terminal phase monte carlo program. In this program, the statistical distributions of the random variables are simulated with well known numerical methods, and all burnout quantities are computed in closed form. Therefore, questions pertaining to the validity of linear transformation techniques do not arise. Furthermore, if it is assumed that the analytical model employed in the monte carlo program is a good simulation of the *Surveyor* spacecraft system operation, the degree of conservatism desired in the design of terminal parameters or constraints (such as the burnout contour) may be controlled with the terminal phase error model. For example, increasing the value for the main retrorocket engine thrust variation to a more conservative choice would result in a requirement for a higher burnout contour, if the failure rate is held constant.

The design of the burnout contour with the monte carlo program is based on the requirement that in 99% of the cases observed, alignment of the spacecraft roll axis with the inertial velocity vector should be completed prior to intercept with the descent contour. In the monte carlo program, the criterion for failure is

$$V_s^2 > V_b^2 + 2(N_n - 1)\, G_m\, (R_s - h_b)$$

where V_s and R_s are the velocity and range at intercept and V_b and h_b are the velocity and range at initiation of the touchdown phase (V_b is nominally 10 ft/sec). In other words, if the above inequality is not satisfied during a given monte carlo cycle, a failure has occurred. The burnout contours shown in Fig. 4 are based on 1% failures; i.e., in 99% of the cases observed, alignment was completed before intercept with the descent contour.

The new burnout contour for a 45-deg unbraked impact angle gives a 3.2 lb decrease in vernier phase propellant consumption and a decrease in the total vernier phase time of 7.8 sec (Table 10). The results also show that, when the new burnout contour and breakpoint are included in the present design, a saving of 4.1 lb of vernier propellant and 9.9 sec of vernier phase time results.

Table 10. Improvements in present design at velocity, or "burnout velocity"; burnout = 368 ft/sec for new burnout contour and breakpoint

Parameters	Present design	New burnout contour	New burnout contour and breakpoint
Time in minimum acceleration phase burnout to intercept), sec	43.6	37.4	34.3
Time in maximum acceleration phase (intercept to touchdown), sec	117.4	115.8	116.8
Total time in vernier phase (burnout to touchdown), sec	161.0	153.2	151.1
Propellant consumed in minimum acceleration phase, lb	17.4	14.9	13.7
Propellant consumed in maximum acceleration phase, lb	90.2	89.2	89.7
Total vernier phase propellant consumed, lb	107.5	104.3	103.4
Characteristic velocity of minimum acceleration phase, ft/sec	181	155	142
Characteristic velocity of maximum acceleration phase, ft/sec	1027	1013	1015
Characteristic velocity of vernier phase, ft/sec	1208	1168	1157
Reduction of time in vernier phase, sec		7.8	9.9
Reduction of vernier propellant consumed, lb		3.2	4.1
Reduction of vernier phase characteristic velocity, ft/sec		40.0	51.0

The present and improved designs and the resultant gains are presented in Table 11. Only 8.0 lb and 18.2 sec of the 9.5 lb and 21.6 sec shown in Table 11 have been accounted for. The difference of 1.5 lb and 3.4 sec is caused, in part, by a decrease in the minimum injected weight of 25 lb (from 2500 to 2475) which decreases the vernier propellant consumption by 0.2 lb and vernier phase time by 0.4 sec. The remaining differences of 1.3 lb of vernier propellant and 3.0 sec of vernier phase

UNCLASSIFIED

UNCLASSIFIED
CONFIDENTIAL

Table 11. Burnout contour design improvement

Area of design improvement	Propellants, lb	Time, sec
Burnout contour and breakpoint	4.1	9.9
Reduced minimum acceleration	0.2	0.4
Changes in nominal acceleration due to change in lunar slope/ flight path allowance	3.9	8.3
Better fit of descent contour	1.3	3.0
Total	9.5	21.6

time result, because for higher performance designs, i.e., higher nominal accelerations, the segment approximation of the descent contour improves. In other words, the segments are a better fit of the continuous descent parabola (if the nominal acceleration were infinite, the fit would be perfect).

The analysis of Section ***b*** and the results in Fig. 7 show that to accommodate lunar slopes up to 15 deg and intercept flight path angles of 25 deg (or approximately 45 deg at burnout), the lunar slope/flight path angle allowance may be reduced from 0.1 to 0.035 g. In addition, the results of Fig. 6 indicate that slope/flight path allowance may be treated as a statistical quantity. Based on these results, Eq. (5) gives a nominal acceleration value of $N_n = 1.89$ lunar g, compared to 1.80 g for the present design.

The segment approximation of the nominal descent contour may be improved by minimizing vernier propellant consumption with respect to the position of the breakpoint between segments 1 and 2. In the case of the 2500-lb A-24, this improvement amounted to 1 to 1.5 lb for unbraked impact angles of 45 deg and a velocity range of 300 to 400 ft/sec (Table 9).

Various problems inherent in the procedure presently used in the design of the burnout contours are circumvented with the HAC terminal phase monte carlo program. The results of Section ***d*** presented in Table 10 show that for an A-24 injected weight of 2500 lb at an unbraked impact angle of 45 deg, a burnout contour based on monte carlo 1% failures decreases the vernier propellant consumption and the time in the vernier phase by 3.2 lb and 7.8 sec, respectively. Table 10 also shows that the combination of an improved burnout contour and breakpoint reduces the vernier propellant consumption by 4.1 lb and vernier length by 9.9 sec (Table 11).

2. *Effect on Retrorocket Engine Propellant Thermal Control on Surveyor A-21 Mission*

a. Summary. Because of the data obtained during solar thermal vacuum (STV) testing of the SC-1 spacecraft, the prelaunch thermal conditioning of the retrorocket engine was modified so that the propellant average temperature at launch would be 70 ±5°F. The resulting propellant average temperature at retrorocket engine ignition is predicted to be between 40 and 70°F. Under these conditions, the retrorocket maximum thrust requirement of 10,000 lb is satisfied and the retrorocket engine burnout dispersions resulting from the above temperature range and estimated operate interval prediction accuracy (1%) are accommodated by the present terminal descent design.

b. Functional requirements. Limitations of the maximum pitch/yaw moment disturbance and dispersions in the retrorocket phase burnout range impose functional requirements on the performance of the retrorocket engine and the thermal control of the retropropellant. These requirements are as follows:

(1) Retrorocket engine maximum thrust less than 10,000 lb

(2) Retrorocket engine operate interval between 38 and 42 sec

(3) Maximum error in prediction of retrorocket engine operate interval for any propellant average temperature within allowable range less than 1% (3σ)

(4) Retrorocket engine average temperature at ignition between 20 and 70°F

(5) Maximum error in predicting retrorocket engine average gain temperature at ignition less than 20°F

(6) Maximum temperature sensitivity of retrorocket engine operate interval to average temperature less than 0.12% per °F

(7) Thrust versus time profile predicted within 1% when averaged over 1-sec intervals.

c. Retrorocket engine thermal control. Data taken during the SC-1 STV tests indicate that the average temperature of the propellant at ignition will be between 55 and 85°F if the propellant temperature at launch is 85 ±5°F. The maximum propellant average temperature of 85°F results in a predicted maximum thrust of 10,600 lb, which exceeds the specification limit. The expected propellant average temperature at ignition of 70°F, as

CONFIDENTIAL
UNCLASSIFIED

compared to the propellant temperature for the retrorocket engine tests of 50°F, degrades prediction accuracy to an estimated 2%. Because the retrorocket engine propellant ignition temperature would exceed the maximum temperature that the retrorocket is designed to accept (70°F), the temperature conditioning plan for the retrorocket engine was revised to produce an average propellant temperature at launch of 70 ±5°F. For this condition, the predicted average temperature at ignition is 55 ±15°F. The STV test data also indicate the propellant thermal gradient will be less than previously predicted.

d. Mission effect of retrorocket engine performance. The predicted maximum thrust for the A-21 retrorocket engine design as a function of propellant temperature is given in Table 12. At the maximum ignition temperature of 70°F, the predicted maximum thrust is less than the required maximum of 10,000 lb. If this requirement is not satisfied, a higher thrust for SC-1 could be tolerated (with reduced margin) since the predicted thrust to vehicle center of gravity is 0.16 in. compared to a required value of 0.18 in., and the moment disturbance (thrust times offset) establishes the required limits (Table 13).

Table 12. Predicted retrorocket operate interval

Bulk mean grain temperature	Maximum thrust, lb	Retrorocket operate time, sec
70	9977	38.59
65	9922	38.79
45	9707	39.59
40	9654	39.79

Also indicated in Table 12 is the predicted retrorocket engine operate interval (from ignition to the time during thrust decay when the thrust reaches 3500 lb) for several values of propellant average temperature. These values for the propellant temperature range, including the predicted limits, satisfy the system requirements.

The expected propellant temperature at ignition is 55°F which is near the temperature determined from STV test for retrorocket engine performance. The present system design assumes a 2% prediction error of retrorocket operate time at a known temperature. The effect on retrorocket engine burnout dispersions is determined by combining the prediction uncertainty (2%) and the temperature uncertainty (±20°F times maximum retrorocket engine temperature sensitivity of 0.12%/°F to yield 2.4%) in an *rss* manner to obtain a dispersion in retrorocket engine operate interval (3.1%). This uncertainty times the partial derivative of burnout range with respect to interval uncertainty (1917 ft/% for A-21) establishes the retrorocket engine burnout dispersion (6000 ft) due to this parameter. The retrorocket engine burnout range dispersion allowable for all parameter variations for the A-21 design is 9000 ft. The predicted temperature range satisfies the temperature uncertainty requirement of ±20 deg.

After a new prediction of propellant temperature (including gradient) is made on the basis of detailed analysis of the STV data, an A-21 retrorocket engine will be tested under this condition and verification of the operate interval prediction accuracy is expected. This test is planned before launch of the SC-1 spacecraft.

Since the thermal gradient for the propellant is expected to be substantially reduced from previous predictions, the thrust time curve should approach that of

Table 13. Effect of launch temperature on mission parameters

	Average temperature of propellant				Pitch/yaw disturbance			Retrorocket engine operate interval uncertainty			Retrorocket burnout range disper., ft	Vernier propel. margin from full tanks, lb
	Launch, °F	Ignition			Max. thrust, lb	Max. offset, in.	Max. moment, in.-lb	Propulsion, %	Temp. (±20°F), %	rss, %		
		Expected from STV test, °F	Uncertainty									
			From STV test, °F	Required, °F								
Specified values				±20	10,000	0.18	1800	1	2.4	2.6	8800	3.8
Predicted	85 ±5	70	±15	±20	10,600	0.16	1700	2	2.4	3.1	9300	3.1
Performance	70 ±5	55	±15	±20	10,000	0.16	1600	1	2.4	2.6	8800	3.8

a retrorocket engine conditioned to a uniform temperature and yield improved accuracy in prediction of this profile. The error in the shape of this profile produces a dispersion in retrorocket engine burnout range, which is not expected to be significant compared to dispersion due to operate time uncertainty.

3. Surveyor *Lighting Calendar, 1967 through 1968*

Recent changes in the *Surveyor* program have caused more emphasis to be placed on the parking orbit ascent mode. *Atlas/Centaur* capability restricts direct ascent trajectories to lunar arrivals that occur when the lunar declination is less than approximately −15 deg, i.e., about 8 days per month. The parking orbit mode can be used for many more days in the month. With this added flexibility, the obvious choice for launch periods is to pick those days of the month when lunar lighting is favorable. With this in mind, the *Surveyor* lighting calendar, Fig. 9, was developed. The lighting criteria are met if landing is made at least 20 hr after sunrise (dawn or night/day terminator) or at least 150 hr before sunset

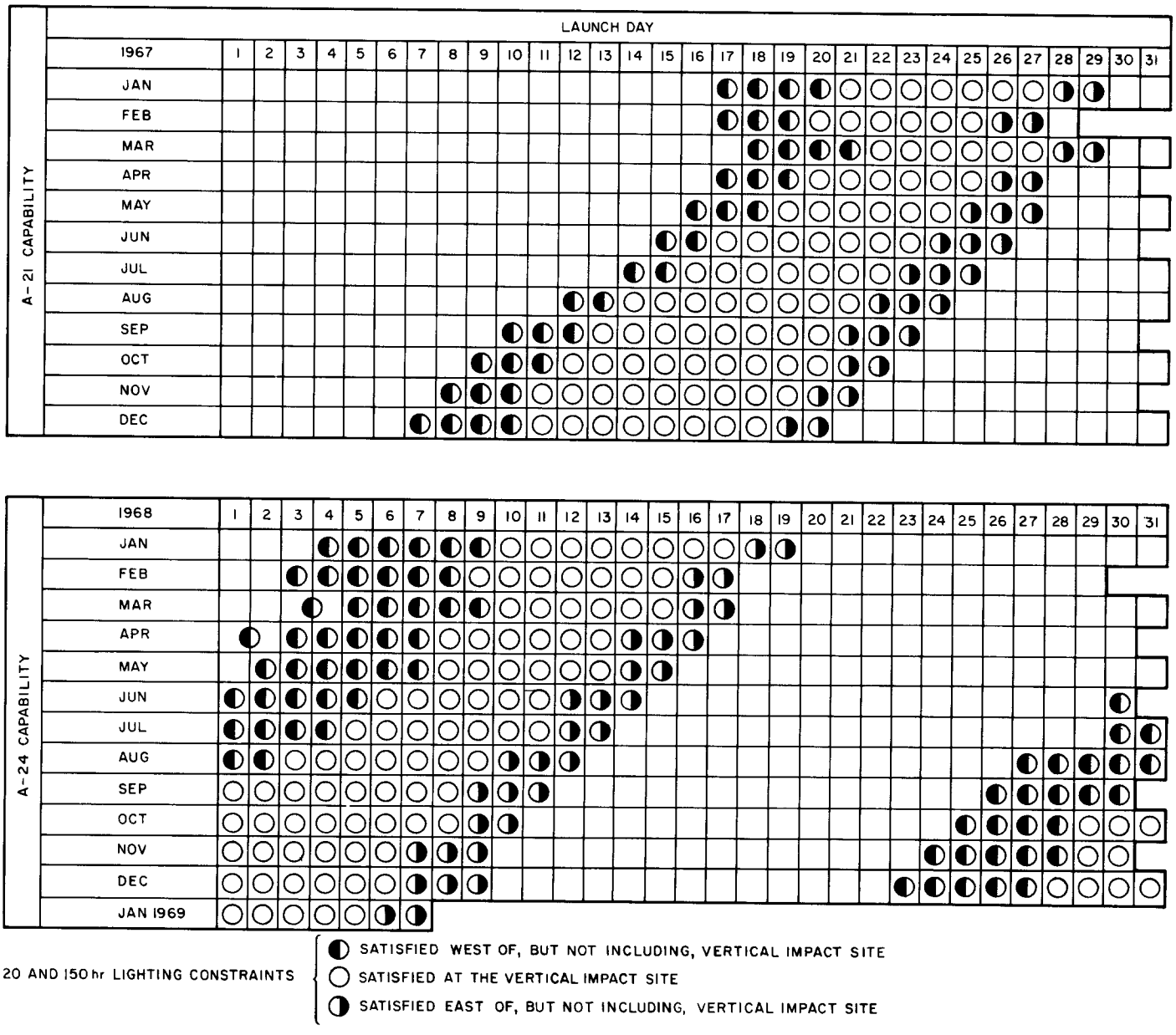

Fig. 9. *Surveyor* lighting calender, 1967 to 1968

UNCLASSIFIED
CONFIDENTIAL

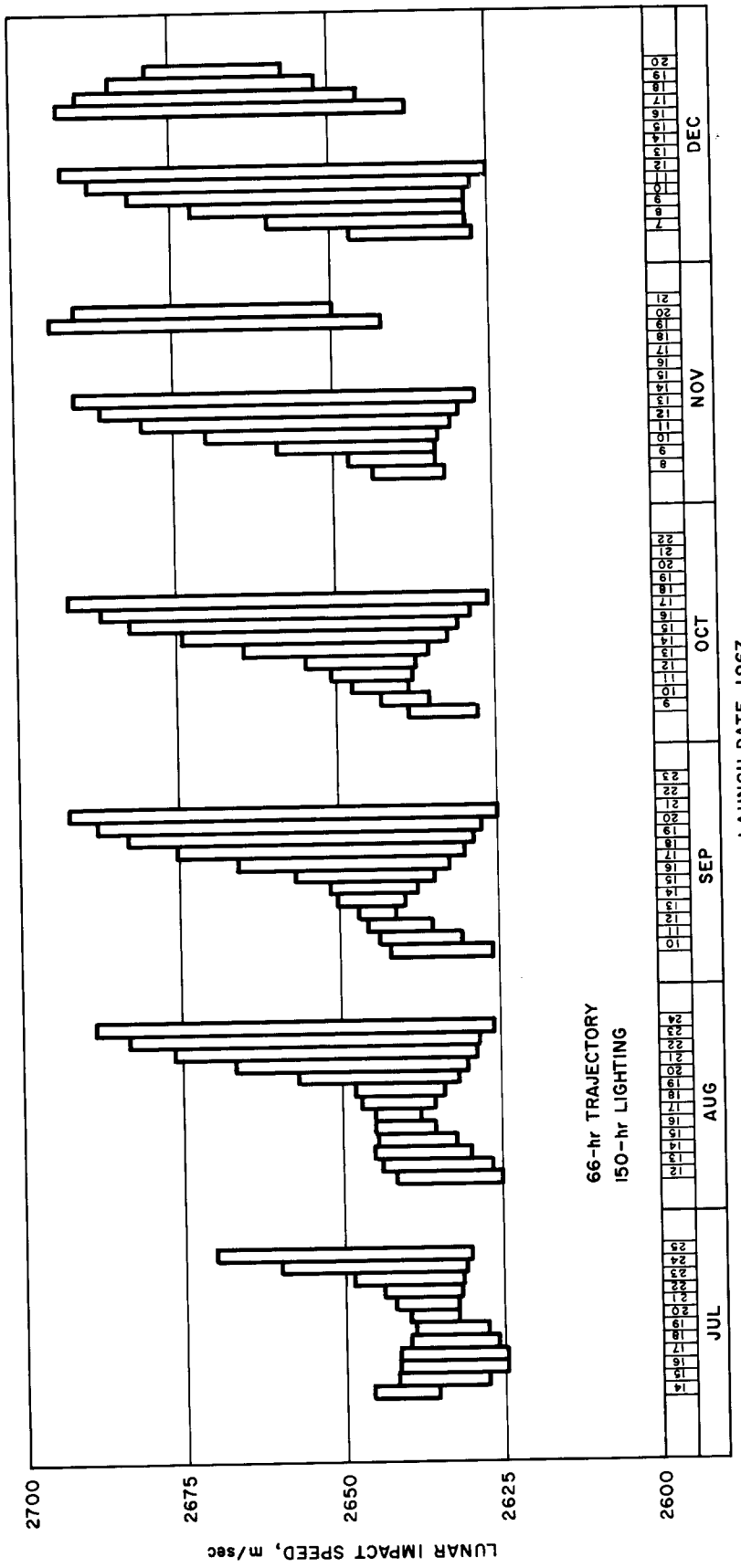

Fig. 10. Variation of parking orbit lunar impact speed, July through December 1967

CONFIDENTIAL
UNCLASSIFIED

UNCLASSIFIED
CONFIDENTIAL

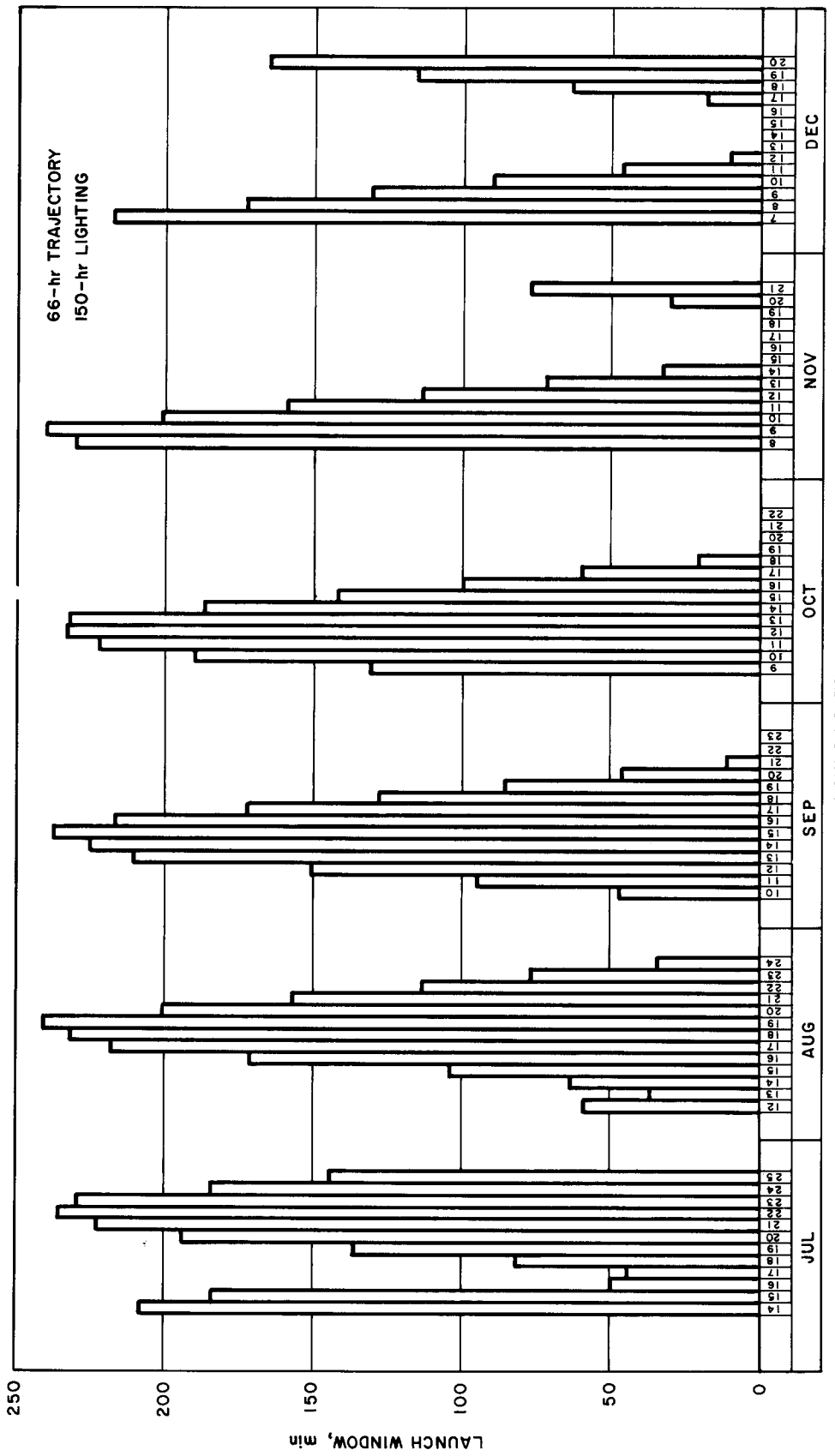

Fig. 11. Parking orbit launch windows, 1967

UNCLASSIFIED
CONFIDENTIAL

(dusk or day/night terminator). These are the lighting constraints toward which HAC is working for parking orbit missions.

The *Surveyor* lunar lighting computer was used to determine lighting. Rather than use the associated assumption that vertical impact occurs 45 deg from the Earth-Moon line, however, the actual locations were used from Ref. 3. For 1967, the A-21 spacecraft capability of unbraked incidence angles up to 25 deg was used. For 1968, the A-24 capability of up to 45 deg was used. This maximum incidence angle constraint establishes the limiting landing site to the east of the vertical impact site. The lunar limb constraint determines the maximum westerly landing site. For this lighting calendar, it is 75 deg from the Earth-Moon line at the landing time.

4. Parking Orbit Trajectory Characteristics July Through December, 1967

The following ground rules were used to generate the data for this study. Detailed analyses and description of methodology are found in Refs. 4 and 5.

(1) Boost vehicle was the *Atlas/Centaur*.

(2) Launches were assumed to take place from Cape Kennedy with launch azimuth restricted to between 80 and 115 deg east of true north.

(3) The coast time was constrained to between 2 and 20 min.

(4) The parking orbit altitude was 90 nm.

(5) Arrival at the Moon had to occur 20 hr after lunar sunrise and 150 hr before lunar sunset for all possible *Surveyor* landing locations (Fig. 9). For 1967, a maximum unbraked impact angle of 25 deg is used to determine possible *Surveyor* landing areas; for 1968, a maximum impact angle of 45 deg is used.

(6) Arrival at the Moon had to occur between 2 hr after Goldstone rise and 3 hr before Goldstone set.

(7) Flight times of the order of 66 hr were assumed.

Fig. 10 shows the variation of parking orbit lunar impact speed for July through December 1967. The top of the bar for each day indicates the impact speed expected for earliest arrival and minimum launch azimuth for that day. The bottom of the bar represents expected impact speed for latest arrival and maximum launch azimuth for each day. Fig. 11 shows the corresponding launch windows available for each day.

5. Lunar Sequence Specification

A preliminary issue of the "Standard Lunar Sequence of Spacecraft Operations for Model A-21," System Specification 224555, has been distributed. This document will control the lunar operations to the extent of HAC responsibilities, and control the lunar phase of the mission sequence tests for the A-21 vehicles. The specification is in two parts: (1) operational constraints and sequence requirements of the spacecraft, and (2) a typical, detailed sequence for use in mission sequence system tests to assure the spacecraft capability to accomplish lunar operations. It is intended that this specification will be maintained current to include the operational capability differences which exist between spacecraft of the A-21 series.

D. Launch Vehicle Integration[1]

1. Spacecraft/Launch Vehicle Integration Schedule

a. Support of Atlas/Centaur R&D flights. Shipment to AFETR of *Atlas/Centaur* No. 8 (AC-8), the *Surveyor* mass model payload, and the HAC supplied S-band transponder equipment, was completed January 25, 1966. System testing, with HAC performing the transponder operations, was completed March 28 and the space vehicle launched April 7, 1966. Flight results were discussed in paragraph 5 below. All HAC supplied support equipment for AC-9 has either been delivered to GD/C at San Diego or placed in bonded stores for delivery when required.

b. Systems test and operations. The difficulty in scheduling joint spacecraft/launch vehicle combined systems testing (CST) (*SPS 37-37*, Vol. 1, pp. 8–12) was resolved and a joint schedule established for SC-1/AC-10 CST and AFETR operations. Key milestones contained within this schedule follow:

Spacecraft/launch vehicle mate at CST	— Feb. 26, 1966
Complete CST and ship to AFETR	— Mar. 12, 1966
Spacecraft/launch vehicle mated for J-FACT	— Apr. 14, 1966
Complete J-FACT and demate	— Apr. 26, 1966
Final mate	— May 26, 1966

[1]Prepared by Technical Section 291.

UNCLASSIFIED
CONFIDENTIAL

The *Centaur* vehicle was erected at the combined systems test stand January 31, 1966. The spacecraft (SC-1) arrived February 19, 1966. A delay in receipt of flight qualified hardware for the guidance system, which is necessary to place the launch vehicle in a flight-ready configuration, extended the AC-10/SC-1 mate date from February 26 to March 4, 1966. The impact of this extension was overcome by spacecraft and launch vehicle personnel working on a three-shift per day basis, and the CST was completed March 7, followed by demate March 8, and the spacecraft was shipped to AFETR March 13, 1966. The *Atlas* was shipped to AFETR March 14 and the *Centaur* March 15, 1966.

Atlas/Centaur mating at AFETR was completed March 31 after an approximate one week delay due to weather conditions and postponements of other NASA launchings. As a result, the spacecraft was mated to the launch vehicle April 17 instead of April 14, 1966, as scheduled. The schedule delay was recovered by extending the work week and workday and the launch vehicle tanking test was completed April 20, followed by spacecraft launch vehicle demate April 26, as scheduled. Final spacecraft and launch vehicle preparations are in progress. Further discussion of SC-1/AC-10 launch operations is contained in paragraph 6 below.

Joint encapsulation procedures (GD/C), the SC-1 and AFETR Test Directives (HAC) and the AC-10 CST and ETR test plan (*Centaur* Unified Test Plan, Section 6.5.8 and 8.10 – GD/C) together with applicable procedures for SC-1/AC-10 have been completed. The joint encapsulation procedures (GD/C AY66-0539-008-13) were employed during the CST of SC-1/AC-10. Changes resulting from this usage were factored into the procedures, and the revised document was followed for the first encapsulation of SC-1 at AFETR.

2. *Interface Requirements*

The proposed amendment to PD-1 concerning injection accuracy (*SPS 37-37*, Vol. 1, p. 9) was revised to reflect: (1) the recent program change, making all of the *Surveyor* missions (A thru G) engineering flights, and (2) utilization of the improved guidance system on all launch vehicles. The proposed amendment now specifies that the rss_{M+T} value of the midcourse maneuver required to make lunar miss plus time of flight corrections for 1-σ injection errors be less than 16.7 m/sec on all missions (A–G). A preliminary draft of the revised amendment has been technically agreed to by Lewis Research Center (LeRC) representatives. A final draft of the amendment has been transmitted to LeRC for approval.

A proposed amendment to PD-1 outlining RFI/EMI requirements has been reviewed and technically accepted by LeRC.

Additional changes to interface requirements which will be documented in PD-1 by amendment or document revision are discussed below. A third revision of the document is being planned.

Additional wiring has been added to reduce line losses between the target lighting power supply and the lights both at the combined systems test stand and at AFETR launch complex 36-A and 36-B. In addition, JPL has installed a 40-v, 5-amp power supply to insure receipt of 28 v at the lights mounted inside the nose fairing. The bulb rating is 5000 $\pm$1000 ft-c at 28 v DC. At this level the survey TV camera can be operationally checked over its range of shutter openings and lens settings while the spacecraft is mounted on the launch vehicle.

A problem still exists on the approach camera which cannot detect the target under the current lighting conditions. Improvements in the target-to-light incidence angle and target reflectance may be required to resolve this deficiency.

Retromotor qualification tests require the motor to be temperature conditioned for 70 $\pm$5°F at launch. As a result, the air conditioning requirement while on the launch pad has been changed from 85 $\pm$5°F to the 70 $\pm$5°F. At two hours prior to opening of the launch window the temperature of the air conditioner is returned to 85 $\pm$5°F. This is to insure the inertial reference unit gyros and the vernier propulsion system fuel and oxidizer lines are above a minimum temperature required at lift-off.

The spacecraft mounted separation sensing and arming devices have been redesigned, which results in significant changes in the forces exerted on the adapter mounted mating pedestals. Preliminary analysis indicates spacecraft separation rates will not be significantly affected and LeRC has accepted the change.

LeRC and GD/C have made some minor improvement changes to the separation springs and separation rate monitoring devices. An improved spring stroke adjustment has been incorporated and better alignment of the separation rate monitoring potentiometers has been

CONFIDENTIAL
UNCLASSIFIED

UNCLASSIFIED
CONFIDENTIAL

obtained. The improved alignment will insure proper measurement of separation spring travel.

Cleanliness requirements have been proposed to LeRC but have not been accepted due to lack of supporting data. It is planned to conduct special tests at a future date in order to acquire the necessary information. Although agreement has not yet been reached on the requirements for inclusion in PD-1, effort to improve cleanliness control has continued. Cleaning procedures have been established for both the spacecraft and the nose fairing/spacecraft adapter assemblies. Special techniques have been employed to purge the air conditioning ducting and a 0.3-μ filter has been inserted in the entrance to the nose fairing air distribution system. A definite improvement in cleanliness has been noted which can be expected to reduce the probability of foreign matter degrading the spacecraft energy conversion, optical and thermal control devices.

3. Interface Control Drawing (GD/C 55-00050)

Although this drawing is revised periodically, it has been determined that a complete redraw is desirable to improve definition of the dynamic envelope, static clearances, mating surfaces, and electrical interface. A list of requested changes together with a request for redraw has been forwarded to LeRC. Studies of the problems involved in producing a new interface control drawing are in progress. Consideration is being given for JPL to produce, maintain, and control the interface drawing.

4. Launch Complex Interconnections

The latest revision (F) of HAC Specification No. 274532 has been reviewed by JPL and forwarded to LeRC along with a list of corrections. LeRC has been requested to incorporate the information in the interface control drawing (GD/C 55-00050). The changes and corrections were primarily in the area of nomenclature and functional usage. A change in the 28-vDC launch complex facility power represents a change in requirements as follows.

The facility power requirement, as presently contained in PD-1, calls for a 28-v, 10-amp DC circuit to the transfer room and blockhouse. Recent calculations and measurements disclosed that the GD/C installed cabling at AFETR (and at the combined systems test stand) would not support this requirement, which was based on future design changes, but would support a 28-v−5-amp requirement to the transfer room as required for SC-1. A 5-amp requirement to the blockhouse, for SC-1 was met by installing additional lines and using available spare pins. Upgrading the installation to meet the 10-amp requirement will be initiated as soon as possible.

5. AC-8 Flight Results

The AC-8 *Atlas/Centaur* vehicle was the seventh in a series of development flights and the second of three vehicles planned to demonstrate a two-burn mission capability for *Centaur*. The first attempt to launch was made March 29. The 1-hr built-in-hold at T−90 min was extended 2 hr and 58 min because the winds aloft were unacceptable. Because of the additional hold time at T−90 min, no additional hold was planned at T−5 min; however, winds aloft were still NO-GO and a hold was initated. After 37 min, the count was resumed and proceeded normally through the *Atlas* engine start sequence at T−8 sec, but at T−3 sec the launch release ladder was interrupted because the *Centaur* aft pneumatic umbilical panel did not eject as programmed. The launch was aborted and rescheduled for April 5.

The countdown for the second launch attempt proceeded normally until T−90 min. The winds aloft were again NO-GO, and the launch was scrubbed after an approximate 4-hr hold.

The third launch attempt was made April 7 and the vehicle lifted off launch complex 36-B at approximately 2000:02 EST, 2 sec after the planned T-O.

A quick evaluation of available data indicated satisfactory *Atlas/Centaur* performance through *Centaur* first burn, and the *Centaur* with its 1730-lb mass model of the *Surveyor* payload was placed in a 90-nm Earth orbit. However, the required second engine firing to transfer the spacecraft into a lunar intercept trajectory, following a 25-min low gravity orbital coast, was not accomplished because of a deficiency of peroxide to operate the boost pumps. Early depletion of the peroxide appears to have been caused by a leak during the coast phase. Further analysis and investigation is in progress.

6. Surveyor Mission A (SC-1/AC-10) Launch Operations

Atlas/Centaur checkout during the CST at San Diego and at AFETR has been excellent. No spacecraft-launch

UNCLASSIFIED
CONFIDENTIAL

UNCLASSIFIED
CONFIDENTIAL

vehicle RFI/EMI abnormalities were experienced during the CST. The spacecraft did not see any perturbaions during the *Atlas/Centaur* quad tanking tests April 20, 1966. All preparations have been made for emergency abort in the event the spacecraft develops a propellant leak or battery pressure rise.

The only gear that remains to be checked out is the stabilizing gear employed for hoisting or lowering the *Centaur* or *Surveyor* in high winds. This is to be accomplished after J-FACT with a dummy spacecraft load on the handling equipment.

A JPL/HAC requested addition to the encapsulated spacecraft handling equipment is being incorporated as a result of concern over the torsional stability of the nose-fairing and spacecraft during hoisting operations. Light torsional loads to the nose-fairing resulted in deflections relative to the spacecraft. As a result JPL built a restraining device that will be used in lieu of a rope lash-up employed at the first mate of SC-1 to AC-10. This torsional stiffner will be used during all lifting operations of the encapsulated *Surveyor*.

7. Launch Vehicle Payload Capability

A summary of current launch vehicle payload capability for the *Surveyor* missions, as of approximately April 1, 1966, is presented in Table 14. The data have been derived from the April 21, 1966 issue of the "*Centaur* Monthly Configuration, Performance and Weight Status Report," GD/C 63-0495-35.

The current status shown in Table 14 includes the following more important changes in payload capability which have been incorporated since the last reporting period:

(1) An approximate 95-lb gain for direct ascent missions A, B and D.

(2) An approximate 85-lb gain for parking orbit missions C, E, F and G.

The above gains result from using improved *Centaur* propellant utilization values to effect reductions in LH_2 bias and flight performance reserve.

(3) An approximate 22-lb loss for direct ascent missions due to the addition of four 50-lb thrust hydrogen peroxide engines for the *Centaur* retromaneuver.

(4) A 12-lb gain on parking orbit missions (C, E, F and G) and a 4-lb gain on direct ascent missions (A, B and D) based on further analysis of the H_2O_2 system and a reduction in H_2O_2 residuals.

GD/C was contractually directed in January to implement the use of *Atlas* SLV-3C (previously referred to as SLV-3X) for *Surveyor* missions, beginning with AC-13. A 51-in. tank extension has been established for the SLV-3C design which provides for 21,000 lb additional propellant load. By increasing flow rates, engine thrust levels at liftoff will be increased as follows: boosters from 165,000 to 168,000 lb each; sustainer from 57,000 to 58,000 lb; verniers from 670 to 1000 lb each. The estimated payload improvement expected for missions E, F and G is 303 lb.

Table 14. Summary of current launch vehicle performance[a]

Mission	Flight	Engineering payload	Ascent mode	Minimum burnout weight[b]	Centaur jettison weight	Payload capability	S/C weight	Margin
A	AC-10	SC-1	Direct	6398	3944	2454	2194	+260
B	AC-7	SC-2	Direct	6352	3905	2447	2184	+263
C	AC-12	SC-3	Parking orbit	6541	4119	2422	2177	+245
D	AC-11	SC-4	Direct	6377	3931	2446	2194	+252
E	AC-13	SC-5	Parking orbit	6541	4116	2425	2179	+246
F	AC-14	SC-6	Parking orbit	6541	4111	2430	2182	+248
G	AC-15	SC-7	Parking orbit	6541	4111	2430	2177	+253

[a] As reported in GD/C 63-0495-35, "*Centaur* Monthly Configuration, Performance and Weight Status Report," April 21, 1966, unclassified.
[b] "Minimum BOW" equals "Nominal BOW" less the "Performance Reserve" of 175 lb for direct ascent missions and 195 lb for parking orbit missions.

CONFIDENTIAL
UNCLASSIFIED

UNCLASSIFIED

E. System Testing

1. T-21 Type Approval Test Vehicle

a. Lunar landing shock test phase. Study and assessment of the telemetry phase lock problem (possible loss of phase lock) during the first T-21 landing shock test is being continued. A possible transient loss of lock and instantaneous recovery can be observed in the oscillograms of shock absorber strain gage signals. This loss appeared during only the first drop; however, the first drop was the only test during which these telemetry signals were received (and recorded) via air link, such that the motion of the omniboom antenna could have contributed to the observed anomaly in the data record (oscillogram).

A review of the accelerometer oscillograms generated from T-21 drop test recordings indicated that for the three different drop conditions, responses at several accelerometer locations exhibited "characteristic" or repeatable rise and decay modes, i.e., oscillograms of generally similar form at a given location. This observation suggested that data reduction to obtain shock spectra could be limited to one presentation (each) for all of the accelerometers except three. The g responses (accelerations) of various components of the spacecraft reported previously have been reassessed and are shown in Table 15. Revisions and additions have been made to the data because of errors in the interpretation of the calibrations from the records. Some data not available at the last report period have been reviewed and are included. Review and analysis continues.

Table 15. Peak acceleration response at various component positions

Component accelerometer	Drop 1	Drop 2	Drop 4
Compartment A (vertical)	7.0	12.0	19.5
Compartment B (vertical)	14.0	15.6	10.2
Omniantenna A			
Vertical	20.0	19.0	22.0
Horizontal	Not avail.	14.6	Not avail.
Omniantenna B			
Vertical	10.0	14.5	11.0
Horizontal	Not avail.	12.4	Not avail.
Antenna/solar panel positioner V40 (horizontal)	14.0	6.0	14.0
Doppler velocity sensor antenna V41 (vertical)	15.0	12.0	12.5
Flight control sensor group V11 (vertical)	9.3	10.8	Not avail.

b. Posttype approval test operations. Following lunar landing shock tests, several units were removed from the spacecraft and transported to the unit area for investigation of open failure reports. The vehicle was then utilized on the alignment dock for development of weight, balance, and alignment techniques and procedures.

2. SC-1 Flight Spacecraft

a. Vibration test phase (retest). Vibration test input control data for the SC-1 flight acceptance retest of January is shown in Figs. 12 and 13. Fig. 12 shows a composite plot of acceleration versus frequency recorded at each

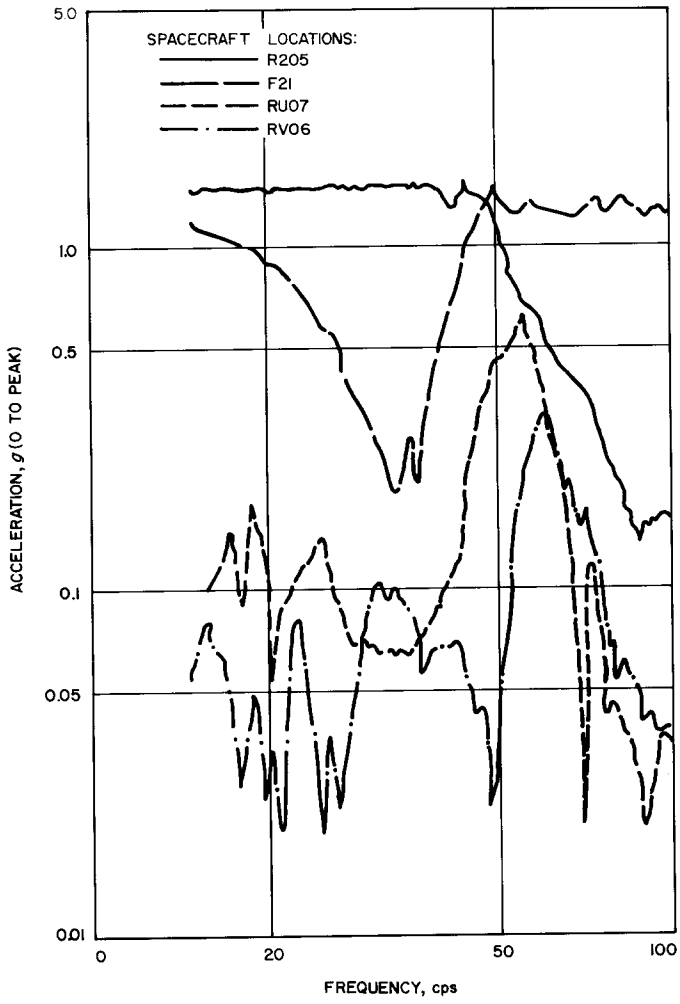

Fig. 12. Composite plot of SC-1 control accelerometers, test run 10A

UNCLASSIFIED

UNCLASSIFIED

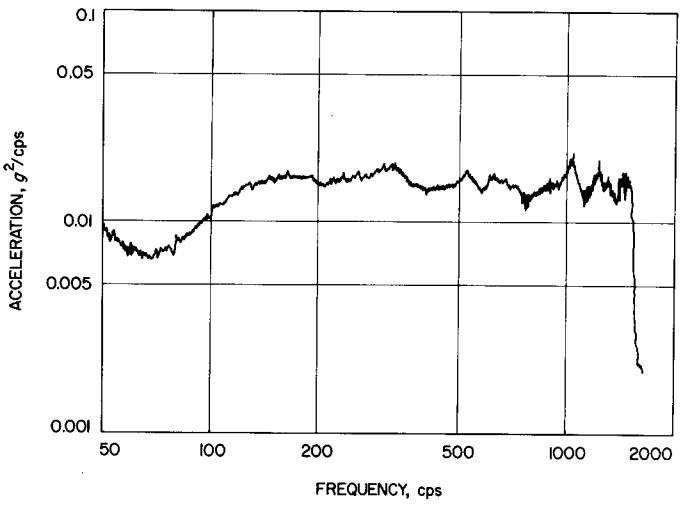

Fig. 13. Power spectral density analysis, run 10B

control accelerometer position. The automatic crossover of control from retrorocket accelerometer RZ05 to fixture accelerometer FZ-1 at 48 cps, accomplished by the selector control adjustable multiple point (SCAMP) unit, occurred with negligible change in level of test magnitude. SCAMP is a device to automatically switch control to the output of the accelerometer in a given system that is experiencing the highest response. Small variations in level above 50 cps were noted as the operator adjusted the level from 1.5 to 1.33 g (0-peak) on a nonstop procedure basis for the reduction in specified level breakpoint at 50 cps. For the combined sine and random test (10B), an acceleration spectral density plot (Fig. 13) shows the control achieved with the MB-80 80-channel equalizer, over the test range 100 to 1500 cps. The objective level of 0.0145 g^2/cps, with a tolerance of ± 3 db in each 50-cps bandwidth in range 100 to 1500 cps is satisfied. This plot indicates an improvement in uniformity of level over the test reference frequency band (100 to 1500 cps), achieved with the MB-80 equalizer, compared to the previous vibration flight acceptance test of June 1965, wherein the 40-channel equalizer was used.

b. Vernier engine vibration test phase. The vernier engine vibration test phase was performed successfully after a few minor problems with the STEA were corrected. The first subphase simulated the vibration environment to be encountered in both the midcourse maneuver and the terminal descent. This subphase was performed with a vibration input of 10 lb rms to each vernier engine. An example of the random force input is shown in Fig. 14. The signal data converter was used in a closed loop with the flight control closed-loop simulator and the radar altimeter STEA. During this test the

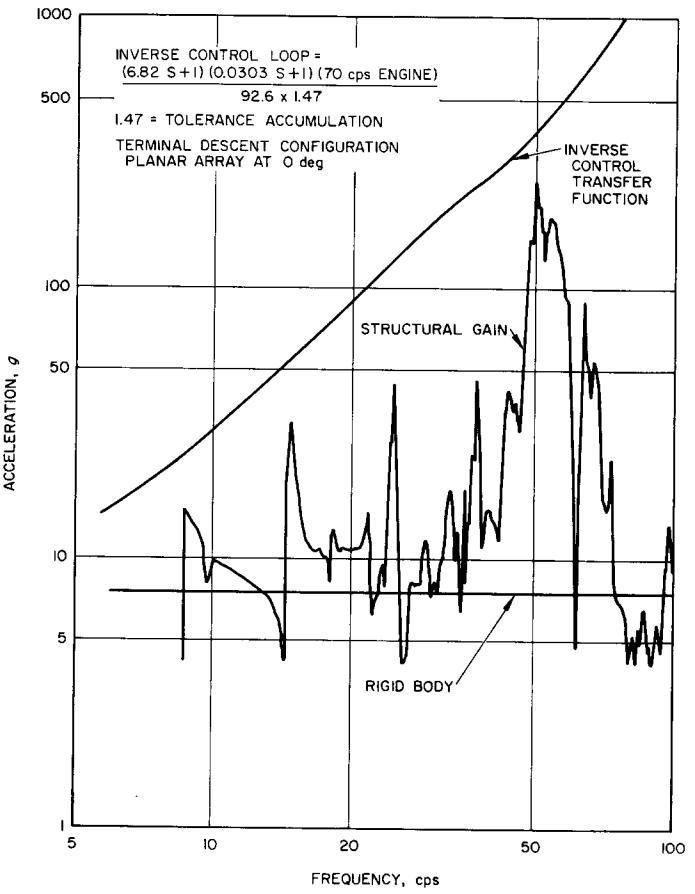

Fig. 14. Structural transfer function between vernier engines and flight control sensor group accelerometers

inputs to the signal data converter were 3 db above threshold. The relationship of range to vertical velocity (R/V_z) was plotted and came within the prescribed envelope for the entire descent. There were no losses of lockon or erroneous lockups of the RADVS during this descent. Several earlier descent attempts were failures because of a damaged cable connecting the RADVS summing amplifier to the SDC.

The second subphase involved a margin test where vibrational forces of 20 lb rms were inserted into each of the vernier engines with no access to the RADVS. The RADVS was required to search without lockup. This excitation is considered to be at least 6 db above the level expected during actual flight. The RADVS operation was good and exhibited no tracker lockups or gain state changes during this margin test.

Prior to the vernier engine vibration test, modal shakers (Stephens ST10A) were attached to the vernier

UNCLASSIFIED

UNCLASSIFIED CONFIDENTIAL

dummy engines and special test 15 was performed (Fig. 15). The structural transfer function from the vernier engines to the flight control sensor group accelerometer was measured during a sinusoidal sweep excited at all three dummy vernier engines simultaneously. The objectives were to verify (1) that the electronic filter modification to the flight control sensor group ("buzz fix"), developed on the basis of structural dynamics model S-2A test data, was adequate for the SC-1 spacecraft and (2) to compile data for estimating the structural transfer function to establish the need for testing subsequent spacecraft.

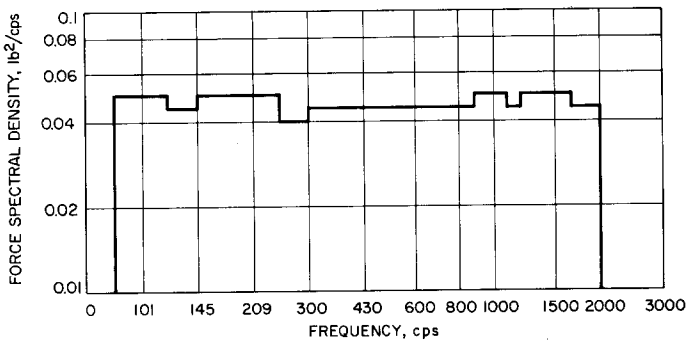

Fig. 15. Vernier engine vibration random vibration force input spectral distribution

The structural gain was determined to be within 4 to 5 db of an instability at 14.5 and 50 cps. The inverse control transfer function shown is for maximum electrical and engine gain, a worst case condition, with the electronic filter modification incorporated. It is evident that this modification is adequate for SC-1.

The structural transfer function was different from that of the S-2A in many respects. SC-1 shows higher gains at the low frequencies and an upward shift of the major resonance from 40 to 50 cps, which should be explained by modal surveys and transmissibility studies to be made on the S-9 structure's test model. It appears, however, that the shift is caused by the increase in vernier engine bracket stiffness. The vernier engine in the SC-1 bracket has a natural frequency of from 45 to 50 cps, whereas 40 cps was observed for S-2A. The results show significant differences in transfer functions between SC-1 and S-2A and small gain margins.

Following completion of test activities in El Segundo, SC-1 spacecraft was turned over to launch operations.

3. SC-2 Flight Acceptance Tests

a. Mission sequence/electromagnetic interference test phase. The SC-2 flight acceptance mission sequence/electromagnetic interference (MS/EMI) test phase was performed in accordance with revised A-21 mission sequence/electromagnetic interference test specification 224822.

Beginning with the system readiness test the EMI environment of the launch site was simulated. When the injection subphase of the real-time mission sequence was reached, the EMI simulation was turned off, the umbilical cable was disconnected, the spacecraft ground connection was removed, and the remainder of the test was performed in the plugs-out configuration. No problems affecting mission operation were found attributable to EMI. Television camera operation was degraded during the systems readiness test by 260 Mc EMI simulating the *Atlas/Centaur* telemetry transmitters, but this problem is irrelevant because *Centaur* spacecraft separation will have taken place long before TV cameras are turned on.

After completion of the MS/EMI test phase, SC-2 went into complete test weight, balance, and alignment procedures that simulated the sequence that will be performed at AFETR.

b. Solar thermal vacuum test phase. Preparation for testing the SC-2 spacecraft in the solar thermal vacuum (STV) phase began immediately following the termination of this test on the SC-1 spacecraft. The test plan has been revised to reflect changes resulting from the operation and post-test analysis on SC-1. In general, however, the STV testing of SC-2 will embody the same test objectives and undergo the three solar perturbated exposures of SC-1. From February 15 to March 23 activity in the STV test area was mainly concerned with redefining the necessary criteria for flight acceptance, which also included new propulsion requirements such as jet valve and flow response. These redesigned and new requirements were engineered and implemented. Preparation prior to receipt of the spacecraft from weight, balancing, and alignment involved the expansion of all preparation steps for the spacecraft mating to the end bell. Such additional implementation refinements as flowmeters for jet gas output, new radiometer mounts, outfitting of the new inert retrorocket engine with a heater and thermocouples, and the realignment of the necessary thermocouples for protection and temperature profile data were representative of the continuing effort to improve the test configuration. Other areas that have been improved

UNCLASSIFIED CONFIDENTIAL

UNCLASSIFIED

involve protective wrapping of the spacecraft during the preparation phases to offset possible thermal degradation of surfaces. The preparation and checkout of the SC-2 vehicle continued through the early part of April. Pretests, including a systems readiness test, abbreviated mission sequence, and various test addendums such as flight control closed-loop testing, and Sun and star acquisition were accomplished. From approximately mid-April to the first week in May, subphases A (low solar) and B (high solar) were conducted. These are back to back tests in STV exposure. Following subphase B, the spacecraft will be prepared for subphase C (plugs-out).

4. Group Tests

Although hardware deliveries for SP-1 and SC-3 have been delayed somewhat, the units shown in Table 16 were group tested.

Table 16. Group tested units

Unit	Hardware part number	Serial number	Planned usage
Boost regulator	274200-11	13	SC-3
Boost regulator	274200-11	12	SP-1
Battery charge regulator	274100-3	14	SC-3
Battery charge regulator	274100-3	13	SP-1
Auxiliary battery charge	273000-2	14	SC-3
Auxiliary battery charge	273000-2	11	SP-1
Receiver	231900-3	21	SC-4
Receiver	231900-3	23	Undetermined
Receiver	231900-3	19	SC-3
Central command decoder	232000-5	2	SP-1
Survey camera	284312-4	13	SP-1
Approach camera	284302-1	14	SP-1
Altitude marking radar	283827-1		SP-1
RADVS			SC-3

The GT-1 STEA (STEA-5) was used in support of SC-1 and SC-2 weight, balance, and alignment and the RADVS special tests.

5. AMR Ascent Pressure Profile Test

Special test 92 was performed February 28 through March 7 to verify the performance of the AMR antenna/electronics assembly during ascent pressure differential exposure. The AMR parabolic dish and some of the structures in the electronics units are constructed of Fiberglas honeycomb material. The test was to assure that the ascent differential pressures did not cause dish deformation due to delamination or functional anomalies. Analysis of the optical and electrical test data verified that there were no anomalies resulting from this test which would affect design performance.

6. T-2N Descent Dynamics Program

Each of the two T-2N vehicles successfully completed an altitude descent test at AFMDC and was returned to Culver City for rework in preparation for the touchdown phase. The T-2N-1 vehicle completed all rework and retest and was returned to Holloman Air Force Base where it is in preparation for an additional altitude descent test (test 6) prior to touchdown tests.

a. T-2N-1 descent tests. The third descent test of the T-2N-1 vehicle was conducted February 24. Performance was normal in every respect, and the programmed Range $-$ V_z profile was followed. A modification incorporated in the recovery electronics assembly which retains power to the vehicle for 40 sec after recovery was tested for the first time. Radar range to ground data was obtained, and the altitude at which the 14-ft mark was generated by the RADVS was determined.

In the mission countdown several anomalies encountered in the behavior of the RADVS were attributed to the test fixture used to verify RADVS performance prior to release, and to telemetry difficulties.

Specifically, as observed on previous missions, when the RADVS test was initiated, V_y and V_z were abnormal, and when the test was terminated the beam 3 tracker remained locked. Jettison of the test fixture did not, as expected, alleviate this condition and it was necessary to recycle power to eliminate the problem. As the countdown continued it was observed that a telemetry indication of a positive V_z of approximately 20 ft/sec was present. Inasmuch as the signal level measured in the beams 1, 2, and 3 preamplifiers was within specification and no tracker locks were seen, the indication appeared erroneous and the countdown was allowed to proceed. With this exception performance of all subsystems during the 16-sec tether test proceeded as expected and the vehicle was released.

Subsequent analysis disclosed the X-3 RADVS to exhibit anomalous behavior in several ways. The RADVS

UNCLASSIFIED

UNCLASSIFIED

was removed from the vehicle and returned to Ryan for analysis, test, and repair as required, and action was undertaken to improve reliability.

The current status of these efforts is as follows:

(1) RADVS test fixture. The wheels on the fixture were capable of producing strong sidebands on which the searching velocity trackers periodically locked. The wheel and cavity were redesigned and a thickness of microwave absorber added to reduce the magnitude of the undesired sidebands. These modifications will be tested on the first mission in mid-April.

(2) V_z indication. This problem has been isolated to the presence of noise in the V_z converter when the signal data converter is subjected to certain combinations of high supply voltage and low temperature. Although not clearly an out-of-specification condition, and one which has no effect on normal operation, a resistance value in the V_z converter has been increased, thereby attenuating the undesired signal.

(3) Delay in range acquisition. This problem was identified in the postmission data review, and was traced to beam spreading in the radar altimeter klystron-modulator assembly. The spare T-2N klystron-modulator has been substituted, and the klystron power supply modulator was retested satisfactorily.

(4) Analysis of the remaining two anomalies has not been completed.

b. T-2N-2 descent tests. The second descent test of the T-2N-2 vehicle occurred March 7. Preparation and countdown of the vehicle proceeded smoothly and on schedule until the RADVS test was commanded approximately 2 min prior to engines on. A typically anomalous result was obtained, and the test was repeated three times before obtaining the proper response. The countdown then continued, and the vehicle was released. All subsystems performed normally during the tether and after release the vehicle followed the prescribed Range $-$ V_z profile achieving all test objectives.

Approximately 5 sec after release a roll oscillation developed, and started limiting one cycle. The oscillation period was approximately 5 sec and remained until recovery. Although in no way detrimental to the primary objectives of the mission, this condition obviously has been the subject of extensive analysis.

Although the precise nature of the initiating disturbance has not been positively identified, the subsequent response of the vehicle and its initiation of roll limit cycling are well understood, and have been long recognized as a potential behavior characteristic. Basically the potential for this response is the result of the relatively high gain (in comparison with the flight spacecraft) of the T-2N roll loop. This condition is due to the reduced rotational moment of inertia coupled with the use of spacecraft thrust chamber assemblies and basic flight control system.

To reduce the possibility of a recurrence, proven changes have been made to the roll loop circuits, enabling the gain to be reduced from 1.32 to 0.58. Also, since evidence indicates that the basic cause is high roll torques induced by aerodynamic forces, caution will be maintained to minimize the exposure of the vehicle to marginal wind conditions and pronounced shears.

A second minor difficulty was encountered when at 1.3 sec before recovery beam 1 lost lock, causing the loss of reliable operate doppler velocity sensor and reliable operate radar altimeter. Although at an altitude of 600 ft and at a velocity of 5 ft/sec radar signal return is quite low, this problem had not been previously encountered. In this instance two causes have been identified. First, the stabilization parachute, with a sink rate greater than 5 ft/sec, drifted below the vehicle and was in close proximity to the beam in question. Although no corrective actions are required in this case, the possible fouling of the vehicle is of sufficient concern to raise the issue of its value. Second, possibly because of coupling from the roll oscillation, a slight lateral velocity built up at that point, causing the velocity along beam 1 to drop to approximately 1.1 ft/sec. This beam velocity combined with the reflectivity obtained at 600 ft has been determined to be sufficient cause for the loss of signal in beam 1 and subsequent loss of lock.

c. Touchdown modification and test. In the touchdown mission, the T-2N spacecraft will fly essentially the same Range $-$ V_z trajectory as in an altitude recovery mission but with the 600-ft bias removed, so that the release altitude will be nominally 900 ft, and the flight will terminate in Earth touchdown. Two minor differences in trajectory will be as follows:

(1) At 7.5 sec after release, the vehicle will be commanded to descend at a constant acceleration of 1 ft/sec^2 until the line segment is acquired. The purpose of this is to limit the maximum vehicle

UNCLASSIFIED

UNCLASSIFIED

velocity, which will provide greater assurance that the engines will not reach the lower thrust saturation limit immediately before crossing the line segment.

(2) During the terminal phase of the descent, the generation of the RADVS 14-ft mark will turn off the klystron power supply modulator high voltage and command the vehicle to descend at an essentially constant acceleration. Thus, the vehicle will continue its descent at a constant acceleration of 1 ft/sec^2. The powered flight is terminated and the engines turned off at an altitude approximately 2 ft above the ground.

Engineering modifications required to perform the touchdown mission were incorporated into the T-2N-1 spacecraft during the upgrade-retest cycle completed March 25. The engineering changes consist of the following:

(1) Minor modification of the flight control electronics unit.

(2) Repackaging of the recovery electronics assembly to provide space for additional circuitry required for touchdown logic.

(3) Addition of a touchdown probe and sensor mechanism.

(4) Provision of a new harness, which includes modified and additional interconnections for touchdown operation.

After incorporation of the engineering modifications, the vehicle was subjected to system testing, including system functional testing — phases 1, 2, and 3, vehicle vibration testing, and a vehicle landing shock test. All unit and system documents, both engineering and test, that were affected by touchdown modifications have been revised to reflect the new requirements.

Testing of the *Surveyor* T-2N-1 in the touchdown configuration was accomplished at the HAC Culver City facility in accordance with the T-2N system functional test plan (228103-1) and the T-2N environmental test plan (225456-1). The primary objective of these tests is to demonstrate the readiness of the T-2N-1 spacecraft to successfully complete the touchdown mission.

Five new test requirements were added to the system functional test specification and four to the environmental test specification. These are listed in Table 17.

Table 17. New T-2N test requirements

Number	Description
FL 016A	One g acceleration and accelerometer checkpost landing enable
RD 034A	Range mark enable touchdown logic
RY 021A	Landing enable
RY 022A	Air bag inflation with 14-ft mark
RY 023A	Touchdown sensor

Completion of the system functional test phase demonstrated the capability of each subsystem to perform its required functions, independently and integrated into a complete system. The vehicle was in the configuration specified by the test plan with no deviations. All test requirements were satisfied.

The environmental test consisted of two parts, vibration and simulated landing shock. The closed-loop simulator verified proper system operation throughout this test phase.

The vibration test consisted of performing closed-loop mission sequences with and without altitude bias for each of the three conditions: (1) previbration, (2) vibration at 10 force lb, rms random noise between 84 and 2000 cps applied at the vernier engines, (3) postvibration. The input level in the 1700 to 1800 cps band was 0.008 lb^2/cps as compared to a required level of 0.05 lb^2/cps. This is attributed to a sticking panel meter in the equalizer console. Since the broadband rms level as indicated on a meter during all three rms was approximately 10.7 force lb and this band represents a very small portion of the overall spectrum, the vibration test will be accepted as valid. Also, no problems have been experienced in this frequency region during previous vibration tests.

The landing shock test consisted of releasing the vehicle above the ground so that the touchdown velocity approximates the actual altitude recovery touchdown velocity (20 ft/sec). After the release two closed loop mission sequence tests were performed, one with and one without altitude bias. All test requirements were satisfied. The elapsed time from probe touchdown to switch activation was 4 msec. The elapsed time from probe touchdown to air bag touchdown as measured from high speed 16 mm film was 17 msec; however, poor film quality made reading difficult.

UNCLASSIFIED

UNCLASSIFIED CONFIDENTIAL

F. Launch Operations

1. Mass Model Operations

On February 8 and 9 special tests were conducted to gather data needed by Deep Space Network (DSN) personnel so that they could plan for the launch of AC-8. Also, flight acceptance testing (FAT) of the test battery was completed successfully.

The premating functional checkout of the transponder was performed February 21 and 22. The data were within specification. Performance difficulties were caused by the vacuum tube voltmeter signal generator and spectrum analyzer of the STEA. Tests were completed with spare items.

The transponder was mated to the mass model in the explosive safe facility February 23. The battery simulator was adjusted to prevent battery discharge. Daily transponder checks were conducted from building AO via the microwave link while awaiting the encapsulation and first mating of the spacecraft. Mating was delayed by GD/C to rework the AC-8 barrel section. The spacecraft was encapsulated March 5 and mated to AC-8 March 10.

On March 11 RF compatibility tests with DSIF 71 were performed. Later in the day, the joint flight acceptance composite tests were performed. Because of discrepancies between HAC and JPL data, the compatability tests had to be rerun. The discrepancies were found to be caused by procedural difficulties. During joint flight acceptance composite tests, the transponder dropped lock several times. This could have been caused by: (1) RF interference; (2) a faulty receiver in the transponder; (3) system test equipment assembly (STEA) problems; or (4) microwave link problems. During a retest on stand March 12, the trouble recurred. The range assured HAC that no interference near the *Surveyor* frequencies was present and, since checks revealed no apparent problems with the STEA or microwave link, the payload was demated and decapsulated March 12 so that the receiver could be investigated. Retests in the explosive safe facility did not reproduce the problem.

The receiver from the AC-9 transponder was substituted in AC-8. The transponder was checked out, reencapsulated, and remated by March 14. Since that time, no unexplainable drop locks have occurred.

The AC-8 receiver was installed in the AC-9 transponder and bench tested to see if it was faulty. The only malperformance occurred when the transponder was connected to the building AO antenna. The trouble is believed to have been RF interference but, by the time a tracer could be started, the malperformance stopped. No interfering source appeared to have been on the air and the break lock anomaly has not been completely explained. To maximize confidence in AC-8, HAC recommended and JPL approved use of the AC-9 receiver. After the launch of AC-8, the exchanged receiver is to be returned to HAC for retest to assure flight readiness for AC-9.

Tanking took place March 17. Transponder operation was normal. Demating and decapsulation occurred March 19. The receiver was upgraded at AFETR March 20 by staking the knurled nuts in the receiver with epoxy. Because of the receiver substitution, a complete functional retest of the transponder was made March 20. Performance was normal.

The flight battery was installed March 21, and DSIF compatibility tests were rerun. Before the tests, procedures were reviewed between JPL and HAC. The tests were highly successful, with complete agreement between DSIF and STEA data, indicating that the previous problems with DSIF data were procedural. Final encapsulation took place in the ESF early March 23. After a brief transponder check, the encapsulated spacecraft was transported to launch pad 36B and mated to AC-8.

Because of GD/C operations around the booster, a transponder checkout after mating, via the microwave link, could not be conducted until March 25. When checkout was attempted, interference was experienced from SC-1 which was under test in the high bay area of building AO. Even with its transmitters hardlined to the STEA, there was sufficient RF leakage to swamp the incoming AC-8 signal. Daily transponder checkout was successfully performed at a time selected to avoid interference with SC-1.

An attempt to launch AC-8 was made March 29. The countdown proceeded smoothly for SD-6 until T −90 min, when an indefinite hold was declared because of high winds aloft. After a delay of approximately 4 hr, the countdown proceeded to T − 5 min when there was a 20-min hold while wind data were analyzed. The countdown then proceeded to T − 2 sec when the launch was held by automatic interlocks because the lower umbilical plate on the *Centaur* had not ejected properly. GD/C made minor changes to the plate eject mechanism,

UNCLASSIFIED CONFIDENTIAL

UNCLASSIFIED

and recycled AC-8 for launch at 0900 EST April 5. Because of conflicts with the Orbiting Astronomical Observatory, which was experiencing launch difficulties in the same time period, the launch of AC-8 was rescheduled to 0005 Eastern Standard Time (EST) April 6.

Countdown started about 1500 April 5 and proceeded smoothly to T − 90 min when a hold was declared because of high winds aloft. After holding for 4 hr, the launch was scrubbed at 0230 April 6, because it appeared the winds would not diminish in a reasonable time. The launch was rescheduled for 2300 April 6.

On April 6 high winds aloft continued with little probability that they would diminish to an acceptable level at the scheduled launch time. The launch was rescheduled for 2000 April 7.

The count proceeded with no accumulated holds up to a few seconds before launch. AC-8 lifted off at 01:00:02.090 (GMT) with an accumulated hold of less than 3 sec experienced in the last few seconds of the count. Mark events were more or less as expected until second *Centaur* motor ignition. Ignition was about on schedule, but cutoff occurred after 17 sec instead of the programmed 108 sec. One engine developed 10% thrust and the other about 70%. Because of the low thrust and short second burn, the mass model separated and continued in a low parking orbit (perigee after 98 nm and apogee about 110 nm, period about 90 min) instead of a transfer trajectory. For this reason, continuous DSIF tracking was not possible.

The spacecraft was first acquired by DSIF-11. Subsequently, it was tracked by DSIF stations 11 (Goldstone), 72 (Ascension), 51 (Johannesburg), and 61 (Madrid). One-way lock was obtained at all stations, and two-way lock was established on some passes. The tumble rate was 24 deg/sec (about 8 times specification limits). Tracking by the DSIF network continued for 26 hr.

2. *AFETR Activities*

a. SC-1. Following successful completion of combined system testing at GD/C, San Diego, the first flight spacecraft arrived at AFETR by air March 14. The spacecraft was moved to the system test stand and preparations for the performance verification test sequence were started.

Because of equipment shortages and operational problems, some minor rescheduling and planning has been necessary to accomplish performance verification testing and the vernier propulsion system procedures within the overall schedule limitations. However, the initial spacecraft checkout facility testing phase of SC-1 is essentially on schedule. The spacecraft was transported on schedule to explosive safe facility for joint flight acceptance composite test preparations.

In addition, several special tests were performed, including a special check of the separation sensing and arming devices, which required mounting the dummy retrorocket engine on the spacecraft and mating the spacecraft to the forward payload adapter on ground transport vehicle (GTV) 2. This test was accomplished with the cooperation of GD/C and revealed that the combined system test (CST) adjustment of the separation sensing and arming devices was satisfactory.

Several special laboratories conducted operations parallel with the main spacecraft effort. These included the flight control sensor group laboratory, where a complete functional test of the flight control sensor group was performed prior to mounting it on the spacecraft, and the solar panel laboratory where functional checks of the flight and backup solar panels were performed. The backup laboratory provided battery support and delivered a test battery for the special test of the separation, sensing, and arming device.

In addition, the explosive safe facility and the launch pad are being prepared for future operations. The high pressure gas installation facility in the explosive safe facility was completed and proofed. Work is under way to validate the propellant and gas handling ground support equipment (GSE).

At the launch pad work is progressing toward tanking and joint flight acceptance composite test operations. This work includes modifications to the ground power supplies and their control systems, a rework of the TV target light system, validation of all spacecraft aerospace ground equipment (AGE) on the complex, and the inclusion of an expanded capability to record AGE parameters.

b. S-6 test program. Lists of expected failures for all electrical tests have been completed and will be provided as an additional section to affected procedures. The affected procedures are performance verification test 1, performance verification test 2, and the system readiness test. Expected failures are those due to open sensors such as battery temperature sensors, compartment cover temperature sensors, and compartment cover temperature

UNCLASSIFIED

UNCLASSIFIED

sensors which may be absent for certain test configurations. A corrected PATE tape for performance verification test 2 was provided February 7, and a major revision is presently in progress and will incorporate numerous corrections received from the SC-1 test team February 7.

The ground rules established for the S-6/AFETR program were as follows:

(1) SC-1 procedures would be used.

(2) SC-1 support equipment would be used.

(3) SC-1 facilities would be used whenever possible.

The major objectives of the program were intended to accomplish the following:

(1) Verify and/or update procedures describing prelaunch activities related to vernier propulsion systems and related AGE.

(2) Verify and/or update procedure for leak-checking gas jet attitude control system (GJACS) by pressure decay method.

(3) Further identify and refine methods and techniques required to leak test helium tank and valve assembly and GJACS nitrogen bottle by plastic enclosure (bag) technique.

(4) Develop and demonstrate method to achieve satisfactory propellant loading within weight and center of gravity accuracies required.

(5) Improve personnel skills associated with preceding operations.

The program began February 14 with delivery of the S-6 vehicle to AFETR and was completed March 28. The S-6 vehicle is being held at AFETR pending further direction from JPL. During the program, approximately 25 procedures were conducted on the GJACS and vernier propulsion system. The only three significant variations from the original plan were as follows:

Because of the labor, technical, and scheduling difficulties, the JPL installed gas distribution system in the explosive safe area could not be utilized. Instead, a representative system of flex hoses (similar to that used during the T-21 program) was used.

The initial propellant loading and weighing operation was not entirely successful. As a result, revisions to procedures and techniques were required, as were weighing system hardware modifications. A second propellant loading, of oxidizer only, demonstrated adequate resolution of the problems.

Because of a conflict with SC-1 requirements for personnel, equipment, and facilities, the plastic enclosure (bag) leak test was conducted on only the GJACS high pressure nitrogen bottle. It was agreed, however, that the techniques developed were satisfactory and directly applicable to the helium tank and valves assembly.

The following operations were performed on the S-6:

(1) Installed helium tank.

(2) Connected pneumatic control console.

(3) Checked vernier propulsion system.

(4) Installed thrust chamber assembly.

(5) Filled flush carts with solvents.

(6) Tested pressure decay leak of nitrogen bottle.

(7) Tested pressure decay leak of helium bottle.

(8) Validated pneumatic control console in building A0 in accordance with document 288385.

(9) Completed bag calibration experiments.

(10) Removed helium from tank, and purged and refilled helium tank with nitrogen in preparation for bag leak test of nitrogen bottle.

(11) Purged propellant lines and tanks and applied blanket of nitrogen.

(12) Depressurized nitrogen bottle.

(13) Moved GTV-1 and bag operation to propellant loading building.

(14) Sniffed S-6 vehicle for trapped helium.

(15) Placed S-6 in the bag on GTV-1 and performed bag leak check.

3. *Combined Systems Test Facilities Activation*

Activation of the CST facility for SC-1 testing was completed February 19. Activation spanned a 2-mo period from mid-December until mid-February. During this period an upgrade program consisting of 54 modifications to STEA-3 equipment was completed, and STEA-3 was given a complete calibration by the GD/C standards laboratory and by HAC personnel.

STEA-3 validation was performed by HAC personnel and by SC-1 test team members. During activation, the

UNCLASSIFIED

UNCLASSIFIED

Goldstone STEA-3 configuration was removed from the system test trailer and reinstalled in the CST facility.

A communication system employing telephone equipment and lines was established between STEA-3 at the CST facility and STEA-4 at El Segundo. This communication system provided for the transmission of the spacecraft telemetry bit stream and the command bit stream to the STEA-4 decommutator at El Segundo. In addition, the STEA inter-communication systems were tied together to provide two-way voice transmission between sites.

A JPL furnished power scanner rack was provided to monitor power voltages, but the equipment arrived in a configuration that was not compatible and which could not be calibrated in sufficient time to be used.

Three teletype printers for recording spacecraft data from the JPL computer data system were installed. Transmission of data was made by telephone company data phone link. The printers were not integrated into the system until after spacecraft testing was begun, but were in use in time to record data during performance verification test 2 and all subsequent tests.

4. Combined System Test, SC-1 and AC-10

The spacecraft was transported from El Segundo to San Diego in air ride vans, arriving at the CST facility at approximately 2300 hr February 19. Receiving, inspection, assembly, and integration functions began immediately and were completed at approximately 1200 hr on February 20. Preparations for performance verification test 1 began immediately, and the test was completed at about noon February 22. Several delays were encountered because of STEA-3 decommutator rack [control data handling console (CDC) bay 6] problems. The rack was replaced with a similar item from El Segundo. Also during this period the CDC command generator was replaced with a modified (ECA 112349) unit which had the capability to transmit interlocked normal and magnitude commands.

Checkout of the CDC bay 6 decommutator and command generator delayed the completion of performance verification test 2 until noon February 24. Inert retrorocket engine wrapping operations were conducted February 22 through 24. Some delays were encountered because of a shortage of the corrrect bonding material. Several troubleshooting sequences and special tests 62 and 99 were performed through March 2. On March 2 a simulated launch-countdown exercise was conducted with the spacecraft on the system test stand.

Joint flight acceptance composite test operations in preparation for encapsulation in the nose fairing began at 2200 hr March 3. These operations included the installation of the batteries and squibs. The encapsulation was completed at about 1000 hr on March 4. Mating operations followed encapsulation and were completed at approximately 1630 hr the same day. Provisions for monitoring battery cell voltage and pressure were made by stringing cables through one of the shroud air conditioning ducts.

A separate gyro preheat power supply into the launch complex equipment was incorporated after the arrival of the spacecraft. The power supply furnished as a part of the modification kit had inadequate overvoltage protection provisions. A power supply from the STEA was obtained and used for gyro preheat, but gyro preheat problems persisted.

Following completion of the mating operations, a CST, which was independent of GD/C operations, was performed on March 5. The joint CST was performed March 7. Two short holds were encountered during the 9-hr countdown.

Problems noted during the CST were as follows:

(1) TV target light illumination was not adequate.

(2) Approach TV camera produced an observable signal but would not produce a definable picture.

(3) Flight control sensor group accelerometer indicated a reading when the vehicle was stationary.

(4) The *Centaur* umbilical indicated a separate condition prior to launch. This problem was traced to a bad connector on the *Centaur* side of the field joint.

(5) A bad connector on the *Centaur* side of the field joint caused problems when driving the spacecraft main power switch from the on to the off condition.

(6) The nose fairing thruster bottle squibs did not receive a go signal.

(7) Following decapsulation it was found that 11 of the 12 retrorocket engine separation squib simulators were burned out. This problem is still under investigation but appears to be caused by procedure error.

UNCLASSIFIED

UNCLASSIFIED
CONFIDENTIAL

Approximately 10 hr of troubleshooting followed the combined acceptance test.

5. CST Facility Operations

At the completion of SC-1 testing the STEA-3 power and prelaunch monitor racks were shipped to El Segundo and subsequently to Goldstone to support T-21 operations. The PATE rack has been returned to El Segundo in support of SC-2 operations. These equipment racks, or suitable replacements, must be returned to the CST facility to support SC-2 combined systems testing at least 30 days prior to the scheduled arrival of SC-2. CDC bay 10, CDC video processor, TV monitor, and the command generator have been returned to El Segundo for upgrading.

The use of STEA-3 equipment on other programs poses problems in furnishing a STEA that is qualified and properly configured to support SC-2 testing. A compromise could result in a schedule delay of the combined acceptance test. The *Atlas* booster was air-shipped March 14, and the *Centaur* booster, payload adapters, insulation panels, and interstage adapters were air-shipped March 16. SC-1 and *Atlas/Centaur* 10 operations have been completed. Preparations for SC-2/AC-7 operations are now under way.

Packaging operations for spacecraft data files and miscellaneous items were completed March 10. The STEA-3 power and prelaunch monitor racks have been returned to El Segundo in preparation for support of T-21 operations at Goldstone DSIF. The STEA-3 PATE rack has been returned to El Segundo to support SC-2 operations.

The CST facility/El Segundo data link performed efficiently in every respect during performance of the J-FACT procedure. Earlier intercom problems were solved through improved impedance matching of STEA-1 with the remainder of the network.

The prejoint flight acceptance composite test procedure has been submitted to JPL for approval. The Brunson optical instruments were calibrated by the Pan American calibration laboratory and returned to the explosive safe facility optical dock. Preliminary checkout and alignment was started.

a. Diesel generator assurance test. The diesel generator assurance test was performed February 16, and satisfactory operation was obtained under varying conditions.

b. Mechanical-propulsion. The vernier propulsion system weighting scales (Fairbanks-Morse) were moved from the south bay of the flight assembly building to the propellant laboratory building, and assembled and calibrated. The scales were calibrated to support the S-6 operation and will be recalibrated for SC-1. The Fairbanks-Morse scales in the high bay of building A0 were leveled and calibrated in preparation for SC-1.

c. AMR RF panel. The RF panel, 226483-11, the microwave power meter, and cable could not be calibrated at AFETR and were returned to El Segundo. The items were calibrated by HAC calibration laboratory, Culver City, and returned to AFETR March 9.

d. S-6. In accordance with the provisions of action directive 244 from JPL, S-6 was sent to AFETR for a series of simulated prelaunch operations.

G. Space Flight Operations

1. Television Science Analysis and Command Surveyor Mission Operations[2]

The science activities related to the actual mission conduct for the first *Surveyor* flights involve primarily the survey television system. The science portion of *Surveyor*, as represented on the early engineering flights, involves real-time analysis of received TV pictures. This analysis is directed toward optimization of the imagery by adjustment of the camera parameters by ground command.

The operational organization which makes pertinent recommendations relative to the science aspects of the mission is the Television Science Analysis and Command group (TSAC). This group functions as a representative of the *Surveyor* Project Scientist in the operational organization. Prior to actual missions, extensive preparations involving training activities and documentation of operational procedures and techniques, are required. During the training and actual flight mission, the TSAC group is under the direction of the space Science Analysis and Command group and functions as its advisor on the scientific use of the camera. The postmission analysis and reporting activities of TSAC are primarily under the control of the *Surveyor* Project Scientist, and involve assisting in the preparation of the mission science report.

[2]Prepared by Technical Section 323.

CONFIDENTIAL
UNCLASSIFIED

UNCLASSIFIED

The mission responsibilities of TSAC involve preparation of standard and nonstandard operational sequences, as well as assimilation and analysis of image data collected during the mission. Utilization of prelaunch calibration data and lunar lighting prediction information allows realistic adjustment of camera parameters for optimum operations on the lunar surface.

Development of a quick look real-time analysis capability for TSAC is based upon prompt availability of positive photographic prints of the TV imagery. This capability is provided by two systems which are under the direct operational control of TSAC for the first *Surveyor* missions.

The principal system is a 35-mm kinescope recording camera which records directly from a slow scan TV monitor. After a lunar picture taking sequence is completed, the film is removed from the camera and passed through a rapid film processor and immediately printed. The prints are then processed, dried and passed to a team for assembly into mosaics and subsequent analysis. The time required, beginning with the removal of the film from the camera to the time the first prints are available for mosaic analysis, is approximately 12 min.

The other quick-time image-recording capability is provided by cameras which view other slow scan monitors and image directly on photosensitized paper. The polarity of these monitors is reversed so that the negative image is recorded as a positive on the paper. This material is then passed through a rapid processing system directly associated with the recording cameras and is immediately available for analysis. The time required from image recording to mosaic availability is approximately 15 sec. This imagery provides quick time, hard photo copy for immediate analysis prior to delivery of the higher quality prints from the 35-mm kine recorder.

Upon completion of the mosaic, scientific analyses and recommendations for subsequent operations on the lunar surface are provided to the mission directors. After the standard operational sequences, or objectives, are satisfactorily completed, then the selection of additional activities can be made from established sequences for several optional television activities.

Through this basic operational plan, the science aspects of the first *Surveyor* missions will be implemented. Additional and more detailed scientific analysis of the imagery will be performed under the direction of the Project Scientist during the postmission analysis period.

H. Aerospace Ground Equipment

1. Operational Ground Equipment

a. Closed-loop test equipment. Data recording and processing techniques used with the closed-loop test equipment do not yield data with sufficient accuracy and resolution to adequately assess spacecraft performance. To correct this problem the JPL computer data system was used to digitize and record the data. The present purely analog method of data recording will be maintained for backup purposes and for performing tests, such as gain and phase margin, which are not readily adaptable to digital techniques. The closed-loop computer data system tie-in will be implemented in two phases. Phase 1 was recently implemented for SC-2 thermal vacuum testing. It provides for the digitizing of all closed-loop parameters without making any modifications to the system test equipment assembly (STEA) and increases the accuracy of the recorded data by a factor of approximately 10. The resolution of several key parameters is still insufficient, however, for detailed spacecraft performance assessment. Phase 2 provides modifications to STEA, mainly scale factor changes, which will enable the computer data system to record the data with sufficient resolution and accuracy to adequately assess spacecraft performance. This phase is planned for October 1966.

Proposals for improving the operability and maintainability of the closed-loop rack were submitted to JPL. These improvements include repackaging the rack-mounted gear in a two-bay rack and adding a digital voltmeter, function generator, frequency counter, and module checker. The problems associated with performing a large-angle approach closed-loop simulation were discussed. The most feasible and least costly method for this simulation would be to use the large computer in the basement of building 366, with signal transmission obtained over leased data phone lines.

b. Primary Sun simulator. Excessive lamp failures encountered in the primary Sun simulation during SC-2 testing were traced to two causes: (1) test procedure changes required the simulator to be operated for a period far in excess of its original design requirements; and (2) a new protective glass cover over the primary Sun sensor (part of the flight control sensor group) reflected excessive heat and light back into the simulator, causing it to operate at increased temperatures. Use of different lamps and the application of a magnesium fluoride coating to the glass cover are being investigated as possible solutions. As a permanent solution, a

UNCLASSIFIED

UNCLASSIFIED

completely redesigned Sun simulator with error angle simulation capability has been proposed.

c. Nitrogen gas jet remote monitoring. Engineering procedures for changing the method of remote monitoring on the nitrogen gas jets were released. The new method uses the electrical signals to the jets for operating the remote lamps and on-off cycle counters and relies on audio perception and/or sense of feel to determine actual jet operation. This procedure will prevent recurrence of electro-pneumatic device problems experienced during SC-1 solar thermal vacuum (STV) testing with no compromise in the level of testing.

d. Radar altimeter and doppler velocity sensor (RADVS). Engineering for the RADVS delay line equipment will permit expansion of the radar altimeter tests to include ranging at a known distance. In the past, this level of testing could not be achieved. RADVS waveguide leakage test equipment was provided. It permits a quick, conclusive check for RF leaks or loose particles in the RADVS waveguide.

e. Intercabling. Work was begun on the modifications and new design of the intercabling between STEA and the flight control sensor group in preparation for SC-3. This will be the first time that a dash -5 flight control sensor group configuration is mated with STEA; considerable differences from previous spacecraft exist in the intercabling requirements.

f. Launch complex safety console. The launch complex safety console and control rack have been modified to provide a capability for supplying gyro preheat voltage to the spacecraft. In addition, modifications were made to the launch console to monitor various voltages and currents applied to the spacecraft.

g. Power monitoring. Design work to isolate the STEA power monitoring circuits from the spacecraft to prevent damage in the event of inadvertent short circuits has been completed. The STV equipment has been modified to include these changes.

h. JPL computer data system. The computer data system intercom system has been modified to accept a four-wire telephone circuit from AFETR, with remote operation to STEA 1 and STEA 5. The purpose of this modification is to provide computer emergency backup to AFETR.

i. Mission Sequence Electromagnetic Interference (MS/EMI) screen room. The new screen room equipment in building 350 has been installed, checked out, and used for MS/EMI testing of SC-2.

j. STV test equipment. Preparations for SC-2 STV testing included numerous modifications to improve testing and to protect the spacecraft and test equipment.

Items affecting the functional performance are as follows:

(1) Modification of JPL-provided separation, sensing, and arming actuation device for use with SC-2. Design of a new unit for SC-3 having a reset capability and approximating the actual separation speed has also begun.

(2) Addition of two squib mufflers for retrorocket engine ignite squibs to allow firing of actual squibs and monitoring of the firing.

(3) GN_2 purge of Canopus view port to prevent fogging.

(4) Flow indicators for attitude jets. These are also used for phasing checks.

(5) TV 3 view port reflections. Reflections that mask the TV 3 target have been reduced by adding an antireflective coating to the view port and the target glass. A shield to help block the light incident on the view port also has been added inside the chamber.

(6) Test adapters. The auxiliary battery test tee has been redesigned for phases A/B, and shielding has been added to the klystron power supply modulator test tee.

(7) The number of circuits in the plugs-out relay box was increased requiring a physical and thermal redesign.

Items designed to protect the aerospace ground equipment (AGE) and/or the spacecraft from damage are as follows:

(1) Covers to protect the AGE flexible waveguide that connects to the RADVS feedhorn adapters.

(2) Supports for the LN_2 flex lines to prevent excessive flexing and resultant failures.

UNCLASSIFIED

UNCLASSIFIED

(3) Covers to protect the AGE end-bell cables when on the test floor.

(4) A stiffened flight control blower mount to prevent the blower from touching the spacecraft.

k. Optical design.

(1) TV 4 Image Shift—An investigation is in progress to determine the reason for an image shift that was noticed when photographs taken by TV camera 4 were checked before and after Z-axis vibration. Lack of proper equipment is delaying some of the necessary operations. However, a critical check was made of the alignment tool and its lens; some design changes have been proposed as a result.

(2) Canopus Simulator Positioning—An extensive study was made of the Canopus simulator positioning mechanism's accuracy. Spatial relationships existing during STV test were duplicated, and a quartz window was introduced between the simulator and test sensor. The backlash of the two units checked was well within limits. The inherent accuracy and repeatability were found to be acceptable, but a design change of the arc plate engraving and the vernier was suggested to allow a readout to 0.01 deg.

(3) Tele-Microscope for Dust Particle Count—A breadboard model of a tele-microscope for dust particle identification and count has been built and will be used for a remote cleanliness check of the spacecraft at AFETR. The design of this equipment is complete except for a suitable mount. The feasibility of the tele-microscope depends largely on the mount since even the slightest vibration would nullify all readings. The mount used in the Zeiss Technoscope is being investigated.

(4) Primary Sun Simulator Lamps—Recent problems with Sun simulator lamp failures, which occur under continuous use, have led to design studies centered on the lamps themselves. Several tests are in progress to determine whether a change of illuminants will correct the problem. If not, a simulator effort to lower the operating temperature of the lamps will be required.

2. Ground Support Equipment (GSE)

a. GSE for GD/C combined systems test (CST) and AFETR. An intensive program of GSE preparation (including selloff to HAC and JPL engineering and quality control) was completed in time to support SC-1 test and checkout at CST, San Diego, and at AFETR. The vast majority of items processed were spacecraft and spacecraft component handling equipment. Approximately 47 GSE line items were delivered to launch operations for shipment to combined systems test to fill out the list of equipment requirements. Immediately upon completion of that exercise a similar effort resulted in 55 line items for shipment to AFETR. These, coupled with the 45 major line items of GSE already at AFETR, completed that portion of AGE designated for the launch preparation activity.

b. Spacecraft auxiliaries. GSE spacecraft auxiliaries provided with each spacecraft were processed for shipment with SC-1. This group included the ground transport vehicle (GTV-1), which is actually the shipping and storage container as well as an occasional test platform, various spacecraft components' protective covers, and approximately 100 spacecraft components and spares shipping and storage containers. Because so much of this equipment had been in use during El Segundo test and checkout of various spacecraft, it was necessary to upgrade and repair many of the items so that they would represent the latest approved configuration and would afford the proper protection to SC-1 and associated equipment. The heavy use of all existing GSE indicated the need for additional quantities of certain items. This need resulted in submittal and approval of 97 line items in the Mod 56 negotiations. Procurement of this additional GSE will begin immediately.

c. RADVS test equipment. Conditional acceptance by JPL of a proposed RADVS test at AFETR has resulted in a need for a new spacecraft rollover and handling fixture and a new trailer larger than the present GTV-2 used to transport the encapsulated spacecraft. The test calls for the fully assembled spacecraft to be inverted, placed on a test stand, mounted on an enclosed trailer, and transported to the test site. The go-ahead for the rollover fixture design was received, and work is proceeding with a target date of May 15 for completion of engineering.

3. Support

a. Aerospace Ground Equipment (AGE) set 2 at AFETR. Department support of AGE set 2 at AFETR is continuing. Final upgrade of the equipment and resolution of critical TFRs are being accomplished as required for checkout and launch of SC-1. In addition to a crew of permanently assigned personnel at AFETR,

UNCLASSIFIED

UNCLASSIFIED

several specialists have been temporarily assigned there to support this critical period.

b. AGE set 3 at CST. AGE set 3 equipment was moved from El Segundo to CST, San Diego, for use with combined systems testing of *Atlas-Centaur/Surveyor*. STEA 3 was reactivated prior to February 18 and was used to test SC-1 between February 18 and March 13. Several minor problems were resolved by temporarily allocating additional AGE personnel to CST and by maintaining a heavy, inordinate supply of standby STEA components. Most of these components were temporarily transferred from other AGE sets in El Segundo.

c. Spares support plan. A concerted effort is being completed to revise and update the AGE spare parts program. Complete lists of all AGE spare parts have been prepared showing items approved by the customer, and their availability, location, and quantities.

4. Reliability Analysis and Engineering Evaluation

AGE reliability has reduced the backlog of open noncritical TFRs by closing out 115 TFRs in the past 2 wk. Critical TFRs are monitored daily and closed out immediately on completion of all corrective action. A new criticality classification system for AGE TFRs was proposed at the HAC/JPL TFR review board meeting March 22. This new system would assign a class code to every open TFR, indicating the criticality of the TFR with respect to each spacecraft, thus simplifying preparations for "Consent" meetings.

5. T-21 Goldstone Tests

All necessary equipment to support the T-21 test at Goldstone was delivered on schedule. Included in this equipment were two major subassemblies from STEA 3 in San Diego. All equipment was redocumented on shippers and all *Surveyor* quality assurance directives brought up to date. Scheduled use for this equipment is 6 wk at which time it will be returned to the proper installation.

6. Surveyor System General Specification

The AGE department input to the *Surveyor* system general specification was completed in first draft form and submitted to the project coordinator. These specifications were prepared for the A-24 spacecraft series in the AFSCM 375-1 format.

I. Flight Control

1. Introduction

The flight control subsystem is comprised of units that provide velocity and attitude control during the transit and landing phase of the *Surveyor* mission. These units include optical sensors, inertial instruments, attitude controls, flight control electronics, and lunar radar.

2. Systems Design

The S-6C closed-loop live firing test report has been published as SSD 5603R. New analytical engine models developed from these tests have been used to explore stability and control limits of the flight control/radar altimeter and doppler velocity sensor (RADVS)/propulsion system via the 6-deg of freedom analog simulator. These studies indicate that the low-thrust dynamics, with helium-saturated propellants, are such that unstable initiation of vernier phase control can occur when velocities are high along all axes and system gain tolerances adversely pyramid; however, the probability of such an occurrence is low. Factors promoting stable acquisition are ability of the thrust chamber assemblies to develop well below 30 lb at the minimum thrust stop (27 to 28 lb is typical) and greater than nominal loop gain near minimum thrust. Analysis of the SC-1 flight control/RADVS/propulsion system indicates that an unstable vernier phase acquisition is unlikely. For later vehicles, a reduction in flight control system lateral velocity loop gain will be implemented ensuring a stable vernier phase acquisition under any specified condition with any engine dynamics demonstrated to date.

3. T-2N Tests

a. Descent test. The Range-V_z trajectories for all tests have been excellent.

Telemetry data for T-2N-2 descent test 2 showed an unexpectedly large amount of roll vehicle motion. Analysis of these data indicates that large external disturbances are the most probable cause of the roll motion. Extensive reevaluation of the T-2N roll loop was accomplished, and a gain change was implemented. The previous T-2N roll loop gain was set as low as possible within the capabilities of the previous T-2N electronics, but the resulting gain was higher than desired for controlling roll motion. With the incorporation of new electronic changes, the T-2N loop gain was reduced to almost the desired value. It is not practical to reduce the gain further because the

UNCLASSIFIED

UNCLASSIFIED

gyro stops would be reached before the roll actuator mechanical stops. The new reduced gain and the old high gain were used in a closed-loop demonstration employing actual T-2N hardware. With the old gain, a 1-sec external disturbance induced a self-sustained limit cycle operation. This operation was known to exist but was not anticipated to be induced because the aerodynamic disturbances were expected to be smaller. With the new lower gain, the limit cycle operation could not be induced by applying the largest expected external disturbance, thus demonstrating considerable improvement in loop stability. The only remaining uncertainty is the magnitude of the expected external disturbance on future missions.

b. Soft-landing design review. At the completion of analog computer studies to determine the effects of vehicle component errors upon a successful soft landing, a design review was conducted. Fig. 16 was presented as a typical soft-landing mission profile. The primary difference in this profile and previous descent profiles is in areas 3 and 9. These areas of 1-g acceleration command are used to allow essentially constant velocity descent during segment acquisition and after radar turn-off at point 8. The results of analog computer studies using the block diagram and error sources shown in Fig. 17 were discussed at the design review. A brief summary of the results indicate that a nominal mission, starting at h = 900 ft, M_0 = 45.56 lb (dry weight of vehicle = 189.5 lb), will yield the following:

Maximum total critical high thrust (T_T)	221.85 lb
Altitude of intercept at 5 ft/sec	31.2 ft
Propellant used at end of mission	35.03 lb
Unused propellant at end of mission	10.53 lb
Total mission time	37.2 sec
Time of 3-sec enable delay (before touchdown)	5.10 sec

The 3-sec enable delay is the time between the axial velocity (V_z) of 10 ft/sec and radar 14-ft mark.

Also in the analog simulation study, the operational uncertainties such as launch altitude of ±50 ft, release weight of ±2 lb, and drag of ±4% and system mechanization, radar, and flight condition errors were considered. Fig. 17 shows the various sources of errors of the trajectory control loop. When all errors were considered individually at their 3-σ specification limits, the following variations occurred:

Total critical high thrust	219.15 to 224.70 lb
Altitude of intercept at 5 ft/sec	16 to 42.4 ft
Propellant used at end of mission	30.4 to 41.25 lb
Unused propellant at end of mission	4.31 to 15.16 lb
Total mission time	32.8 to 43.5 sec
Time of 3-sec enable delay (before touchdown)	3.0 to 8.6 sec

Considering these same errors in a root-summed square manner on a 3-σ basis the following results are achieved:

Total critical high thrust	221.85 ±4.43 lb
Altitude of intercept at 5 ft/sec	31.2 ±15.02 ft
Propellant used at end of mission	35.03 ±6.06 lb
Unused propellant at end of mission	10.53 ±6.06 lb

These results indicate that sufficient margin exists for a successful soft landing.

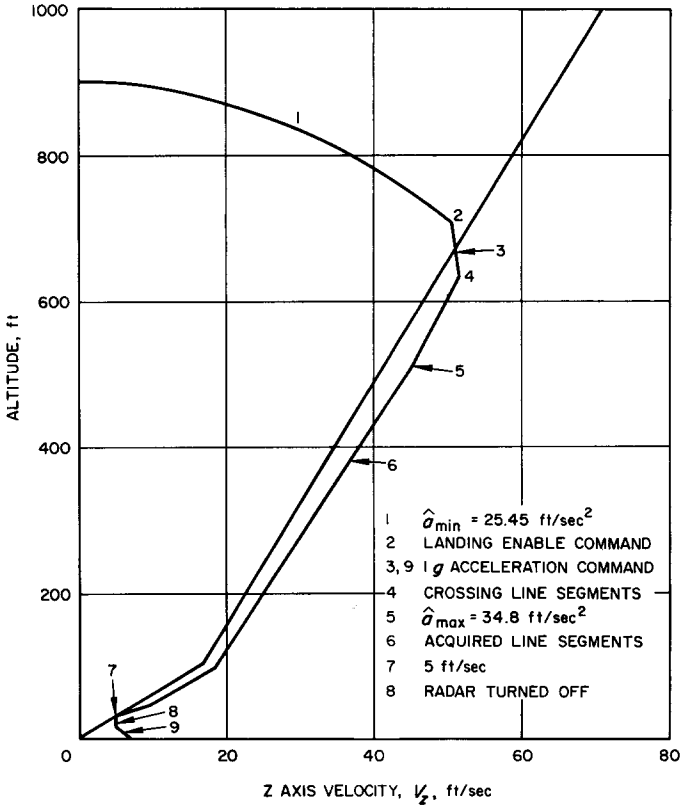

Fig. 16. Typical T-2N soft landing mission profile

4. Flight Control Electronics Unit

Tests on proposed changes to the thrust phase power on and off command circuits have been completed. These tests determined the sensitivity of critical command lines when subjected to specified noise pulses. As a result of

UNCLASSIFIED

UNCLASSIFIED CONFIDENTIAL

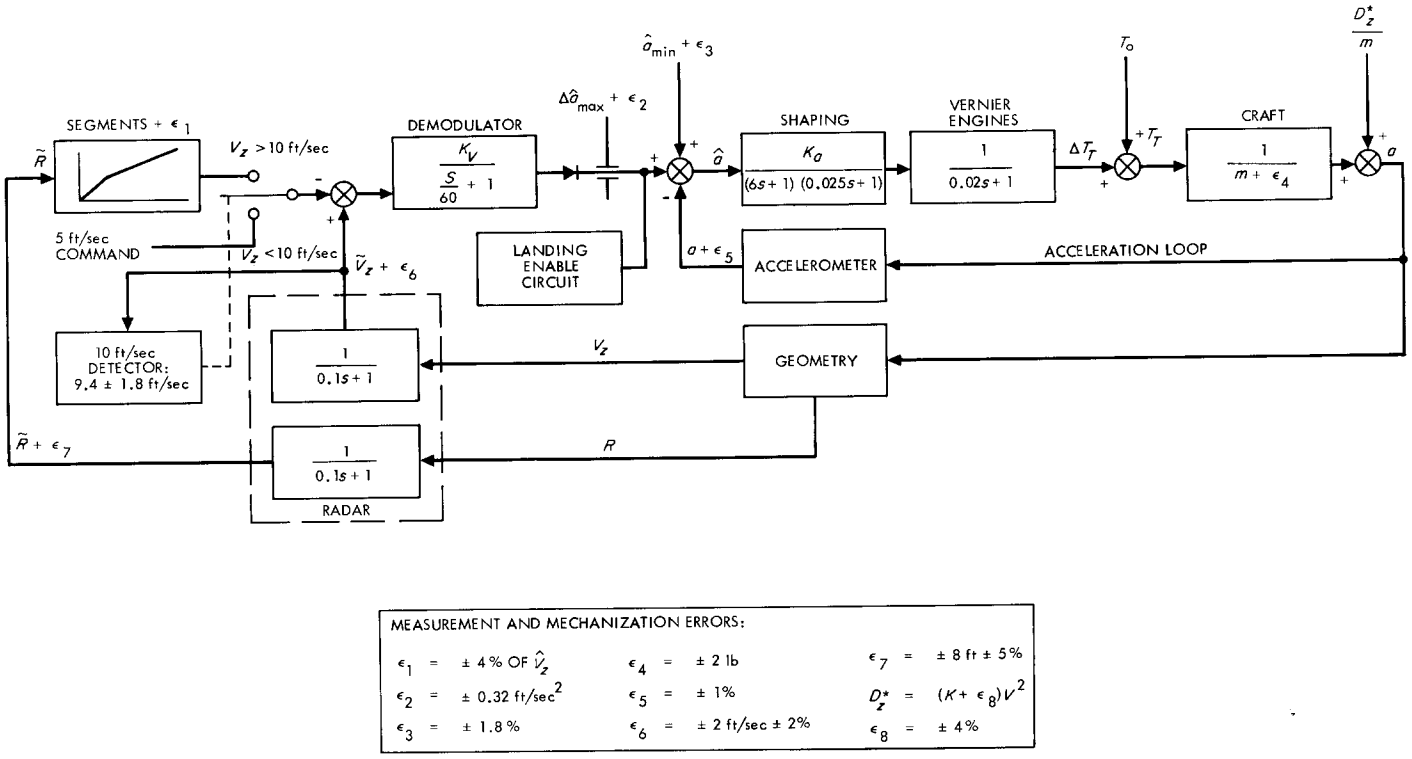

MEASUREMENT AND MECHANIZATION ERRORS:

ϵ_1 = ± 4% OF $\hat{V}_z$	ϵ_4 = ± 2 lb	ϵ_7 = ± 8 ft ± 5%
ϵ_2 = ± 0.32 ft/sec^2	ϵ_5 = ± 1%	D_z^* = $(K+\epsilon_8)V^2$
ϵ_3 = ± 1.8%	ϵ_6 = ± 2 ft/sec ± 2%	ϵ_8 = ± 4%

Fig. 17. Block diagram of T-2N trajectory control loop

these tests, a modification consisting of adding a passive R-C filter to the input of each command line was recommended.

Design and drafting of significant changes for SC-5 are complete. All drawings are released, and hardware fabrication has been started. Checkout of the SC-5 chassis is partially complete, and the remaining checkout will be completed before unit delivery. The significant changes are as follows:

(1) *Squib Firing Circuit Changes* — These changes, which affect chassis 1A6, redesign the squib firing circuitry and make the squib command pulse generating circuitry for retrorocket engine ignition and separation independent of each other.

(2) *Unit Housing Change* — The screw mounting hole pattern of the unit housing is altered as a result of a change in the design of the programmer chassis, which employs threaded inserts mounted in the center of the chassis sandwich.

(3) *Roll Shaping Amplifier Redesign* — This change causes a partial redesign of chassis 1A5. The electrical changes consist of modifications in the roll shaping amplifier to accommodate the ±12-deg roll actuator.

5. Inertial Sensors

a. Gyros. Inertial reference unit (IRU) test bed P-3 underwent 420 hr of special testing including flight control sensor group flight approval test, thermal vacuum exposure and a one-and-a-half mission solar thermal vacuum (STV) exposure as part of the S-10 test vehicle. The three gyros in the inertial reference unit are of particular interest when considering the decreasing gyro transfer function. Gyros 54 and 58 previously exhibited permanent decreases in transfer function after usage in IRUs, but the decrease subsequently ceased. Gyro 38 had a relatively stable transfer function. All three gyros survived testing with little or no change in transfer function. Investigations of the physical chemistry of the damping fluid and possible changes in signal generator behavior are continuing.

b. Accelerometer. As a result of the deformed diaphragm observed after type approval test, a complete evaluation of the relationship between fill procedure, completeness of fill, and deflection versus temperature of the fluid expansion compensating diaphragm has been accomplished. Based on this evaluation, the instrument vendor has agreed to a modified fill procedure and verification measurements of diaphragm deflection versus

UNCLASSIFIED CONFIDENTIAL

UNCLASSIFIED

temperature, which will greatly enhance confidence in a bubble-free fill.

As shown in Fig. 18, diaphragm deflection is related to temperature and the presence of a bubble. Since the slope decreases as bubble size increases for a given fill procedure, the slope can be used as the criteria for determining the presence or absence of a bubble.

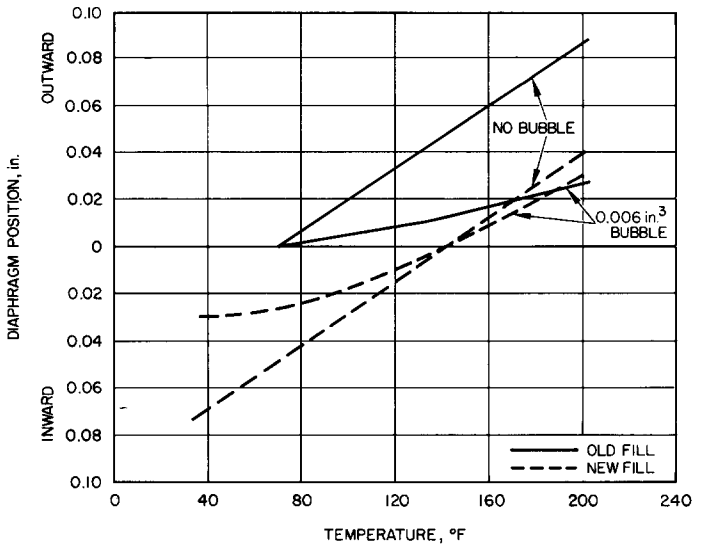

Fig. 18. Diaphragm position versus temperature for IRU accelerometer

A fill procedure, initiated in mid-March 1966, provides for degassing of the fluid cavity, film degassing of the fluid, and a slow fill at 120°F. The sealed inner case is temperature cycled three times prior to assembly into the outer case. During this time, diaphragm position is measured. These degassing provisions will further reduce the possibility of a bubble, and the 120°F fill will result in a positive fluid pressure at room temperature without causing excessive diaphragm deflection at higher temperatures. The temperature versus deflection measurements will aid in determining the presence of a bubble.

c. Inertial Reference Unit (IRU). Considerable effort was directed to defining the gyro operating temperature restrictions since it was not generally understood that the IRU may not come up to operating temperature in the prelaunch environment. Concern with this possibility was expressed in the recent SC-1 consent-to-ship meetings.

During SC-1 combined systems test, the telemetry temperature sensors on the IRU structure reached 163 to 169°F, whereas 169 to 174°F would correspond to the normal gyro operating temperature of 180°F, the temperature at which the gyro heaters cycle on-off. Another desirable but not mandatory temperature point to reach before exciting the gyro spin motors is 150°F, as indicated by the sensors. During combined systems test, approximately 155°F was reached with 85°F shroud air. During system readiness test, shroud air was only 70°F, and the temperature reached was approximately 145 to 150°F. These temperatures were reached with the operate heaters excited from 25 to 26 v. During operation of the spacecraft battery, the output of which was 22 v, temperatures dropped 8 to 13°.

The desire to have the gyros above 150°F at spin motor excitation results from safe practice standards rather than from test data. Cold start testing has not resulted in any immediate failures; however, it is not possible to accurately assess its contribution to later degradation in performance. Areas of concern with cold starts are the spin motor bearings running in a different track and the fine wire flex leads being pulled through high viscosity fluid as a result of precession which would occur with the motors running.

Although it would be desirable to have gyro heater control at normal operating temperature during prelaunch testing and at liftoff, it is not mandatory. The heater circuits have operated reliably in the past and, with a satisfactory check just prior to encapsulation, there will be confidence in proper flight operation. Precise temperature control of the gyros is not required until the attitude maneuvers prior to midcourse. Stabilized operating temperature is predicted within an hour after Sun acquisition.

Remote voltage sensing will be provided at the vehicle during prelaunch operations in order to maintain the heater voltage near 26 v until the voltage is switched to the batteries. Also, attempts are being made to have one or both cooling air ducts which exit toward the IRU redirected or blocked off. These measures probably would provide the margin necessary to ensure the two desired temperature conditions during IRU operation in the prelaunch environment.

6. Canopus Sensor

Recent testing of the new Canopus sensor shield showed that at extreme acquisition launch window settings, i.e., 105 and 75°, moonlight interference can cause loss of Canopus lock owing to reflection from the edge of the forward-most shield baffles. This condition has

UNCLASSIFIED

UNCLASSIFIED

been corrected by increasing the sensor shield field-of-view by increasing the depth (acquisition direction) of the shield to remove the interfering baffles. The reworked shield has been tested and eliminates the interference.

Sun and star data recently obtained using the production Sun/star simulator revealed that Canopus sensors were improperly set because of a simulator calibration error. This error, which was further verified through actual Sun and star checks, resulted in the Canopus appearing too bright to the sensor when viewed in outer space. The brightness would cause Canopus to fall outside gate brightness levels and would not be recognized in the automatic mode. Since the Canopus sensor operates on a Sun/star relative brightness principle, correction of this error can be accomplished by increasing the light transmissibility of the Sun filter which, in turn, effects a change in the automatic gain control so that the star intensity (voltage) can be properly centered within the Canopus brightness gate levels. New Sun filters have been made and tested. A new shield and Sun filter are now on SC-1, and the Sun/star simulators have been recalibrated to correct brightness levels.

7. Gas Jet System

a. Gas supply. Tests to optimize charging valve torque requirements and to determine valve leakage have been made on engineering tank 0013. Tests run at 5000 psig (4600 psig is the normal charge pressure) indicated that the previously established torque of 55 to 60 in.-lb is ample for satisfactory valve closing. Examination of the valve stem packing O-ring after these tests showed very little crazing. The needle valve point seating area and mating valve seat area were not damaged. Leakage varied from 0.4 to 0.7 $in.^3$/hr standard temperature and pressure (STP) which was more than expected, but acceptable. Another tank will be tested to gain additional confidence in the valve. A change in the gas supply flight acceptance test (FAT) specification of the measurement of charging valve leakage at 50 to 60 in.-lb torque is being implemented.

b. Attitude jets. Tests of two jet valve armatures incorporating a hard chrome-plate (Microplate process) were satisfactorily completed. The armatures were initially tested for 100,000 cycles with periodic disassembly for inspection of wear. After installation of new spacers, another 100,000 cycle test was completed without intervening disassembly and inspection. During the initial 100,000 cycles and after the second 100,000 cycles, wear on the armature was negligible, and tube wear was much less than with the previous copper-nickel-chrome plating process. Spacer deformation and scoring was greater than with the previous plating, but was considered to be within satisfactory limits. After the second 100,000 cycles, the valves were reassembled and cycled 1 million times, then disassembled and inspected. Increase in armature and tube wear was slight. However, the armature spacers were expanded and cupped, and small pieces were detached. Response time at room temperature was normal. Side L_2 maximum leakage was 14.4 cm^3/hr after 75,000 cycles, but decreased to 6.6 cm^3/hr after completing 1 million cycles. Side L_1 leakage never exceeded 1.7 cm^3/hr. Maximum permissible leakage before launch is 18 cm^3/hr.

c. System installation and testing. The landing leg flexible line flexure tests on SC-1 and SC-2 type lines were satsifactorily completed. A total of 5500 flexure cycles were accomplished under maximum possible operating pressure, each cycle equivalent to an extension and retraction of the landing leg. Gas contamination measurements indicated a decrease in particulate matter as the number of cycles increased. However, total particulate matter count indicated that the flexing generated additional particles. There was no leakage or indication of failure. Flexure tests will be repeated on SC-3 type lines when parts become available.

Four combinations of B nut-tube flare fittings were torqued to maximum torque 15 times, each time with new conical seals installed. There was no leakage or failure.

Gas system installation and test procedure 230058 is being changed, effective with SC-3, to include tank pressure measurements, tank temperature, pressure relief valve leakage, pressure regulator lockup pressure, and jet valve leakage. Also, a total system leak test, with gas tank charged with 2500 psig helium, using the bag-leak method will be incorporated.

8. Roll Actuator

The model B ($\pm$12-deg range) roll actuator detail design has been completed, and the engineering drawing released. A preliminary drawing release was made earlier to solicit comments regarding the production of the detail parts, the structural integrity of the design, the compatibility of the thermal finishes to the allowable temperature extremes, and the adequacy of the part dimensions from an assembly and installation standpoint. The comments received have been reviewed, and appropriate changes

UNCLASSIFIED

UNCLASSIFIED

were incorporated before the formal drawing was released. An advance bill of materials has been forwarded to the manufacturing area to assist in the procurement of hardware and the fabrication of test and flight units.

The test program will consist of an engineering type approval test (TAT) as per the same specification used for the SC-1 type roll actuator and will include vibration, acceleration and, thermal-vacuum exposures. After extensive interference study, a suitable location was determined for the pin puller on the top of the roll actuator housing.

9. New Technology (Closed-Loop Testing)

The closed-loop tests with the SC-6 test vehicle have demonstrated a new technology, namely, the closed-loop testing of system dynamics where primary system components are separated by distances on the order of tens of miles. The technique of utilizing telephone data links was originally considered as the most practical and economic means of integrating a large and complex analog simulation of *Surveyor* vehicle and flight control dynamics with a live *Surveyor* propulsion test vehicle; it was not feasible to move either facility to the site of the other.

The SC-6 live firing flight control system is shown in Fig. 19. While initial tests showed that lag introduced by the data sets and a short (5 mi) checkout link was negligible in terms of effect on system dynamics, calibration of the longer (35 mi) actual links used in the tests indicated the existence of sufficient lag to produce an appreciable degradation of closed-loop system damping. Compensation was, therefore, designed and introduced which cancelled effects of the lag in the significant control frequency band without introducing significant adverse effects in the time domain. Comparative test runs without tie lines, and with compensated tie lines, showed practically identical results. The design of compensation for a given system tested by this technique becomes more critical as the tie-line length increases; a practical limit to the separation distance of the major components will exist, depending upon inherent system dynamics.

The economic advantages of the telephone tie-line technique in a test of this nature are substantial, though perhaps not readily computed as a specific cost savings. Cost of installation and usage charges for the lines involved in this test setup were approximately 2000 dollars; the cost of leasing and setting up analog equipment of comparable capability on-site would have run one to

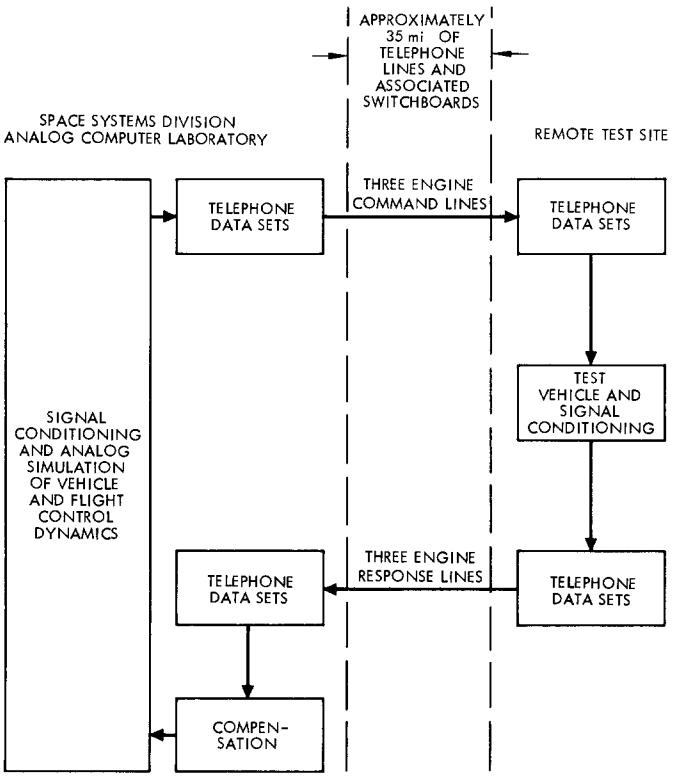
APPROXIMATELY 35 mi OF TELEPHONE LINES AND ASSOCIATED SWITCHBOARDS
SPACE SYSTEMS DIVISION ANALOG COMPUTER LABORATORY
REMOTE TEST SITE
TELEPHONE DATA SETS
THREE ENGINE COMMAND LINES
TELEPHONE DATA SETS
TEST VEHICLE AND SIGNAL CONDITIONING
SIGNAL CONDITIONING AND ANALOG SIMULATION OF VEHICLE AND FLIGHT CONTROL DYNAMICS
THREE ENGINE RESPONSE LINES
TELEPHONE DATA SETS
TELEPHONE DATA SETS
COMPEN-SATION

Fig. 19. SC-6 live firing flight control system

two orders of magnitude higher. Thus, this new technology resulted in a maximum of usable data at minimum cost.

10. Surveyor Inertial Instruments[3]

A portion of the in-house support given by JPL to the *Surveyor* program consists of detailed evaluation of selected systems and components from the *Surveyor* spacecraft. The most recently completed test program was performed on the guidance gyroscope. This gyro is used in the inertial reference unit (IRU), which is part of the flight control sensor group.

The gyro used in the *Surveyor* IRU is the Kearfott model C702514008. It can be basically described as a single axis, floated rate integrating type, utilizing a pivot and jewel suspension and a ball bearing spin motor. This spin motor operates from 26-v, 3-Φ, 400-cps power and turns at 24,000 rpm providing an angular momentum of 100,000 gm-cm²/sec. It also incorporates an integral spin motor running detector which produces a 1600 pps signal when the motor is at synchronous speed.

[3] Prepared by Technical Section 344.

CONFIDENTIAL
UNCLASSIFIED

UNCLASSIFIED

The gimbal position pickoff is a microsyn type operating at 400 cps while the torquer is a moving coil and permanent magnet type with the unusually high sensitivity of 800 deg/hr/ma.

The gyro is a wide angle design providing a minimum input storage angle of ±10 deg. This large storage angle capability necessitates the use of a very viscous high density flotation fluid which in turn must be accurately temperature controlled at 180°F.

Serial No. 40 gyro was chosen for evaluation, a rebuilt type approval test (TAT) unit considered unusable for flight due to an out of specification condition on one parameter, g insensitive drift, also known as reaction torque (RT).

A series of long term performance tests were made on this gyro under normal laboratory environments. No rigorous environmental tests such as vibration, shock or thermal vacuum were performed during this evaluation.

Initial examination and measurement of basic conditions such as resistances and case dimensions did not disclose any discrepancies. Precision testing of the four main gyro parameters which affect system performance was then started. These tests are performed on an optical dividing head, tumble table or precision servo table as determined by the nature of the test. The important parameters obtained from these tests are: torquer scale factor; g-insensitive drift (RT); g-sensitive drift component along the spin axis (MUS); and g-sensitive drift component along the input axis (MUI).

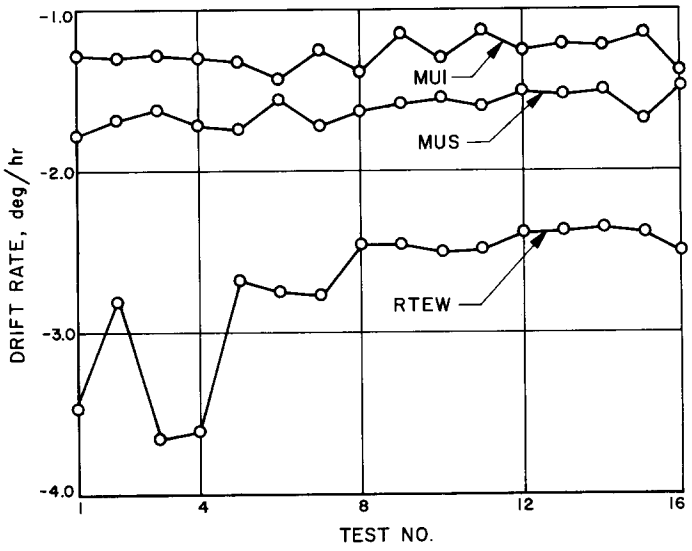

Fig. 20. Heading test data summary

The eight position heading test phase covered a period of approximately two weeks with 8 days of actual data taking. Each day's data were taken in a series of 3 runs of eight positions after a 1-hr warm up period. The gyro was then allowed to cool to room temperature for 1½ hr and then reheated and three more runs taken. In this manner a total of 48 determinations of the gyro's performance was obtained. These data are shown in Fig. 20. Each data point is the average of 3 runs, representing ½-day of testing.

Polar axis tumble testing yields the same type of data but from a different method of testing. This and the servo test-cogging data are both dynamic gyro tests, as opposed to the static method used in the heading test. Figs. 21 and 22 show the performance obtained by these

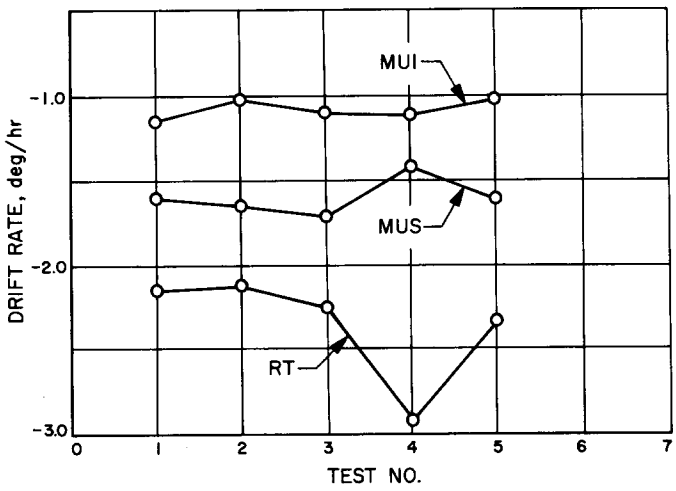

Fig. 21. Tumble test data summary

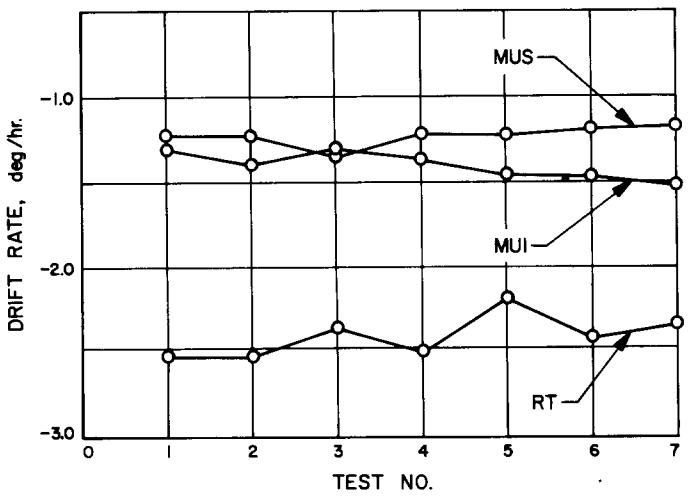

Fig. 22. Cogging test data summary

UNCLASSIFIED

test methods. Each data point represents one day's testing. Correlation of data obtained by these three different methods is excellent for a gyro of this type. These data confirm the out of specification condition for the RT term ($\pm$1.0 deg/hr maximum). The g-sensitive drift terms are within specification limits.

The torquer scale factor was measured by the servo table method at several temperatures and current levels. Performance is shown in Fig. 23. These values are also within specification and indicate satisfactory linearity of the gimbal torquer.

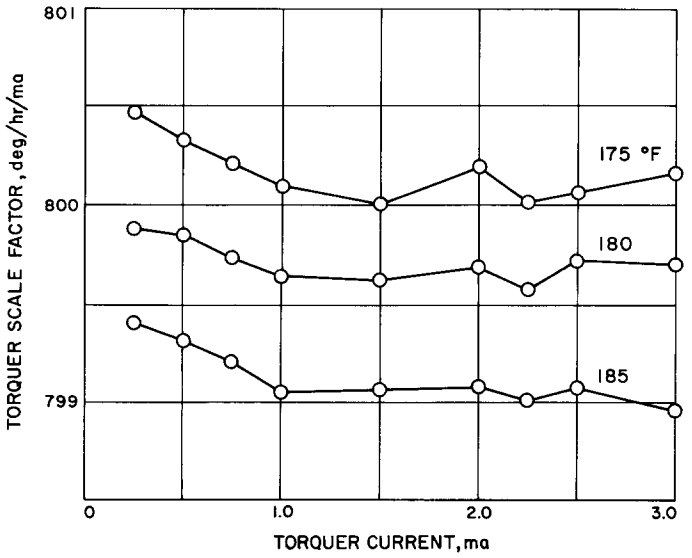

Fig. 23. Torquer scale factor

J. Electronics

1. Auxiliary Engineering Signal Processors

Design improvements, which will be incorporated in SC-5 and the following spacecraft, were completed for the engineering signal processor (ESP) and auxiliary engineering signal processor (AESP) as follows:

(1) Alloy type commutator output switch transistors will be replaced by higher reliability epitaxial switch transistors (ECA 112095).

(2) A more reliable and higher accuracy bootstrap unloader circuit will replace the old circuit. Improved ESP signal measurement accuracy, as well as improved ease of manufacturing and testing of the modules, will be a direct result of this change (ECA 112308).

(3) The X-Y commutator flip-flop modules were improved to increase their current handling capability (JPL IOM, 2737-65-412) (ECA 112267).

(4) Routing of the 29-v return line was corrected (ECA 112390).

(5) For SC-3 and following spacecraft, the null error amplifier circuitry was modified.

(6) Contour cables were upgraded (SC-5 and following spacecraft). The cables will be made with H-film material. The connector will be encapsulated with resilient potting compound which is more resistant to moisture penetration (ECA 112457).

An investigation is underway to determine the amount of output capacitance reduction required to decrease the temperature measurement current generator settling time.

A complete laboratory breadboard of the ESP was completed during this period and is being used to evaluate the present (and future) design changes which will be incorporated in the ESP/AESP.

2. Engineering Signal Processor (A-24)

Several of the design improvements to be incorporated in the A-21 were also completed for the A-24 ESP. They are as follows:

(1) The alloy type commutator output switch transistors will be replaced by higher reliability epitaxial switch transistors.

(2) A more reliable and higher accuracy bootstrap unloader circuit will replace the old circuit. Improved ESP signal measurement accuracy will result from this change.

(3) The X-Y commutator flip-flop modules were improved to increase their current handling capability (JPL IOM, 2737-65-412).

An investigation has been started to determine the amount of output capacitance reduction required to decrease the temperature measurement current generator settling time, and a laboratory type breadboard of the ESP was completed for use in evaluating the present (and future) ESP design changes.

3. Product Design Engineering

Design effort on A-21 digital equipment was accelerated to meet schedules established by mod 56. Major additions and modifications are discussed in the following paragraphs.

UNCLASSIFIED

a. Advance flight control programmer (AFCP).

(1) Midcourse maneuvering timing capability was increased, resulting in a major modification of six modules and two etched boards (ECA 111874-1).

(2) Disable AFCP keys were extended and separation circuitry was modified. This change was reflected in board interconnections, as well as module redesign (ECA 112194).

(3) Prevent firing of vernier engines was implemented by the repackaging of one module (ECA 112140).

(4) Wiring and assembly of the AFCP was simplified by the redesign of the board mounting clips. This new usage of internal mounting clips will be reflected in an improvement of the AFCP reliability (ECA 112345).

(5) Magnitude information transfer module was repackaged to provide greater noise immunity and add an interlock (ECA 112149).

b. Central command decoder (CCD).

(1) ECU driver turn-on circuit was modified to make it independent of the system test equipment assembly (STEA) transmitter. One board was redesigned by having a direct coupling to the 29-v bus of the receiver (ECA 112352).

(2) One capacitor and one diode were added to the subsystem turnoff amplifier in order to isolate an undesirable signal from another circuit. Several major design modifications were incorporated in the ground equipment. These additions and modifications are identified as follows:

ECA 133200: Logic change to provide interlock against accidental transmission of sequence numbers as commands.

ECA 112349: Logic change to provide capability for transmitting interlocked normal and magnitude commands.

ECA 112046: Logic change to improve tape reader timing.

ECA 133204: Modification of two nixie driver circuits to provide signal voltages from the command generator to operate a nixie tube numerical display at a location remote from the command generator.

ECA 112134: Design change and addition of a pulse delay circuit (FF counter) to generate a pulse on the command sync delayed line to simulate the video processor camera advance pulse. This is done to permit testing and evaluation of the TV synchronized survey mode operation.

ECA 112061: Logic change to provide a command transmission signal for recorder.

4. Central Signal Processor (A-21)

Five ECRs were written on the A-21 central signal processor. The following recommendations were made:

(1) Short protection for the *Centaur* booster switch.

(2) Short protection for the −12-v inputs to the central signal processor master switches.

(3) Change in tolerances in the clock pulse conditioner to achieve higher frequency analog to digital converter operation.

(4) Isolation of the central signal processor analog to digital converter output from the TV auxiliary in case of shorts.

(5) Redesign of the central signal processor digit time amplifiers to protect against the catastrophic results of a single short.

Work has begun on a central signal processor to be used for circuit and group test evaluation.

5. Central Signal Processor (A-24)

Three ECRs written against the A-24 processor recommended the following:

(1) Redesign of the digit time amplifier to prevent shorted timing signals from affecting the operation at the analog to digital converter (ECR 319309).

(2) Short circuit protection for the −12-v inputs to the central signal processor master switch (ECR 211003).

(3) A redesign of the analog to digital converter, replacing the null error amplifier with a comparator and a zero, binary voltage weighter which nulls out comparator off-set errors (ECR 308654).

The circuits modified under ECA 111909 were also evaluated.

6. Low Power Transmitter (ECA 112229)

The low power section of the *Surveyor* transmitter is now being redesigned because the output power fell

UNCLASSIFIED

UNCLASSIFIED

below specifications in thermal vacuum environment. There are two causes for the power falloff:

(1) Components in the A4 module operating at high temperatures during high-power operation.

(2) Module mounting and sheet metal assembly, with high thermal impedance, interfaces in a vacuum environment restricting thermal transfer from the A4 module and internal dissipators to the spacecraft thermal tray.

The redesign consists of a power amplifier and a X24 varactor multiplier with shunt connected varactors for thermal transfer. The output is 300 mw at S-band. The existing A1, A2, and A3 modules will provide RF drive at 95.6 MHz to the new A4 power amplifier. The input current to the power amplifier is 220 ma for an output of 3.5 w at 95.6 MHz. A block diagram with power levels for the new design is presented in Fig. 24.

To accommodate the additional current for the new A4, it was necessary to increase the capability of the low-power switches in the electrical conversion unit. The original parallel transistors were replaced with a Darlington circuit for this increased current capability and improved reliability.

To improve the thermal transfer paths, additional heat sinks and spacers with added surface area have been incorporated into the electrical conversion unit structure and plates. The new spacers will be soldered to the top and bottom sheet metal plates and will provide a solid path for heat transfer around the edges of both plates to the sheet metal conversion unit structure and on to the thermal compartment tray. This additional surface area will lower the module mounting surface temperature by approximately 35°F.

A new power monitor design authorized by ECA 112230 will also be included in the new transmitter configuration. The new power monitor will be retrofitted on the present transmitters 263220-4 assigned to SC-3 and SC-4. The new design will use a diode with a 15 v breakdown rating and will provide a telemetry dc output of approximately 2.0 v with the transmitter delivering 10.0 w in high power. The package will remain basically the same.

A set of prototype modules is now in fabrication and will be installed on a Class III *Surveyor* transmitter for thermal-vacuum testing. The X3 and X2 multipliers are complete and have been tested. All prototype hardware is being fabricated to released drawings. The prototype fabrication testing will be completed in early April. The thermal transfer improvements will also be incorporated into the prototype transmitter. The first flight hardware will be fabricated and ready for test early in June. This new design will be effective for SC-5 and following spacecraft.

7. Boost Regulator

The preliminary circuit and product design review for the 3024240 boost regulator was held at Culver City March 16. The 3024240 unit will be used in conjunction with the new 3024260 battery charge regulator and the flat solar cell array for the A-21 configuration.

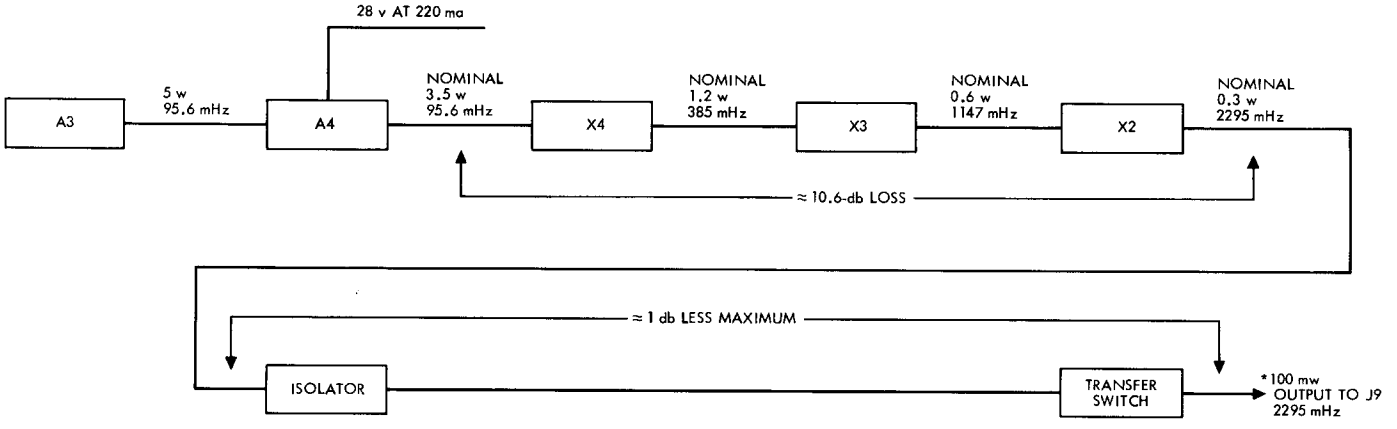

*100 mw MINIMUM OVER TEMPERATURE RANGE

Fig. 24. Power level block diagram

UNCLASSIFIED

UNCLASSIFIED
CONFIDENTIAL

The package outline for the new boost regulator is essentially the same as for the SC-1 configuration. Design improvements will include the use of larger terminals to accommodate interchassis wiring, modularized filter capacitors, Tetalon insulated wire, epoxy glass honeycomb core chassis, and provision for mounting without removing the unit cover.

Circuit improvements provide for a general updating of semiconductors and other components to the present state of technology. Other changes include an improved voltage boost circuit with a preregulated bus capable of accepting power directly from the solar panel and delivering it to the post regulators. An unregulated bus filter is also included in the boost regulator package. This filter will minimize converter-noise feedback to the spacecraft unregulated bus.

Two Class III units will be assembled to facilitate early testing of the flight configuration 3024240 boost regulator. One of the Class III units will be made available for the system integration tests. Component orders for both the Class III and Class IV units were placed, and approximately 50% of the Class III fabricated hardware was put to work. Manufacturing drawings were completed and submitted for drafting check.

8. Battery Charge Regulator

The preliminary circuit and product design review for the 3024260 battery charge regulator was held March 16. This unit will be used in conjunction with the flat solar cell array and the present 3024240 boost regulator in the A-21 configuration.

The new battery charge regulator will retain the same package outline as the 274100 battery charge regulators. Current functional requirements for the A-21 system are reflected in changes to the battery charge regulator circuits and to the internal physical design of the unit. An optimum charge regulator is not required.

The new circuitry is comprised essentially of that switching and control logic required to transfer solar panel power to the battery charging circuit or to the boost regulator preregulated bus. A small dc-dc converter and filter supplies the necessary bias potentials. All command inputs are designed to reject spurious noise signals, and filtering is provided in all telemetered signal lines.

The packaging design of the 3024260 battery charge regulator utilizes replaceable etched circuit chassis rather than cordwood modules. Thus, all circuit elements are more accessible and more readily modified to accommodate future requirements. Tetalon insulated wire is used in all internal cabling and intrastructure wiring.

Two Class III units will be manufactured to support an early test program at the unit level and at systems integration. Component orders were placed for the Class III and the Class IV requirements. The product layout effort was completed, and work is continuing in the drafting phase.

9. Altitude Marking Radar (AMR)

The launch profile decompression test requirement was successfully met by a specimen AMR. This represents a significant advance in the development of the AMR. This requirement was imposed upon the AMR by JPL as a result of bad experiences with honeycomb Fibreglas structures used on the *Mariner* program. The purpose of the decompression test was to verify the ability of the AMR Fibreglas honeycomb antenna structure to withstand the stresses imposed on it by a sudden loss of atmospheric pressure, as in the case of a spacecraft launch. Arrangements were made to use SN-11 (SP-1 spacecraft) as the sample unit. Negotiations also were made to obtain the use of the C5b chamber at the space simulation laboratory. This chamber, owing to its very large pumps, is capable of rapid pumpdown rates simulating pressure loss rates experienced in an actual launch (often referred to as a launch profile). The test was conducted in four phases: (1) the radar was carefully examined electrically (functionally), photographically, and optically; (2) then it was placed in the chamber and subjected to a launch profile decompression; (3) while still under vacuum, it was turned on and briefly checked; (4) it was returned to atmospheric pressure and reexamined. The AMR performed this test sequence without any sign of change, degradation, or damage.

K. Electrical Power Supply

The SC-1 solar panel has been successfully tested at AFETR, and the SC-1 spare is being delivered to AFETR.

Under high-current discharge, the most recent lots of batteries have fallen below minimum voltage requirements. An extensive investigation is under way.

CONFIDENTIAL
UNCLASSIFIED

UNCLASSIFIED

1. Solar Panel

The status of flight panels is as follows:

(1) Solar panel 1 (SC-1 spare)—delivered to bonded storage and shipped to AFETR during the third week of March.

(2) Solar panel 2 (SC-1)—delivered to AFETR. Sunlight test at AFETR successfully completed.

(3) Solar panel 3—solar cell replacement completed. Panel being prepared for delivery for SC-2 vibration testing.

(4) Solar panel 4—solar cells being replaced.

(5) Solar panel 5—solar cells being replaced.

Analysis of solar panel strain gage data from T-21 drop tests showed loads on the solar panel substrate to be well within acceptable limits.

2. Batteries

a. Main battery hardware status.

Serial number	Status
35	Used successfully in SC-1 plugs-out test and in special SC-2 tests; returned to power laboratory and recharged with no degradation observed.
36	Used successfully in SC-1 vibration; recharged in laboratory and shipped to AFETR for special SC-1 tests.
37	Used successfully in SC-2 mission-sequence tests; spacecraft data shows 137 amp-hr removed; battery recharged in power laboratory; no degradation observed.
38	At AFETR for SD-5 tests.
39	Flight acceptance test (FAT) completed; battery thermally wrapped and delivered to AFETR for SD-5 launch.
40	Used successfully in SC-1 combined systems testing at San Diego; returned to power laboratory and awaiting recharge; cell voltages indicate no problem.
41	FAT and thermal wrapping completed; preparation under way for shipment to AFETR for SD-5 backup.
42	FAT complete; scheduled for SC-2 solar thermal vacuum test.

The most recent lot of batteries (serial numbers 43 through 47) fell outside specification requirements in electrical testing at the manufacturer, Electric Storage Battery Company. When pulse discharged at 85 amp, battery readings averaged 16.8 v versus the required 17.5-v minimum. Previous lots of batteries had voltages in the 18.5- to 19.0-v range under the same discharge.

Materials and manufacturing processes used in the batteries in question are being investigated. Quality control data have been reviewed, but no conclusive reasons for battery behavior have been established. Some tentative conclusions are as follows:

(1) The fault is not in the negative mix because the same material has been employed since battery 30.

(2) Potassium hydroxide electrolyte in one of the out-of-tolerance batteries had also been used in previous batteries. The electrolyte is not considered the major problem.

(3) The Q-cell sample, though acceptable, did indicate a change in electrical performance. Q-cell requirements will be tightened to better reflect battery acceptability.

(4) Test equipment used in the electrical test was in calibration, and the procedure was correct.

(5) Cell jar dimensional check showed no change.

(6) Increase in lead lengths (correction incorporated to eliminate electrolyte wicking problem) accounts for only 0.22-v drop at 85-amp discharge.

(7) Dry thickness and weight of the cellophane separator was correct.

(8) Specific gravity of electrolyte verified as correct.

The investigation is continuing. Samples of the positive plates, potassium hydroxide electrolyte, and cellophane separator systems are undergoing analysis at the Electric Storage Battery Company research center. The Q-cells will be dissected and examined. A four-cell matrix test has been initiated; each cell will contain one of the questionable materials. Manufacture of four batteries with all new materials has begun in order to meet SC-1 flight dates. Three of the questionable batteries (serial numbers 43, 44, and 45) have been shipped to HAC as Class IVT and will be used in SC-2 systems testing. Thus, the SC-2 schedule will not be jeopardized, and a better understanding of battery behavior in systems test will be obtained.

CONFIDENTIAL
UNCLASSIFIED

UNCLASSIFIED
CONFIDENTIAL

The monobloc test plan was published, but the test program is being delayed because of the high-discharge test problem previously discussed. Six monoblocs have been assembled at Electric Storage Battery Company but fall in the same category as the batteries. An objective of the monobloc program is to use cells identical to those in the SC-1 flight battery. Three of the monoblocs will be shipped to HAC and tested as part of the high-discharge problem investigation.

In an effort to extend battery operating life, the FAT procedure was changed to eliminate complete discharge cycle and to lower float voltage from 27.3 to 26.9 v. The 26.9 float voltage does not provide sufficient input capacity; increasing the float voltage to 27.1 v is under consideration. With a fully charged battery, a 26.9-v float is satisfactory. However, when 10% or more of battery capacity has been removed, as is often the case in systems test, recharging at a constant 26.9 v is insufficient.

b. Auxiliary battery hardware status.

Serial number	Status
30	Used successfully in SC-1 vibration.
32	Used successfully in SC-2 mission sequence tests; approximately 27 amp-hr were removed.
35	Used successfully in T-21 drop tests.
36	Used successfully in SC-1 combined systems test.
37	SC-1 combined systems test backup but not needed.
31, 33, 34 and 38 through 47	Delivered to bonded stores; unactivated.
48 through 53	Delivered to HAC and undergoing initial FAT process.

c. T-2 batteries. FAT of T-2 main batteries 132 and 133 has been completed. T-2N-1 and T-2N-2 are now being upgraded for an altitude drop followed by actual soft landing touchdown instead of using recovery parachutes. The last lot of ten batteries has been received from Electric Storage Battery Company. Four gondola batteries have been received from Willard Battery Company.

3. Surveyor Electrical Power Subsystem Evaluation

Testing will take place under thermal vacuum conditions, with individual units mounted in their proper spacecraft attitudes on individual thermal trays. This mockup, based on existing design, will be evaluated to establish unit and subsystem performance characteristics, capabilities, and limitations.

Special tests have been conducted to investigate the problem of battery charge regulator oscillations in the optimum charge regulator bypass mode. This problem occurs in the system test equipment assembly (STEA) solar panel simulator when simulator voltage is greater than bus voltage; the oscillation stops when bus voltage and simulator voltage are equal. A corrected design of the solar panel simulator is being evaluated.

Unexplained fluctuations in unregulated bus voltage during systems readiness test and prelaunch countdown tests at San Diego are also being investigated. Attempted simulation of the anomaly, using one of the prelaunch power supplies, has been unsuccessful. The second (or slave) power supply is now being returned from San Diego for use in the test setup.

All drawings, specifications, and other documents associated with the power subsystem and/or individual units are being collected and listed for review and reference.

L. Propulsion

1. Summary

a. A-21 main retrorocket engine. Both the flight and flight spare engines for SC-1 are at AFETR. A third flight retrorocket engine, the SC-2 spare, is scheduled for delivery at AFETR May 18. Storage capability of at least 23 mo has been verified with the successful firing of a previously unused qualification engine.

b. A-24 main retrorocket engine. Fabrication of the case forgings is proceeding without difficulty according to the new schedule, which required revision because of a labor dispute at the material vendor's facility. First hot firing in the program, initial nozzle overtest, was successfully accomplished February 24. A similar test was only partially successful because of a heavyweight case burn-through.

CONFIDENTIAL
UNCLASSIFIED

UNCLASSIFIED

c. A-21 vernier propulsion system. The last items (not yet qualified) successfully completed qualification testing. These items included the propellant tank assembly, the relief valve, the charging valve, and the fill and vent valve. Lunar survival test preliminary results indicate that a vent system for A-21 will not be needed. The system can safely contain the increased pressure resulting from solar heating after lunar landing.

d. A-24 vernier propulsion system. All vendors have made good progress on deliveries of component hardware. Type approval testing of most component-level items has been completed. Engineering testing of control items has been initiated. The redirected program outlined in mod 56 resulted in a minimum of test effort at HAC facilities; thus, interaction of the A-24 program on A-21 work has been reduced to a negligible proportion.

e. T-2N. The propulsion system operated completely satisfactorily in the one tether and four descent tests performed during this report period. Both vehicles are in upgrade preparatory to the soft landing tests planned for this spring.

2. Main Retrorocket Engine

a. A-21. Installation of the thermal control insulation on inert retrorocket engine A-21F was accomplished at General Dynamics/Convair (GD/C), San Diego, during the week of February 21 for support of SC-1 combined systems test (CST). This operation also provided an excellent opportunity for training additional personnel in insulation installation techniques under near actual AFETR environments.

Safe and arm devices 702 and 703 have undergone thermal control surface preparation at HAC and were subsequently shipped to Thiokol for flight approval test and installation into the retrorocket engine.

Operations are under way at AFETR on flight preparation of the SC-1 retrorocket engine and its spare, A-21-26 and A-21-27, respectively. The flight retrorocket engine has been fully prepared and returned to storage. The spare retrorocket engine preparation has been delayed because of a defect in the safe-arm unit. The engine was returned to Thiokol for installation of another safe-arm and will be returned to AFETR by May 1 for final prelaunch preparation.

The SC-1 spare main retrorocket engine (A-21-27) was originally delivered to AFETR March 19. The total propellant weight, as assembled, is 1250.07 lb. No propellant cutback was accomplished in order to protect the suitability of the engine for use on future spacecraft. Should it be necessary to use engine A-21-27 on SC-1, a total ballast of 14.4 lb will be required, making the injected spacecraft weight 2204.64 lb.

If engine A-21-27 is not required for SC-1, it will be used for SC-2. Based on the planned August-through-October launch period, the engine could be used without propellant cutback. A total ballast of 12 lb would be required, resulting in a spacecraft injected weight of 2206.5 lb.

The SC-2 spare retrorocket engine (A-21-28) is being processed at Thiokol for delivery to AFETR by May 18. This engine was cast with the A-21 configuration core to a propellant weight of 1250 lb. No propellant cutback is presently contemplated for support of the SC-2 mission.

No acceptance engine was cast in conjunction with the loading of A-21-28 because the same purpose was achieved by the concurrent loading of the Douglas Aircraft Company "Improved Delta" and Boeing "Burner II" variations of the engine.

Engine A-21-15, an unused qualification engine, was successfully fired at Thiokol April 6. The three primary test objectives were as follows: (1) to prove the storage capability of the basic engine design at the 23-mo level; (2) to provide data for a procurement specification change allowing portions of the propellant to be at 10°F as opposed to the former minimum of 20°F; (3) to provide an evaluation of performance at a temperature gradient that reflects the SC-1 solar thermal vacuum test data.

The test was preceded by an inspection sequence that included visual and X-ray examinations at 10°F and a pressure check for O-ring integrity.

The engine was conditioned to the above thermal gradient and fired. The quick-look data indicated that performance was as predicted at the new gradient condition.

b. A-24. The A-24 retrorocket engine development program is proceeding on a revised schedule. The planned case utilization schedule and the program schedule have been modified.

A review of the case stress analysis was held March 4 at Thiokol and the design was deemed conservative. Thiokol

UNCLASSIFIED

UNCLASSIFIED CONFIDENTIAL

was given authorization to proceed with case fabrication. All other component procurements are proceeding on or ahead of schedule.

The initial nozzle overtest engine was fired February 24. The pressure-time trace is shown in Fig. 25. Measured maximum pressure was 720 psia, and burn time was 40.5 sec. The engine (A-24-1) was loaded with 1643 lb of propellant and was fired at 85°F.

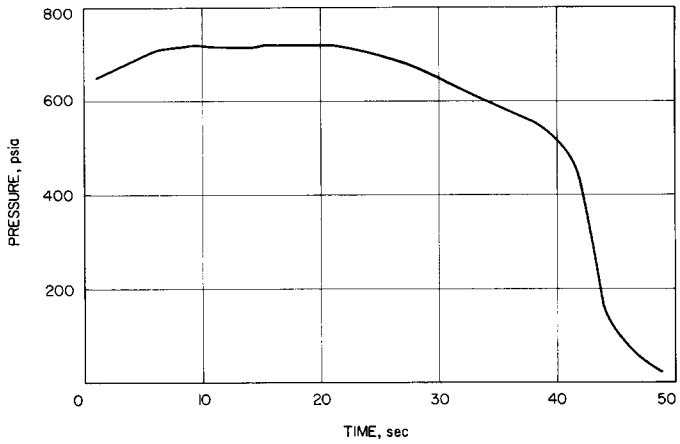

Fig. 25. Engine A-24-1, pressure versus time

Nozzle throat erosion was as predicted and was 13.8% of initial area. Postfire examination of sections of the fired nozzle indicate that the insulation thicknesses are sufficient. Some indications of helical erosion patterns were present in the exit cone liner.

The second nozzle (fired on engine A-24-2) differed from the first in that the helical pattern angle was increased in the exit cone. This change was made to further decrease the shear loads imparted by the gas stream and thereby improve the overall surface condition.

The test of engine A-24-2 was conducted April 7 at Thiokol. After 25 sec of operation a burn-through occurred at the forward weld of the heavyweight (nonflight) case. Prior to the burn-through chamber pressure had increased to 850 psi, as opposed to the expected 715 psi.

It is believed that an unbonded area existed between the release boot and the propellant grain, thereby providing a larger burning surface and causing a rise in chamber pressure with resultant case failure.

The A-24 retrorocket engine posttransit temperature gradient prediction is in process. The computer program being employed is based on the program developed by HAC for the A-21 retrorocket engine. HAC will factor in the information obtained in the SC-1 and thermal control model solar thermal vacuum tests.

Thiokol presented a polished A-21 retrorocket strut to HAC for use on the A-24 retrorocket engine. The strut met all requirements, and the process was approved.

The National Bureau of Standards was contacted February 28 to determine whether they could play a leading role in the establishment of propellant thermal properties. The Bureau expressed a reluctance to work with live propellant but is quite willing to work with Thiokol, using the thermal inert propellant as the standard. HAC will coordinate the activities of both parties in arriving at a reasonable test program.

A planning meeting was held in February at Arnold Engineering Development Center where four type approval tested motors are to be static fired under simulated high-altitude conditions. A 6-wk cell occupancy schedule was generated, enabling the motors to be tested in accordance with the program requirements.

3. *Vernier Propulsion System*

a. System analysis. Vernier propulsion system leakage allocations have been reviewed in the light of launch operations and testing experience. The review revealed that the permissible leakage rates may be substantially increased beyond those experienced in recent testing.

In tests completed during this report period, propellant and pressurant loading accuracies were re-examined. Studies indicate that less than 0.0025 $in.^3$ of helium at pressure per cubic inch of propellant per oxidizer tank can be liberated during a typical *Surveyor* mission. This results from decreasing helium solubility with decreasing temperature. No system difficulties are predicted from this quantity of helium.

Trouble and failure report (TFR) processing and closeout is proceeding on a normal basis. The major open TRF against the vernier system is chargeable to the propulsion system and concerns propellant tank expulsion bladders. Both SC-2 leg 2 propellant tanks were found to have bladder leakage during the filling operation preparatory to solar thermal vacuum (STV) test. The tanks were replaced and upon disassembly a slit-type hole was found in the lower hemisphere of each bladder. The slit ran circumferentially in each bladder. Intensive failure

UNCLASSIFIED CONFIDENTIAL

UNCLASSIFIED

analysis began immediately. Dimensional and physical properties tests were run and microphotographs were taken and analyzed. No discrepancy was found in material or workmanship in either bladder. An investigation is now centering on the processes both common to all tanks and peculiar to these two. A transparent tank is being fabricated and, when complete, a thorough research of bladder dynamics during usual and unusual tank and vehicle leak-test, loading, and other related operations will be conducted. The test program will start approximately May 4.

Nickel coupons were suspended in vessels swept by a slow flow of air at relative humidity levels of 0, 5, 10, 25, 50, and 100%. A small jet of oxidizer (MON-10) vapor was directed at an area on the face of each coupon. Two tests of 7 days duration were carried out at ambient temperature. The results are shown in Fig. 26.

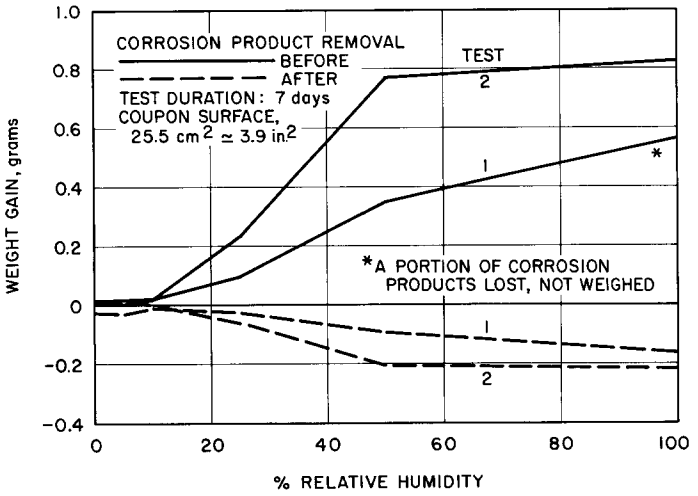

Fig. 26. Weight changes of nickel coupons exposed to MON-10 vapors as function of relative humidity

The results indicate that the corrosion rate of the coupons depends on the relative humidity. The rate of nickel loss varied from zero at low relative humidities to a little over 1 mg of nickel per cm² surface per day over the 7-day period. Hence, it appears that desiccant filled blow-off covers on the thrust chamber assemblies could alleviate the clogging problem.

Rocketdyne has experienced a flow rate decay phenomenon while flowing nitrogen tetroxide (N_2O_4) across a high-pressure drop, such as a needle valve. This situation was discovered while flow calibrating turbine flowmeters. It was determined that the flow decay was caused by a buildup of a semisolid substance on the valve needle. The substance was difficult to obtain when exposed to atmospheric conditions since it sublimes at atmospheric pressure. However, it was finally isolated and analyzed as an iron compound. If the same phenomenon occurred when flowing MON-10 (90% nitrogen tetroxide + 10% nitric oxide, NO_4) it could adversely affect *Surveyor*. Rocketdyne was visited to examine the flow bench test setup and to discuss test procedures. Using this information, a test program has been proposed to first verify the buildup phenomenon using N_2O_4, and then, using the same test apparatus, MON-10 will be flowed. The tests will be run at the Placerita Canyon Test Facility.

Prior to vehicle launch, the helium low pressure system is pressurized to 300 psig. Because of unavoidable leaks in the system, this pressure can decay to zero. If it does, helium which has permeated the bladder and gone into solution at the higher pressures may come out of solution at the decreased pressure and form a bubble inside of the bladder. A test plan has been prepared at the Placerita Test Facility to investigate whether or not this phenomenon will occur.

b. Valves. The remaining unqualified components on the A-21 vernier propulsion system, the relief and high-pressure charging valves, completed qualification testing. These components were submitted to type approval test after successful service on the helium tank and valves assembly that passed control item type approval test. The components were then subjected to the specified environments not experienced on the control item. These included a series of engineering informational nonqualifying tests for the high-pressure charging valves, i.e., lunar survival, endurance and proof pressure, and both qualifying (thermal cycling and propellant exposure) and nonqualifying (lunar survival and proof pressure) tests for the relief valves.

For SC-3 and subsequent spacecraft, all low-pressure quick disconnects on the vernier propulsion system will be replaced by a HAC-designed and-fabricated fill and vent valve. This valve passed its type approval tests and was subjected to the following qualifying tests: propellant exposure, vibration, shock, thermal vacuum (0 and 100°F), and acceleration. Additional tests performed for engineering information were lunar survival, endurance, and proof pressure.

c. Propellant tank type approval test. All tests remaining on the propellant tanks were successfully completed. On March 11 the review committee met, accepted

UNCLASSIFIED

UNCLASSIFIED

the results, and declared the tanks qualified. A brief summary of the test results follows.

Vibration, thermal vacuum, and acceleration tests were completed and reported previously. Expulsion tests, the last required environment, were begun on the oxidizer tank with the goal of 11 full expulsions without leakage. However, the bladder leaked on the eleventh cycle. After a thorough re-evaluation of bladder life requirements, it was determined by HAC and JPL that a four-expulsion cycle durability would provide ample margin for the *Surveyor* mission which consists of one complete expulsion. Hence, the type approval test requirement was adjusted to four expulsions at specified temperatures without leakage, and the fuel tank was put into test.

The fuel tank cycles consisted of three 90 to 95% expulsions at 0, 100, and 70°F, respectively, followed by a 99% expulsion of 0°F. Monomethyl hydrazine (MMH) was used, tank pressure was 730 psig, and average flow rate was 250 $in.^3$/min. The tank met all requirements, and expulsion efficiency on the last test was an excellent 99.46%, with no leakage after test.

As a penalty run for the oxidizer tank, a T-2N-1 tank assembly was selected for test. This assembly had been exposed to vibration, shock, and thermal vacuum test plus two partial expulsions (90 and 95%) using MON-10. The additional tests subjected the tank to two 90% expulsions, flange up, at 100 and 0°F, respectively, and then to a complete expulsion, flange down, at 0°F. The tank passed the test series without difficulty and on the last expulsion achieved an efficiency of 99.51%.

d. Lunar vent system. Development of the lunar vent system was delayed pending the outcome of the propellant tank lunar survival tests. Both vent system designs, squib-actuated valve and fusible plug, appear feasible and capable of early development. A compatibility test of two fusible alloys in contact with oxidizer for 30 days has been completed with excellent results.

Results on the lunar survival test series prove that no lunar vent system is required for A-21. In the first test a tank was selected from the S-7 vehicle. The tank had been exposed to both the vibration levels of vehicle type approval test and shock loads of the pressurized drop test. Hence it had been exposed to environments at least as severe as those a lunar landed *Surveyor* tank will have experienced. In this test the tank was loaded with a representative quality of residual oxidizer (9 lb), pressurized to the regulator lockup pressure of 840 psig and stored for 15 days at 240°F. This temperature is the maximum calculated temperature the tank will experience on the Moon. The tank survived with no problem. In a subsequent burst test, also at 240°F, 1300 psig was required to rupture the tank, indicating an ample safety margin. To provide further confidence in the structural integrity of the tank, a duplicate test was conducted except that storage was at the temperature of 270°F, higher than the expected temperature on the Moon. Storage was for 14 days and the tank pressure peaked at 1069 psig. No problem was encountered and in the subsequent burst test at 270°F, 1367 psig was required to rupture the tank, again demonstrating margin safety.

e. A-24. The helium regulator has successfully completed type approval testing and regulator capability tests which were conducted following the type approval test program. The capability test series demonstrated acceptable operation of the regulator under extreme test conditions of higher and lower temperatures and higher and lower flow rates than the specified operational requirements.

All flight regulators have been delivered.

Type approval testing of the propellant tank shells has been successfully completed except for final burst tests. Sufficient tanks have been procured to support assembly type approval tests and ground test systems S-11 and S-12A. Deliveries of shells for flight spacecraft have been halted by partial termination of this subcontract.

The helium tank shell has successfully completed all type approval testing except for the final burst tests, and all flight hardware has been delivered. All flight hardware of the helium release and dump valve has been received, and the type approval test program has been completed.

The antimigration check valves have begun type approval testing. Initial delivery of flight hardware has been made. Engineering prototype models of this component have also been delivered. Type approval testing of the fuel and oxidizer fill valves has been initiated, and all flight hardware has been received.

All component parts for the helium check and relief valve have been received. Type approval testing of the A-24 helium relief valve has been initiated, and engineering testing on the control item has begun. The helium fill valve has successfully completed type approval testing. Most of the flight hardware has been delivered. Initial assembly and engineering testing was started on the propellant tank assembly.

UNCLASSIFIED

UNCLASSIFIED

f. T-2N. The T-2N-1 vehicle satisfactorily completed two altitude descent tests while the T-2N-2 vehicle was subjected to one tether and two altitude descent tests. All tests were successful except the first T-2N-2 descent test which was recovered prematurely (10 sec after release). Recovery was commanded by the safety console operator because of data display malfunction. Propulsion system operation was completely satisfactory during all the above listed missions. The vehicles are currently in an upgrade cycle during which modifications for soft landing the vehicle will be incorporated.

4. Surveyor Vernier Engine Plume[4] Interactions with the Lunar Surface

a. Summary. The object of this study was to examine the shear stress applied to the lunar surface by the exhaust plumes of the *Surveyor* spacecraft vernier engines during the terminal descent phase of the *Surveyor* mission. Analysis of the vernier engine exhaust plume indicates the vernier engine/lunar surface interaction occurs in the transition regime between continuum and free molecular flow. Analytical and experimental work described in the literature have investigated this interaction as a continuum flow problem. Solution of the equations for this rarefied gas transition regime is quite complex; consequently, the problem was analyzed in two ways, first assuming free molecular conditions to prevail, and second assuming continuum conditions to prevail.

For the free molecular flow case, the gas-surface interaction is described by elastic collisions between molecules and the surface and diffuse reflection of molecules from the surface. This analysis yields maximum shear stresses which are one or more orders of magnitude greater than the maximum shear stresses predicted by the continuum analyses. For a vernier engine cutoff altitude of approximately 5 ft, the maximum possible shear stress for the three engine interaction flow field is approximately 0.9 lbs/ft^2. This is more than an order of magnitude less than the minimum value of 14–28 lbs/ft^2 predicted for the lunar surface shear strength. This minimum shear strength is an order of magnitude less than the nominal expected shear strength.

Based on this study, dust transport due to interaction of the vernier engine exhaust with the lunar surface is not expected for vernier engine cutoff altitudes of 5 ft or greater, provided the minimum predicted surface shear strength is correct within two orders of magnitudes. Base heating of the spacecraft for vernier engine cutoff altitudes of 5 ft or greater was also investigated and found to be negligible.

b. Introduction. Detailed consideration of the lunar descent phase of the *Surveyor* spacecraft mission leads to speculation on a possible dust cloud raised by the action of the vernier engines on the lunar surface. Such a dust cloud could cause degradation of thermal-control and solar panel surfaces on the spacecraft and, additionally, could impair radar altimeter and doppler velocity sensor operation. Desirable, also, is a reduction of landing stresses in the spacecraft by lowering the vernier engine cutoff altitude.

Concerns such as these have led to this analysis of the vernier engine interaction with the lunar surface to obtain an estimate of the magnitude of dust transport phenomena during the final descent maneuver.

To obtain insight into the nature of the problem, Table 18 was prepared giving the values of the density and mean free path of the gas as a function of position in the vernier exhaust plume; also shown are the values of the mean free path following a shock wave at the point in the plume, assuming the shock wave to be very strong.

Table 18. Density and mean free path as a function of position in the vernier engine plume

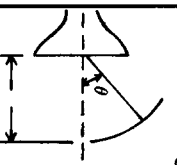

$\lambda_{ahead} = \dfrac{0.677}{\pi v \sigma^2}$; $\sigma = 3.32 \times 10^{-8}$ cm; v = number density

$\theta = 0$ deg

H/R_e	ρ, lb_m/ft^3	λ_{ahead}, in.	λ_{behind}, in.
25	7.5×10^{-7}	0.24	0.031
35	3.2×10^{-7}	0.58	0.076
50	1.5×10^{-7}	1.2	0.156
100	3.8×10^{-8}	4.8	0.625

$\theta = 30$ deg

H/R_e	ρ, lb_m/ft^3	λ_{ahead}, in.	λ_{behind}, in.
25	8.8×10^{-8}	2.0	0.261
35	5.2×10^{-8}	3.5	0.456
50	2.3×10^{-8}	7.9	1.06
100	5.8×10^{-9}	31.0	4.04

$\lambda\{^{ahead}_{behind}\}$ = mean free path $\{^{ahead}_{behind}\}$ a strong shock wave

[4]Prepared by Technical Section 384.

UNCLASSIFIED

UNCLASSIFIED
CONFIDENTIAL

One can see that at an altitude of 50 exit radii, approximately 10 ft, the surface and the plume interact in the hypersonic continuum/free molecular transition flow regime, i.e., the mean free path of the gas is of the order of dimensions typical of the problem. A survey of the literature pertinent to this problem shows that all related analytical and experimental work deals with continuum flows.

Rigorous analytical investigation of this rarefied gas problem requires solution of the Boltzmann equation, an extremely difficult undertaking for this complicated geometry. Consequently, the present analysis makes estimates of the surface shear stress for both the continuum flow and free molecular flow models. These estimates are then compared with the predicted shear strength of the lunar surface to determine the magnitude of associated dust transport phenomena.

The engine and exhaust gas properties used in this analysis are described below.

Vernier engine	*Surveyor* vernier thrust chamber assembly, Thiokol-RMD Model No. TD-339, Reaction Motors Division (RMD) of Thiokol Chemical Corp.
Exit mach number	5.2
Ratio of specific heats (frozen polytropic exponent)	1.313 applicable at and downstream of the engine exit plane and is considered constant.
Maximum expanded velocity of engine exhaust gases	10,000 ft/sec
R_e exit radius	2.545 in.

c. Characteristics of the vernier engine exhaust plume. Constant Mach number contours in the vernier engine plume are shown in Fig. 27, where the length scales are referenced to the engine exit radius R_e. These contours were calculated by considering the behavior of properties in single streamtubes as the flow expanded from the vernier engine throat. This exhaust plume was empirically fit using an inverse square decrease of density with distance and an exponential decrease of density with angle from the centerline of the plume. The following equation describes the plume to an accuracy of about $\pm 25\%$ for angles up to 30 deg and distances greater than 25 exit radii. The region up to 30 deg contains more than 85% of the mass expelled by the engine.

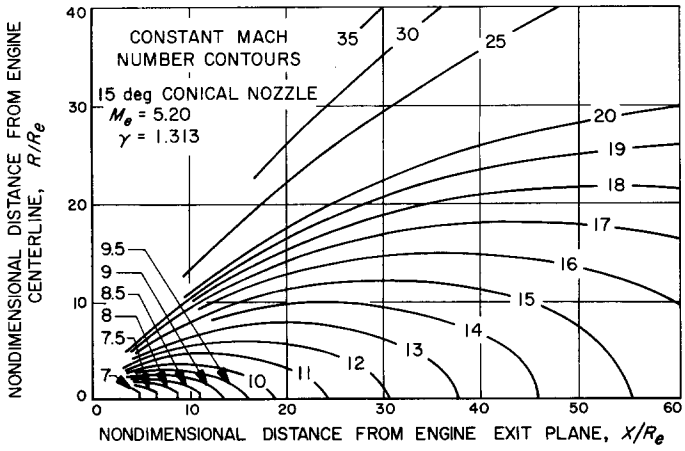

Fig. 27. *Surveyor* vernier engine plume

Along a line normal to the central streamline in the plume, the density is written as

$$\frac{\rho}{\rho_r} = \left(\frac{h_r}{h}\cos\phi\right)^2 e^{-(\phi/\phi_T)^2}$$

where

ρ_r = is the density at the reference distance taken from a numerical analysis of the vernier engine plume.

h_r = is the reference distance.

ϕ = is the angular distance from the central streamline to the point of interest.

ϕ_T = 22.7 deg for this engine.

h_r = is taken as 50 exit radii, 10.604 ft; at which point, on the centerline, the density is 1.5×10^{-7} lb_m/ft^3.

d. Free molecular flow analysis. For this study the flow field in the range of interest is governed as much by intermolecular interactions (continuum flow) as it is by the gas molecules individually (free molecular flow). Due to their complexity, the appropriate governing equations are not solved; instead the methods appropriate to both the overlapping regimes are applied. Since this is a physical problem, flow properties can be expected to behave continuously and uniformly. Consequently, the free molecular and continuum analyses will circumscribe the real situation and yield meaningful estimates for the transition regime.

UNCLASSIFIED

Since only the continuum problem is available in the literature, it was necessary to do the free molecular flow analysis in this study. This analysis was based on the following assumptions.

(1) Near the lunar surface, gas molecules never interact with one another and the gas molecules strike the lunar surface exactly once.

(2) Incident gas molecules undergo elastic collisions with the lunar surface.

(3) Gas molecules are diffusely reflected from the surface.

(4) The geometry is approximated by considering the vehicle descending vertically onto a macroscopically smooth, horizontal flat plate, see Fig. 28.

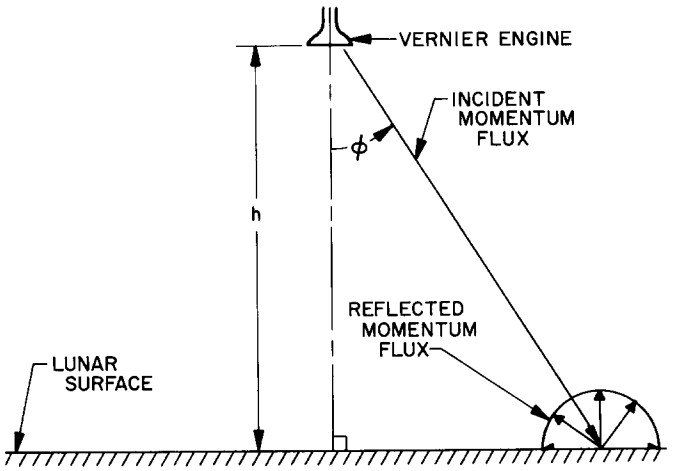

Fig. 28. Descent geometry and illustration of assumptions

The assumption of elastic collisions between the molecules and the surface and the assumption of diffuse reflection tend to maximize the horizontal momentum flux of the reflected jet, thus leading to a conservative estimate of the surface forces.

Consider a small stream tube around a streamline in the plume. The flow field along the surface induced by a single vernier engine is found by assuming that each stream tube, upon intersecting the surface, creates a hemispherical source as shown in Fig. 28, where diffuse reflection with elastic collisions is assumed. An elastic collision implies that the speed of the exhaust molecule before and after impact with the surface is identical; diffuse reflection implies that the mass flow (per unit solid angle) from the source point is the same in all directions above the surface.

It is further assumed that the reflected flow from each point does not interact with the incoming flow from the engine or reflected flow from other source points.

The total forces on an object on the lunar surface are those due to direct impingement by the incident exhaust gas molecules from the engine and those due to impingement by reflected molecules. These forces are equivalent to the momentum fluxes of incident and reflected molecules multiplied by the appropriate cross sectional areas. The momentum flux due to the incident molecules is the horizontal component of the momentum flux contained in the incident streamtube. The horizontal momentum flux, that momentum flux attributed to reflected gas molecules, is found by a weighted vectorial summation of the momentum flux from each of the sources distributed on the lunar surface. The weighting function is proportional to the solid angle that the object subtends from the source point.

The resulting equations for momentum flux can be shown to be similar, such that a plot of momentum flux times vehicle altitude squared against horizontal distance along the surface from the stagnation point divided by vehicle altitude is a single curve for all vehicle altitudes.

The total momentum flux at a point on the surface was found by numerical integration using the method just described. The results are shown in Figs. 29 and 30, where the horizontal momentum flux due to a single vernier engine is plotted as a function of distance from the stagnation point for engines 10.604 ft (50 exit radii)

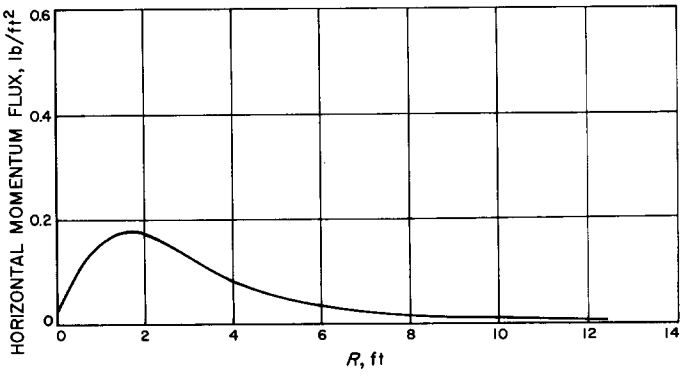

Fig. 29. Single jet horizontal momentum flux as a function of distance from the stagnation point (H = 10.604 ft, H/R_e = 50)

UNCLASSIFIED

UNCLASSIFIED
CONFIDENTIAL

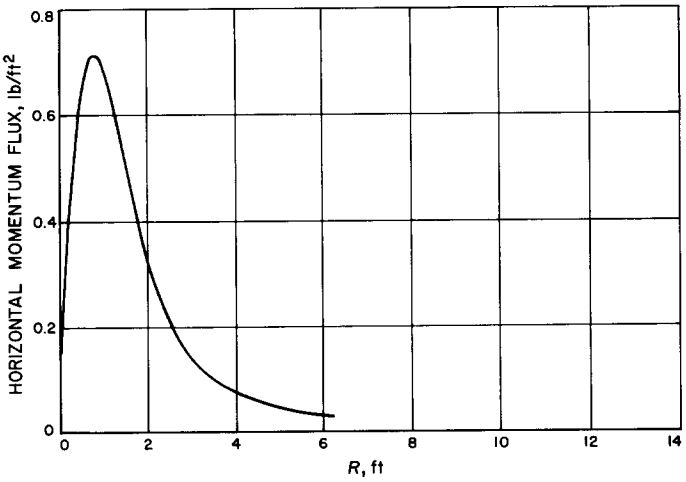

Fig. 30. Single jet horizontal momentum flux as a function of distance from the stagnation point (H = 5.302 ft, H/R_e = 50)

and 5.302 ft (25 exit radii), respectively, above the lunar surface.

In the free molecular flow analysis, for the spacecraft altitudes considered, the scale of the horizontal momentum flux distribution is of the order of the spacing between engines. Thus, the horizontal momentum flux at a point on the surface is influenced by the contributions from all three vernier engines and is the vector sum of these contributions.

Under free molecular flow assumptions, shock waves, which involve strong intermolecular interactions, do not exist and the surface flow field induced by each engine is purely radial. Once the flow field from an individual engine has been established, it is a simple matter to find the flow field due to the interaction of all three vernier engines by vector superposition.

The flow fields for three engines are presented in Figs. 31 and 32. These flow fields are contours of constant horizontal momentum flux on the lunar surface beneath the descending spacecraft. Fig. 31 is for a vehicle altitude of 10.6 ft and Fig. 32 for an altitude of 5.3 ft.

The difference between the two contour maps is due to a transition from a flow whose momentum flux is radially outward (10.603-ft case) to a flow whose more central momentum flux is directed in toward the spacecraft projected center (the 5.302-ft case). In the latter instance the momentum flux can be looked upon as essentially radial from each of the engines, with interference

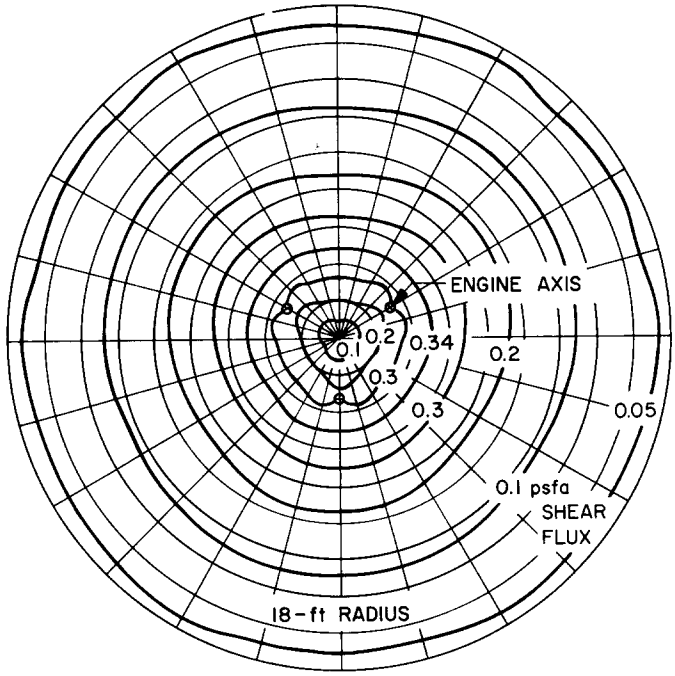

FLUX RADIATING OUTWARD FROM SPACECRAFT PROJECTED CENTER

Fig. 31. Constant momentum flux contours (H = 10.604 ft, H/R_e = 50)

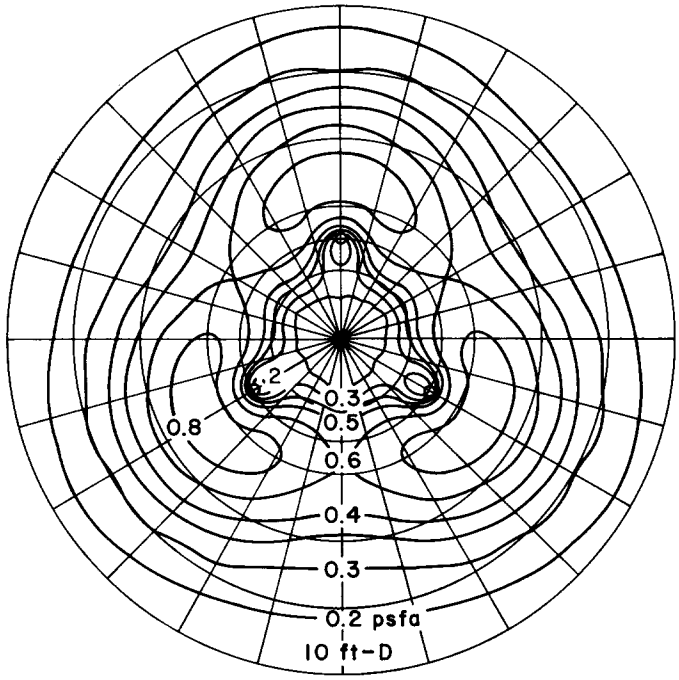

FLUX RADIATING APPROXIMATELY OUTWARD FROM PROJECTED CENTERS OF VERNIER ENGINES

Fig. 32. Constant momentum flux contours (H = 5.3 ft, H/R_e = 25)

CONFIDENTIAL
UNCLASSIFIED

UNCLASSIFIED

effects causing the pronounced warping of the lines of constant horizontal momentum flux.

e. Other analytical work. As outlined initially it is necessary to compare the results of the above free molecular flow analysis with the predictions of continuum flow models as applied to the *Surveyor* engines during the descent maneuver.

Roberts' analysis (Ref. 6) is predicated on a density variation in the vernier engine plume somewhat different from the one assumed here. He assumes the density along a line normal to the central streamline to be

$$\frac{\rho}{\rho_e} = B\left(\frac{h}{r_e}\right)^{-2} \cos^{k+2}\theta,$$

where

h is the distance from the engine exit plane

$( )_e$ refers to conditions at the engine exit plane

B is a constant equal to $k/2$

θ is the angle from the central streamline to the point in question

k is a constant related to the gas and engine considered

$$k = \gamma(\gamma - 1) M_e^2$$

This function does not fit the density variation determined from Fig. 27 well.

For purposes of comparison Roberts' work was used to predict maximum shear stress in two ways:

(1) By using his approach and his assumed form for the density variation in the exhaust plume.

(2) By using his analytical approach but substituting the form of the density variation in the exhaust plume developed in Section II.

The free molecular flow analysis was also compared with the work of Edwards (Ref. 7) who used much the same form of the density variation in the vernier engine plume as is used here. The engine parameters originally used by Edwards were for another engine. For this comparison the maximum shear stress at the lunar surface was predicted using Edwards' method with the parameters for the present vernier engines.

The maximum shear stress for vehicle altitudes of 50 and 25 exit radii, approximately 10 and 5 ft, respectively, are presented in Table 19. The four ways in which these

Table 19. Maximum horizontal momentum flux on the lunar surface

Prediction method	Maximum horizontal momentum flux (lbs/ft²)			
	Vehicle altitude = 10.6 ft ($h/R_e = 50$)		Vehicle altitude = 5.3 ft ($h/R_e = 25$)	
	Single engine	Three engines	Single engine	Three engines
Free molecular flow	0.18	0.34	0.71	0.90
Roberts' method using:				
(1) Roberts' plume density function	0.042	0.042	0.12	0.12
(2) Plume density function appropriate to *Surveyor* vernier engine	0.0022	0.0022	0.0061	0.0061
Edwards' method	0.00015	0.00015	0.00043	0.00043

were calculated correspond to (1) the present free molecular flow analysis; (2) Roberts' method of calculation using his form of the assumed density variation; (3) Roberts' method using the density variation from Section c, and (4) Edwards' analysis using parameters for the present vernier engine.

The free molecular flow analysis itself is based upon a force balance on an object projecting above the lunar surface (Fig. 33). The incident molecules are reflected diffusely and elastically (see Section d), and associated with this is a shear equal to the horizontal component of the incident momentum flux. The object is also acted upon by the reflected momentum flux from other incident molecular beams. The vector sum of these forces is termed the horizontal momentum flux, that is, the momentum convected through a unit area normal to the lunar surface in unit time. This momentum flux is the force on a unit area required to stop the flow.

In comparing these analyses, it should be noted that the free molecular flow model includes two terms in the

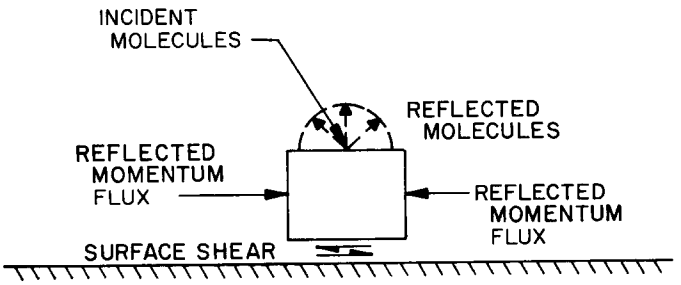

Fig. 33. Illustration of force balance

UNCLASSIFIED

UNCLASSIFIED

horizontal flux: one the force required to redirect the incident flow, the other the momentum convected past the point of observation. This latter term is analogous to a "dynamic head." However, the continuum analyses calculate the viscous shear force only; that is, the retarding force exerted on the flowing fluid by the surface. In these analyses this dynamic head term is not included; and consequently, their predicted viscous shear stresses are expected to be lower than the predictions of the free molecular analysis.

The free molecular analysis assumes that all molecules undergo elastic collisions with the lunar surface. This is the same as assuming a thermal accommodation coefficient of zero. A more realistic estimate of this coefficient would place it nearer unity (Ref. 8), and would lead to significantly reduced values of the horizontal momentum flux. Thus, the present free molecular analysis tends to predict values of the horizontal momentum flux significantly greater than one would expect to observe.

f. Experimental investigations. To the authors' knowledge, four pieces of experimental work pertinent to this problem have been generated. Stitt (Ref. 9) investigated the effect of various de Laval nozzles on dusty surfaces by measuring pressure distributions and observing, qualitatively, erosion patterns. Spady (Ref. 10) blew down a small de Laval nozzle in an evacuated bell jar onto a (balsa wood) dust-covered surface. Land and Clark (Ref. 11) blew down a nozzle in a large, evacuated environmental chamber onto a simulated lunar surface. Data on crater erosion and normal pressure information as a function of position under the jet were generated.

Marte and Fox (Ref. 12) investigated the behavior of yarn tufts on a flat plate beneath a scale model of the *Surveyor* spacecraft using cold nitrogen jets to simulate the vernier engines. Their purpose was to investigate possible induced backflow from the interaction of the plumes in the vacuum environment and no quantitative data germaine to this study were obtained.

Shock standoff distances and shapes predicted by both Roberts and Edwards were compared with Schlieren photographs by Land and Clark. The predictions of Edwards compared quite well with the experimental results, while Roberts' predictions compared well at the centerline but deviated considerably for angles greater than about 20 deg. While this sort of comparison does yield a high degree of confidence in the analytical ability of these authors, especially Edwards, to predict the shape of the shock layer, it does not completely validate their shear stress predictions since these latter calculations are based on additional assumptions. Comparison of the shape of the erroded crater found by Land and Clark does seem to lend qualitative confidence in the shape of the shear stress functions calculated analytically by Roberts and Edwards.

As in the analytical work, the experimental work was done well within the continuum flow regime and thus is not directly comparable to the rarefied gas transition flow regime under examination in this study.

g. Analysis of spacecraft heating. In this free molecular flow model there is no energy exchange between incident gas molecules and the lunar surface. This leads one to question the amount of heating the spacecraft may undergo due to impingement by these reflected gas molecules.

To answer this question strictly adhering to the model with which the shear stress seen by the surface is calculated leads to a rather tedious integration over the entire interaction flow field on the lunar surface for each point on the spacecraft. To obtain a first cut on the answer with little difficulty, a crude, extremely conservative solution was obtained by assuming the total energy of the flow to be its kinetic energy content, and considering this energy to be hemispherically re-emitted from a point on the lunar surface directly below the spacecraft center.

For a descent from 50 ft to a cutoff at 10 ft at a constant, vertical velocity of 5 ft/sec, the maximum total heat input to the underside of the spacecraft is 0.194 BTU/ft^2; for a 10-mil thick sheet of aluminum this corresponds to a temperature rise of approximately 10°F. For a similar descent to a 5-ft cutoff point, the maximum total heat input is 0.46 BTU/ft^2; and the corresponding temperature rise is approximately 20°F.

h. Conclusions. The results of this study, contained in Table 19, indicate that the shear stress on the lunar surface will be between 0.0004 and 0.9 lbs/ft^2 at an altitude of 5.3 ft. The actual shear stress expected at the surface is nearer the lower of these values. It can be said with confidence that the shear stress on the lunar surface due to the jet is less than 0.9 lbs/ft^2. Estimates of the lunar surface shear strength (derived from Refs. 13 through 17) indicate the shear strength of the lunar surface is nominally 1 psi (144 lbs/ft^2) and is not less than 0.1 psi (14 lbs/ft^2). By comparing this with the maximum possible shear stress of 0.9 lbs/ft^2 it can be concluded that the vernier engine exhaust plumes will not transport dust

UNCLASSIFIED

UNCLASSIFIED

for a cutoff altitude of 5.3 ft. if the predicted minimum shear strength of the lunar surface is accurate within one to two orders of magnitude.

Spacecraft base heating due to surface reflection was also investigated and found to be of no concern for a cutoff altitude of 5.3 ft.

5. Helium Relief Valve Tests[5]

Work was completed at JPL on the program to perform limited environmental tests of selected upstream components for the purpose of evaluating, on an independent basis, the capability of these components to meet the *Surveyor* requirements.

The final component to be evaluated under this program was the helium relief valve designed and manufactured for HAC by the M. C. Manufacturing Co. The purpose of these valves in the vernier propulsion system is to prevent overpressurization of the propellant tanks in the event of a malfunction of regulator lock-up.

Previous testing of this component at JPL followed the HAC approval test specification 262695 and results were reported in *SPS* 37-36, Vol. 1, p. 100.

As an additional test this valve was given an exposure to oxidizer vapors to verify propellant compatibility. This test consisted of directly exposing the test valve to the vapors in equilibrium with liquid oxidizer (a mixture of 90% N_2O_4 and 10% NO) at ambient temperature. The exposure consisted of 152 hr at 75°F followed by 60 hr at 100°F and 24 hr at 75°F. (Total of approximately 10 days exposure.)

In actual spacecraft use, although the vernier propulsion system may contain propellants up to 30 days, the relief valve would not normally be exposed directly to the vapors but would see only those vapors which permeated through the propellant tank bladders. For this reason it is considered that the exposure test was conservative.

Following the oxidizer exposure, functional tests of cracking pressure, reseat pressure, and leakage were conducted. The functional tests were performed at ambient temperature (75°F), low temperature (0°F), and high temperature (100°F).

The results of the leak tests indicated no detrimental change in leakage due to either the oxidizer exposure or the high and low temperature functioning. Leakage was within the specification value of 1 cc/hr of helium at standard conditions.

The cracking pressures in the ambient and high temperature tests were below 840 psig, thereby meeting specification requirements. However, the cracking pressure in the low temperature test was 849 psig, which is higher than the specification allowance. The cracking values at ambient and high temperature were respectively 832 psig and 830 psig. Had the initial cracking setting been lowered by 10 psig it appears that this value would have passed all cracking requirements.

The reseat pressures were consistently below the minimum specification value of 800 psig. At ambient conditions the reseat pressure was 790 psig; at low temperature, 781 psig; and at high temperature, 792 psig. The fact that this particular valve had a larger spread between crack and reseat pressures at low temperatures than allowed by specification is not considered a serious problem, since testing of other valves of this design are meeting crack and reseat specifications.

Upon completion of testing, the relief valve was disassembled for inspection. Several parts showed evidence of corrosion from the oxidizer vapors. The return spring was corroded excessively. The piston was slightly corroded along the outside diameter nearest the seat. The bore was corroded moderately at the areas nearest to contracting the seat supports. There were no apparent effects of the test on either the piston nose seal or the seat.

On the basis of the limited testing conducted to date, the M. C. Manufacturing Co. helium relief valve appears to be able to meet the requirements of the *Surveyor* vernier propulsion system. A more complete qualification testing program on this design is now being performed by HAC.

6. Thrust Chamber Assembly[6]

The program for *Surveyor* vernier engine [Reaction Motors Division (RMD) Model No. TD-339] evaluation continued with 17 firing tests, 4 propellant flow calibrations, and a simulated thermal cycle, all at ETS in March and April, and two tests at JPL's environmental test facility during the last half of February and March.

[5]Prepared by Technical Section 384.

[6]Prepared by Technical Section 384.

UNCLASSIFIED

UNCLASSIFIED

Following is a summary of these activities.

Group	*Test No.*	*Test Date*	*Purpose*
22	–	Feb 15 – Mar 23	Injector salting
23	DY 86 to DY 99	Mar 2 – Mar 29	Reduced water content in fuel
24	DY 100	Apr 4	Propellant line conditioning
25	DD 119	Apr 6	Thrust vector
26	DY 101	Apr 8 – 22	Pyrochrome paint confidence test
27	–	Apr	Shutoff valve poppet material improvement

a. Injector salting test—Group 22. The thrust chamber assembly (TCA) under certain conditions has experienced an undesirable oxidizer injector restriction which results in reduced oxidizer flow rates. This problem has been identified as being due to the formation of nickel salts $Ni(NO_3)_2$ in the nickel injector resulting from a chemical reaction between residual oxidizer (MON-10), the nickel injector material, and moisture from the atmosphere. This condition has been experienced both at Holloman Air Force Base (HAFB) on the *Surveyor* T-2 descent program and at RMD of Thiokol Chemical Corp. after test fire shutdown of sea level engines.

These salts, being water soluble, are easily removed by flushing with water. In fact this procedure is now employed at HAFB as part of the post-test operations whenever flow tests indicate a salting condition.

Altitude engines employed on flight spacecraft will not experience injector salting following midcourse firing due to the absence of moisture and the purging action of the space vacuum. However, under the prelaunch conditions at the AFETR with an expected 20-to-30-day period from propellant loading of the spacecraft to launch, the thrust chamber assemblies (TCAs) will be exposed to limited humidity conditions. During this period the spacecraft is handled in an air-conditioned building until encapsulation in the shroud. Following encapsulation, conditioned air is supplied to the shroud.

The propellants are contained in the vernier propulsion feed system and the TCAs under a pad pressure of approximately 300 psig. The TCA shutoff valve prohibits the propellants from entering the injector until the moment of firing. Under these conditions one would not expect injector salting to occur. However, the TCA shutoff valve has a small but finite leakage rate, so the question was raised whether this leakage through the shutoff valve and the injector over the maximum prelaunch period and humidity conditions could result in detrimental salt formation.

A test program was conducted in the JPL environmental laboratory to simulate the AFETR storage conditions to check on the extent of injector salting. Two thrust chamber assemblies, serial no. 532 and 522, were loaded with oxidizer, pressurized to pad pressure levels, and subjected to an environment of 65 to 72% relative humidity at $75 \pm 5°F$ for a period of 20 and 33 days, respectively. The selected test conditions represented an upper bound to the humidity environment expected in either the air-conditioned building or the air-conditioned shroud. The pad pressure was gradually reduced during the test period to simulate the pressure decay which actually occurs on a spacecraft.

Prior to testing, each engine was subjected to proof and leak check, water flush, and a reference flow calibration. At the end of the exposure the TCAs were again flow calibrated, water flushed, and recalibrated. No significant change in flow calibration was noted for either the 20-or-33-day exposure TCAs.

Based upon the results of this test it was concluded that it is highly unlikely that any detrimental accumulation of nickel salts will occur at the AFETR, even with the maximum possible exposure period of 30 days.

b. Reduced water content in Fuel—Group 23. In view of the low over-all performance (nominal to -3σ) which has been exhibited by a number of the production TCAs, the fuel propellant blend (monomethylhydrazine monohydrate) was restudied to see what improvement in performance could be gained by reducing the water content.

UNCLASSIFIED

UNCLASSIFIED

At the same time it was desired to reconfirm the margin of cooling that was available in the TCA under transient conditions with the hydrated fuel. An earlier analysis indicated that the total impulse and heat capacity were both maximized with 28% hydrated fuel for an oxidizer-to-fuel ratio (O/F) of 1.5.

However, there were some data from the RMD margin limit test series that indictaed a possible disproportionate increase in injector efficiency with the attendant increase in specific impulse at an O/F of 1.5 for fuel containing 20% water.

To explore this fuel blend further, a series of 14 firings were performed at Edwards Test Station (ETS) on TCA serial no. 519 (modified with sea-level nozzle), 535 and 538 (flight types). Each test series was defined by a specific thrust profile (ETS profile A, Fig. 34) composed of two firing periods. The first firing period started with cyclic operation of 2.5 to 80 Hz imposed on mid and low thrust to confirm dynamic response, and steady-state points to confirm specific impulse. Step transitions from high to low thrust were employed to evaluate fuel cooling characteristics. The second firing followed engine shutdown by 1 hr to check restart and repeatability of performance. Propellants for all tests were at ambient temperatures and saturated with helium.

In order to evaluate performance changes each TCA was tested with fuel containing 28% water for reference data (Test No. DY 86 and 87 for TCA 538, DY 94 and 95 for TCA 519, and DY 96 and 97 for TCA 535). All other tests were with fuel containing 20% water (Test No. DY 88 and 89 for TCA 538, DY 90 to 93 for TCA 519, DY 98 and 99 for TCA 535).

A small increase in performance was observed. For TCA 535, from mid to full thrust, there was an 0.8 to 1.5% increase in Isp and c*. The range of increase represents data scatter and not any effect of thrust level. The theoretical increase predicted was approximately 1.5%.

There was no change in performance for TCA 538; however, there was an indication of a fuel leak for the 20%-water-in-fuel test that would negate any valid comparison.

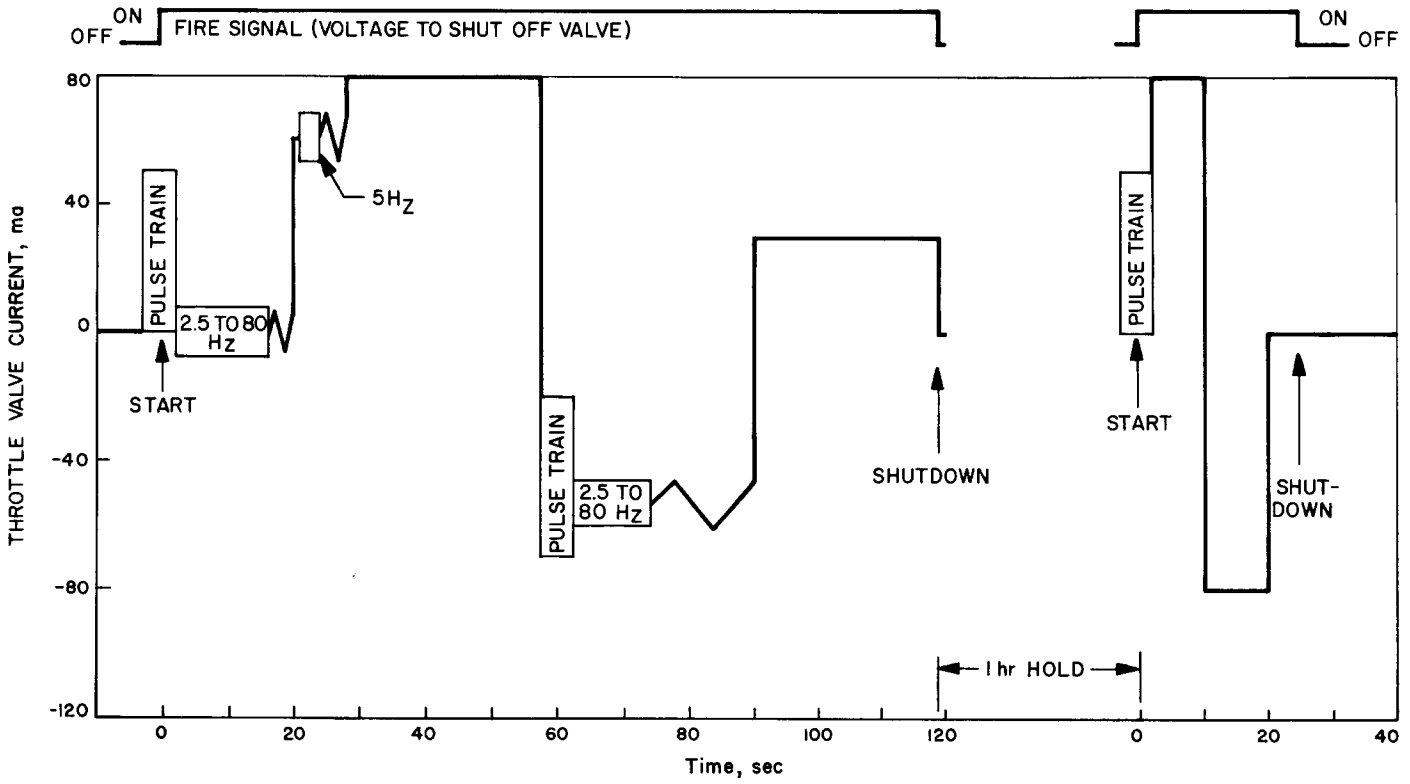

Fig. 34. ETS profile "A"

UNCLASSIFIED

UNCLASSIFIED

A larger increase in performance was noted for TCA 519 with the sea level nozzle. The Isp increased from 1.8 to 2.9% with 1.5 to 2.0% increase in c*. The difference between the data obtained with the TCAs is probably due to changes in nozzle performance (between altitude and sea level nozzles) and the fact that TCA 519 is a high-performing engine while 535 is a low one.

In one of the two tests with 20%-water fuel, where TCA 519 was restarted after a 1-hr hold, there was a delayed start. This is characteristic of a reduced margin of fuel cooling which allows heat soak-back after shutdown to decompose fuel in the cooling jacket.

In summary, it is concluded that although a small increase in performance for 20%-water fuel is possible, it is offset by the reduced fuel density when considering the total impulse for the vernier engines, as constrained by the spacecraft tankage volume. Furthermore, the indication of a detrimental reduction in cooling margin makes it undesirable to reduce the water content from the present value of 28%.

c. Propellant line conditioning—Group 24. A recent study has shown that if various portions of the spacecraft are allowed to drop below their lower specification temperature limits during the period when the spacecraft is in the Earth's shadow, then the available launch window durations can be significantly increased.

Two of these items which would cool below presently-allowed temperatures are the propellant feed lines to one of the TCAs. Analysis has shown that under the shadow conditions the lines could drop to −30°F but would then heat up again above the present limit of 0°F well before the midcourse firing.

During the cooling period the TCA would always remain above its 0°F lower limit, so that the only real concern is whether the fact that the propellant feed lines chill and then heat up could cause any unexpected problems. Since the normal freezing point of the oxidizer is approximately −10°F, the oxidizer would be expected to start freezing during the shadow period and then thaw before midcourse firing.

In order to determine the effect of low temperature (−30°F) conditioning of the propellant feed lines on vernier engine start performance, a test was conducted simulating the shadow conditions. The test was performed at ETS in altitude test stand DY. The propellants were 75 to 100% saturated with helium at 300 psig at ambient temperature conditions. The propellant lines were vacuum filled with a subsequent bleed of ½-gal for each line to assure saturated propellants to the shutoff valve.

The propellant feed lines within 1 ft of the TCA were enclosed in a bag, Fig. 35, and conditioned with cold N_2 gas to −45 ±5°F for ½-hr and then allowed to warm up to a minimum of 35°F for at least 30 min prior to firing. The orientation of the TCA was with the thrust axis and the cooled portion of the propellant lines horizontal, minimizing any gravity effects that might stratify, with non-uniform freezing, the MON-10 oxidizer.

The results of this test (DY-100) are summarized below and compared with a previous test (DY-86) performed on the same TCA under nominal conditions.

Run Number	*DY-86*	*DY-100*
Type of test	Reference-nominal conditions	Conditioned-freeze-thaw
Propellant conditioning	He-saturated	He-saturated
Test program	ETS profile "A" (Fig. 34)	20 Sec of ETS profile "A"
"Fire relay" to ignition	45 msec	48 msec
Ignition to 1st thrust peak	50 msec	45 msec
Thrust at "fire relay" plus 150 milliseconds	56 lb	58 lb

It was noted that there was no discernable effect on TCA performance caused by temperature cycling of the propellant lines. The data from both tests were found to fall within the time-thrust envelope of JPL specification SAM-50355-DSN-A and are considered normal.

d. Thrust vector—Group 25. The thrust vector data from tests DD-115 and DD-118, which were reported in *SPS 37-38*, Vol. I, pp. 62–70, had shown that a small

UNCLASSIFIED

UNCLASSIFIED

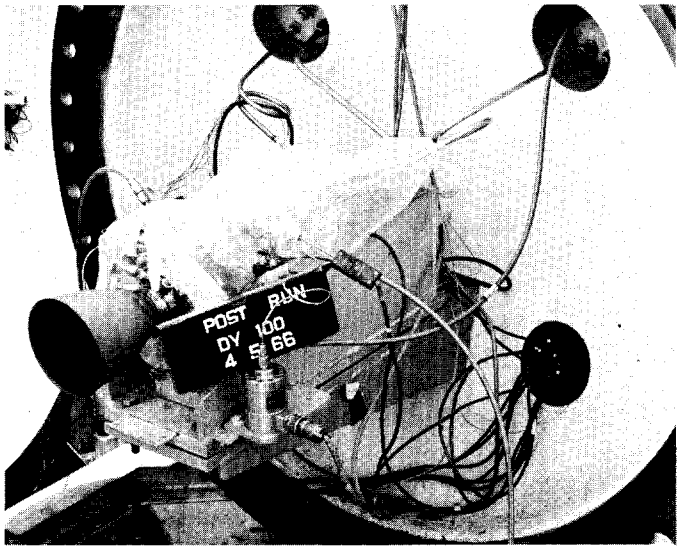

Fig. 35. TCA with propellant feed lines enclosed in temperature conditioning bag (test DY-100)

thrust vector side force had been observed during each firing predominately in the vertical downwards direction. A review of the setup and test procedure was made to see if some unknown factor or coincidence caused the two different TCAs to have the same side force in magnitude and direction.

One procedure was questioned. The TCA had been aligned with the thrust vector stand axis with the unit in a horizontal position. It was theorized that the weight of the alignment fixture, which is cantilevered from the TCA nozzle extension, was heavy enough to deflect the nozzle extension downward. When the fixture was removed after alignment the nozzle would then cant upward.

To test the theory another TCA alignment was made with the thrust vector stand in a vertical position (Fig. 36). A 60-sec test firing (DD-119) was performed with TCA 535 cycling twice to minimum, mid, and maximum thrust.

Measurements of the side force and tabulated angles which were derived through application of the appropriate correction factors are noted below for the case of a commanded thrust of 100 lbs.

Plane	*Side Force, lb*	*Angle, deg*
Horizontal	0.093	0.050
Vertical	0.010	0.017

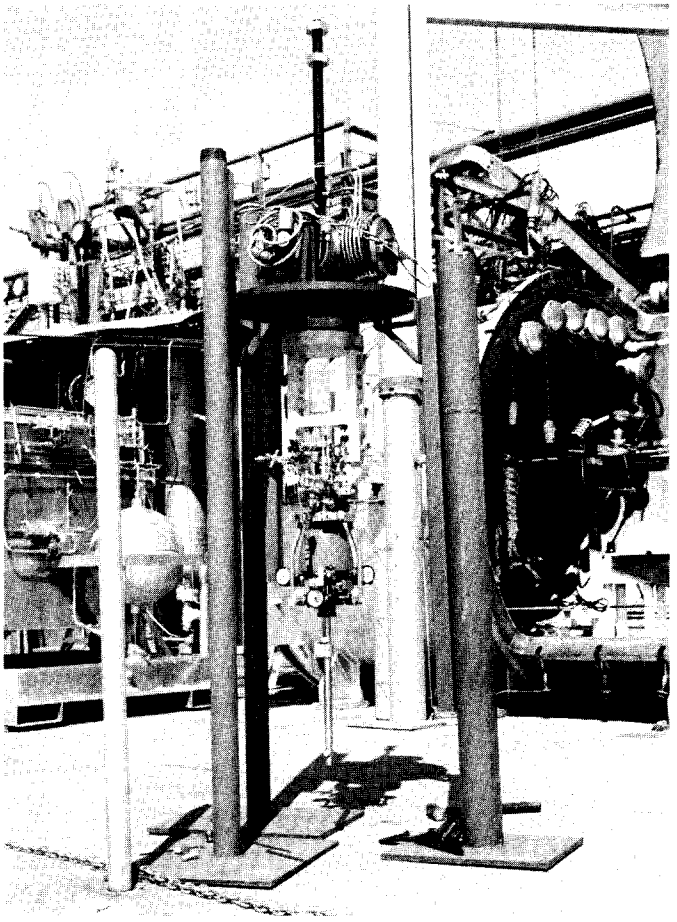

Fig. 36. TCA undergoing alignment in vertical fixture (prior to test DD-119)

The side force is very small and for this test was primarily in the horizontal plane. There apparently was a bias introduced into the thrust vector measurements by the previous alignment procedure that has been minimized in this test. It was also observed recently that with such small side forces the system friction, while small, may bias the measured data by several hundred percent but even with this bias the angles are acceptable. The measured thrust vector angle at maximum thrust for test DD-119 is about ⅛ of the specification-allowable angle of 0.3 deg for flight TCAs.

It is concluded that the data reported previously (*SPS 37-38*, Vol. I, pp. 62–70) are in error but the conclusion reached at that time, namely that the thrust vector deviation angle is within specification, still is valid.

e. Pyrochrome paint confidence test—Group 26. Testing of a vernier engine under simulated ground handling and launch environments through midcourse firing was

UNCLASSIFIED

UNCLASSIFIED

initiated at the end of this period to establish confidence in the integrity of the nozzle pyrochrome paint. The testing was to establish whether flaking of the pyrochrome paint could result in particles of sufficient size and number to affect other parts of the spacecraft, particularly the Canopus sensor.

TCA serial no. 559 was subjected to a number of ground-handling operations including nozzle joint conductance testing, a simulated thermal paint bake cycle, flow test, and thrust vector alignment. It was then subjected to launch vibration, shock, rapid pressure pump down and a midcourse firing (DY-101). Size and number of liberated particles were determined for each of the critical operations.

Preliminary results indicate that the number of particles of pyrochrome paint (or any other materials which may flake from the TCA) is sufficiently small that the probability of any such particle drifting into the field of view of the Canopus sensor is insignificant.

f. Shutoff valve poppet material improvement—Group 27. Data from the material compatibility tests reported in *SPS 37-38*, Vol. I, have shown that both plain and filled Teflon are compatible with the monomethylhydrazine hydrate at lunar survival temperatures.

A review of some of the early RMD development work indicated that although several types of Teflon-based poppet seals had been explored, a plain Teflon poppet had not been tried in the fuel side of the valve. One of the designs that had been tried employed 25% laminated glass filled Teflon but was found to leak due to quality control associated with the direction of lamination. It was felt that the leakage path followed the laminate. In addition a Teflon-coated stainless poppet was tried, but there were problems of process control and low resistance to wear under repeated cycling. The present design employs a Nylon 101 poppet.

Based upon the encouraging results of the previously reported JPL compatibility investigations and the early RMD work, a program has been initiated at JPL to evaluate further the use of Teflon in the valve. A poppet with a plain Teflon seat has been machined and assembled in a shutoff valve and is ready for test. Filled Teflon (nonlaminated) has been analyzed to check the filler material and the data are being reviewed. Additional quantities of the material are being obtained for further evaluation and test.

M. Spacecraft Vehicle and Basic Bus Mechanisms

1. Spacecraft Vehicle

Vehicle activities reported in this section include the design and fabrication of spacecraft and substructure and the assembly of complete vehicles for flight and test spacecraft. Fabrication, assembly, and tests of the thermally controlled equipment compartments, wiring harness, and landing gear are also included. Items such as overall spacecraft configuration studies and weight reports are reported in the following discussion.

a. A-21 flight and test vehicle status. Final drop testing was completed on the T-21, thus concluding the test program. At JPL's request, T-21 was shipped to Goldstone March 21 where it will be used for personnel training.

SC-1 was shipped from HAC February 18 for combined systems test with the *Atlas/Centaur* at GD/C, San Diego, This test was satisfactorily concluded, and the vehicle was then air transported to AFETR March 13.

SC-2 was returned from initial systems checkout to the fabrication area for upgrade, weight, balance, and alignment. SC-2 was delivered to the optical alignment dock with the planar array solar panel and radar altimeter and doppler velocity sensor system missing. Consequently, the procedure sequence was changed in order to conduct the actual mass property determination at the end of the weight, balance, and alignment schedule.

Several problems were encountered (and solved), and the overall weight, balance, and alignment operation was considered successful. This is the first time a spacecraft has gone through the complete operation, utilizing the full direction and control procedure. SC-2 was then returned to the system test area.

Fabrication and final assembly was completed on SC-3, and the initial systems checking was started.

Final inspection buy-off problems with the material review board on the SC-3 spaceframe have necessitated re-evaluation of the spaceframe and substructure engineering drawings. A complete dimensional tolerance study is being undertaken to create a firmer engineering baseline from which to make material review board buy-off decisions.

SC-4 is proceeding through final assembly.

UNCLASSIFIED

UNCLASSIFIED

The engineering for SC-5 through SC-7 is approximately 80% complete and is proceeding on schedule. Engineering drawings for the new thermal compartments A and B have been released for building the developmental hardware.

S-9 engineering payload structural test model and S-10 thermal test model vehicles continued in various phases of testing.

b. A-24 flight and test vehicle status. Major emphasis has been placed on the A-21 series. A limited program for the A-24 model is discussed in the following paragraphs.

The detailed specifications for the touchdown dynamics instrumentation subsystem landing gear potentiometer were completed and released, and the detailed engineering drawings were completed. TAT and FAT specifications were prepared and submitted for comment prior to final signoff and release.

The detailed specification for the touchdown dynamics instrumentation subsystem lunar contact switch has been written and distributed for approval, but implementation in detailed design has met with difficulties. Two major design problems are that the switch must be capable of sensing lunar surface materials ranging from zero crushing strength to that of granite, and that the switch, operating with these extreme conditions, must have sufficient dwell time to produce a suitably long signal pulse so that it will not be masked by noise spikes.

Work continued on weight saving concepts with material evaluation being narrowed to substitution of 6AL4V titanium and Lockalloy (beryllium-aluminum alloy) tubing. Procurement time spans and increased fabrication difficulties or special required in-house fabrication facilities seem to preclude use of these materials in the mod 56 program.

Investigations were also made to improve the design concepts of spaceframe, substructure, and compartments. These studies reaffirm that within current schedule and cost constraints, the current 7075 aluminum tubular structure is the most desirable design.

c. Testing. The flexline assembly that transmits propellant and hydrogen to the gimballed 1 thrust chamber assembly is undergoing tests to verify its compatability with the parallel backup design of a 12-deg roll actuator.

2. Basic Bus Mechanisms

a. Antenna/solar panel positioner (A/SPP). The A/SPP provides mounting, positioning, position indicators, and launch and landing locks for the planar array antenna and solar panel. The antenna support structure includes controllable axes for roll, elevation, and solar and polar rotations. The drive for each axis uses a solenoid stepper motor for power and a wirewound potentiometer for position indication.

A/SPP drive test results from the SC-2 FAT in January required that lubricants and bearing materials in all transmission gear journals be modified. Nine drives incorporating the modifications have been fabricated and tested. Four of these drives completed FAT in A/SPP 287580-1 with no indication of degradation. Four other drives installed in A/SPP 2 completed the same number of steps as required for FAT with excellent performance.

The remaining drive completed an extended life test and was subjected to 260,000 steps at combined loads of 0 to ± 64 in.-lb unbalance load, 24 in.-lb friction, and 5 slug-ft^2 inertia. The drive successfully completed the test at 250 and -250°F with no degradation of performance. Following the test, all parts of the transmission and motor were disassembled and inspected for wear. All wear was minimal, and the gears and journals were in excellent condition.

The performance of the A/SPP drive motor, when subjected to conditions of extremely high vacuum, high temperature, and continuous drive, has been the subject of several investigations of both the drive mechanism and the complete A/SPP. Tests are in process to determine design modifications to lower coil temperatures and increase operational reliability of the wire insulation.

The new lockpin puller/switch module design, which is self-aligning and capable of being bench adjusted, has been completed. All detailed drawings for classes III and IV lockpin puller/switch hardware have been released, and tooling required for fabrication, assembly, and test is being fabricated. Fabrication of class III hardware to be used in developmental tests is 90% complete; class IV hardware is 25% complete. A developmental A/SPP will be used in design verification testing and will be employed to confirm the retrofit and installation procedure.

Testing of the cone worm and sector gear at 70 and -250°F at ambient pressure has been completed. The torque transducer specifically designed for operation in

UNCLASSIFIED

UNCLASSIFIED
CONFIDENTIAL

vacuum in the −250 to 250°F temperature range has been installed in the test fixture and calibrated.

b. Advanced antenna/solar panel positioner. The jackscrew design A/SPP development program has been initiated as a major design revision for SC-5. The major objectives of this change include the following:

(1) Replacement of the existing worm and sector gear polar axis drive with a jackscrew drive three-bar linkage mechanism.

(2) Redesign of the solar and elevation axes to a torque tube drive design.

(3) Redesign of pin puller installation design.

(4) Provision for incorporation of the high-torque stepper motor and the improved design transmission in all axes.

(5) Redesign of the solar panel support arms.

(6) Revision of the A/SPP wiring harness.

Preliminary design loads have been established based on factoring of the existing A/SPP experimentally determined loads.

Concurrent with the design layout preparation, sizing of the axes' radial, thrust, and jackscrew bearings to provide acceptable dynamic and operating loads bearing stresses has proceeded. Table 20 provides a list of the preliminary bearing stress and material selection for landing impact loading.

The varying lever arm of the jackscrew drive produces a variable polar angle step increment per stepper motor pulse as a function of polar angle. To determine the jackscrew's threshold of irreversibility, a study of the nut restraining torques produced by nut-to-lead screw and nut thrust bearing friction was performed to determine irreversibility dependence on the coefficient of friction (μ). For the selected lead angle of 10 deg and other design details, the screw is irreversible for μ greater than 0.06 deg.

Table 20. Jackscrew design A/SPP preliminary bearing stress and materials selection (Maximum lunar impact loading)

Axis or bearing	Impact load		Bearing stress, psi		Bearing material
	Bending movement, in.-lb	Axial force, lb	Radial	Thrust	
Solar	12,400	480	2,470	332	Fluorosint
Polar pivot	20,200	1,210	13,750	515	DU (combination of metal and teflon)
Elevation	26,300	706	5,790	297	Fluorosint
Roll	28,400	760	5,160	319	Fluorosint
Jackscrew gimbal bearing		2,765	19,600		DU
Jackscrew ball end		5,530	34,600		Dry lube 7075-T6
Jackscrew nut thrust bearing		5,530		5,350	DU

Layouts of the jackscrew polar axis, elevation and roll axis, solar axis, antenna support structure, solar panel support arms, and pin puller subassembly have been completed.

Tentative material selections have been made for all radial and thrust bearings and are listed in Table 20. Tests of the coefficient of friction of these materials at the operating loads while exposed to high vacuum (10^{-8} torr) and low temperature (−250°F) are in process.

Table 21. Candidate jackscrew and nut material combinations

Material	Finish	Lubricant	Material	Finish	Lubricant
7075-T6 aluminum alloy	Anodize 16 rms finish	Lubeco 905 burnished dry lube	7075-T6 aluminum alloy	Anodize 16 rms finish	Lubeco 905 burnished dry lube
7075-T6 aluminum alloy	Hard anodize 8 rms finish	In nut material	Westinghouse lubricant compacts	Anodize 32 rms finish	MOS_2 and teflon in nut material
7075-T6 aluminum alloy	Hard anodize 8 rms finish	In nut material	LNP polycarbonate composites	Anodize 32 rms finish	Teflon in nut material

CONFIDENTIAL
UNCLASSIFIED

UNCLASSIFIED

Verification of the low-temperature impact loading capability of these materials is also being performed.

Several combinations of jackscrew and nut materials will be screened through frictional torque, low-temperature dynamic loading, and wear tests to determine the most suitable selection. Combinations to be investigated are listed in Table 21. Additional materials and finish combinations, such as Boeing Company lubricant compacts, are being considered.

Test planning is divided into three categories: design verification, flight acceptance, and type approval testing. Design verification test plans to ascertain adequate performance of the major subassemblies, including critical environmental exposures, have been prepared. Test fixtures and equipment are being assembled. The major subassemblies are as follows:

(1) Solar axis and solar panel support arms.

(2) Jackscrew—polar axis subassembly.

(3) Elevation and roll axes subassembly.

(4) Pin puller subassembly.

(5) Wiring harness.

(6) Antenna support structure.

Materials and lubricants screening and physical properties identification tests are being conducted to verify acceptability of the design selections. Potentiometer high-vacuum exposure life tests are also in process to verify lubrication techniques.

An alternate to the new A/SPP design is model 293275 which embodies minimal changes to the existing A/SPP but enhances reliability by increasing the web thickness of the sector gear and the wall thickness of the antenna support tube and elevation axis motor housing.

Two layouts and 14 new or revised drawings were required for this new configuration. Layouts are complete, and all new drawings have been completed. Fabrication of the redesigned portions of the A/SPP has been initiated for developmental test purposes. A formal design review was conducted on March 16.

c. High-torque motor and transmission design. The design was completed for the plug-in planetary gear transmissions for the 293275 and 293300 A/SPP units. A gear consultant has been retained and is currently reviewing all transmission designs. Mechanics Research, Inc. is reviewing the static and dynamic loads on the gear transmissions.

d. Test. Component tests determined linear solenoid force versus armature displacement under various coil current magnitude conditions. Another component test determined detent torque versus displacement. Other tests determined the output torque profile including the power stroke and the detent stroke effects during the 40-deg step of the motor.

Motor thermal rise tests were performed at sea level, vacuum, and room temperature conditions. The motor was pulsed at the rate of 2 pps with 65 msec pulses at an amplitude of 18 v. The vacuum test was instrumented with additional thermocouples to indicate conduction heat losses to the heat sink.

Motor endurance tests were also conducted. Following replacement of the sprocket with one fabricated of fluorosint, the motor endurance test was successfully completed. Examination of the cam surfaces following disassembly indicated no significant wear.

e. Thermal switches. A study and test program is being conducted to improve thermal switch performance by replacing the aluminum-backed mirrors with silver-backed mirrors. In the past, silver backing has not had the required adherence for thermal switch use. Optical Coatings Laboratory of Santa Rosa, California, has developed a process that provides greater adherence of the silver backing which may prove acceptable for thermal switch use.

Since silvered mirrors exhibit an absorptivity half that of aluminized mirrors, compartment heat dissipating capability could be increased by 100% without a weight increase or a mechanical design change. Silvered mirrors have been received and, following laboratory tests, will be assembled to thermal switches for testing the value of incorporation.

f. Omnidirectional antenna mechanisms. The two omnidirectional antenna mechanisms (A and B) use tapered Fiberglas cloth tubes bonded to aluminum hinge bracket assemblies. They deploy and lock the two omnidirectional antennas into operating position before separation from *Centaur*. A review is in progress on the alignment requirements as they affect the present hardware geometry. The Fiberglas tubes have been reinspected and found to be discrepant. Rework possibilities are being considered.

CONFIDENTIAL UNCLASSIFIED

UNCLASSIFIED

g. Separation, sensing, and arming devices. Three separation, sensing, and arming devices for each spacecraft provide redundant actuation of the postseparation squib firing circuits and vernier engine solenoid circuit after the spacecraft separates from *Centaur*. A review of the *Surveyor/Centaur* interface showed that a modification to the separation, sensing, and arming devices was needed to assure that switching would not occur during boost. This decision is the result of spacecraft and *Centaur* dynamic deflections during launch. The ease and simplicity of adjustment with the pedestal on *Centaur* was also considered. A redesign was initiated, and units of this new 293400 configuration are scheduled to be retrofitted on SC-1. The qualification of this design is scheduled to begin April 19.

h. Pyrotechnic devices. Three full sets of pyrotechnic devices for SC-1 completed FAT and were shipped to AFETR.

i. Manufacture of class III hardware. Drawing releases have been made for class III high-torque motors and gear trains. An advanced bill of materials has been issued for the ordering of class IV long-lead time items for the high-torque motor.

j. Subcontract. The subcontracting effort has been terminated because of the lack of adequate responses from eight suppliers. The best response received would have required extensive development effort. It was also too costly, and was overweight and oversize.

N. Scientific Payload

a. Testing. Cryogenic testing of *Surveyor* vidicons is being conducted to determine the probability and nature of any failures or changes in operating characteristics of the photoconductor or other parts of the vidicon tube. Thus far, 27 tubes have been subjected to cryogenic testing.

Failure of the photoconductor appears to depend on the absolute temperature and appears to be independent of the rate of change of temperature or prolonged exposure at low temperature. Catastrophic failure occurred in two tubes at a temperature of −148°F (Fig. 37). There was minor crazing, at the dark current corner references, in four older type tubes (Fig. 38). There were nine failures for open cathodes, grid shorts, and leaks. In addition, small changes in corner resolution were observed. These were attributed to shifting of the tube's structure and were probably caused by stress relief and differential

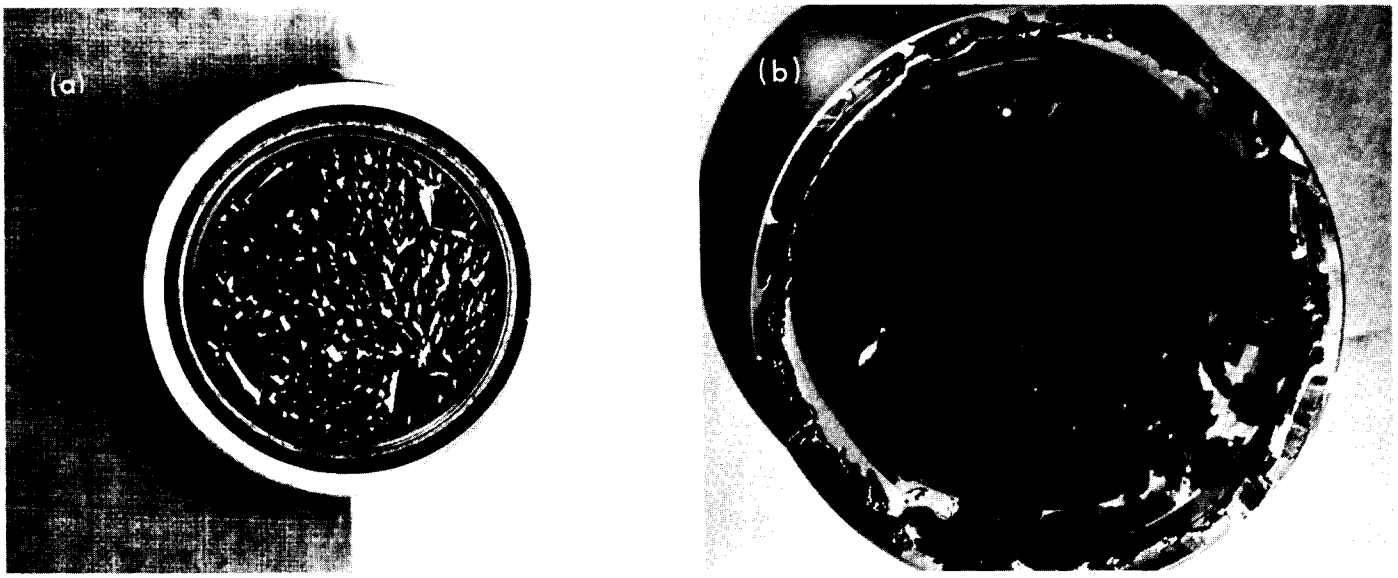

Fig. 37. Failure of photoconductor on older type vidicons after exposure to −118°F: (a) front view of photoconductor looking through faceplate; (b) rear view of photoconductor surface with faceplate removed

UNCLASSIFIED

UNCLASSIFIED
CONFIDENTIAL

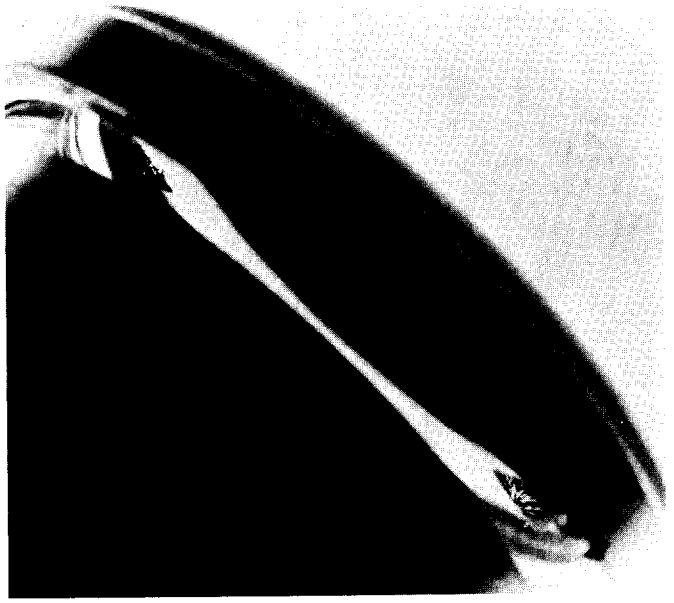

Fig. 38. Minor crazing of photoconductor on older type vidicon after exposure to −292°F

expansion. Wrinkling of the G-5 grid was observed in 24 of the tubes tested; the degree of wrinkling depends on the temperature. It was first apparent at −58°F as a slight puckering at the edge where the mesh was clamped to the support ring, and became progressively more pronounced after exposure to lower temperatures. Preliminary measurements indicated that wrinkling of the G-5 grid may contribute to shading. Some degree of self-straightening of this mesh with time occurs.

Previous tests showed that some vidicons are capable of withstanding a 48-hr exposure to liquid nitrogen while others fail catastrophically in this environment. Presumably the capacity to survive low temperature is completely dependent on tube manufacture. However, all five qualification vidicons used in this series of tests survived the 48-hr exposure satisfactorily. During September 1965 the first of two new vidicons of potential flight quality were exposed to a temperature of −292°F for 48 hr and failed catastrophically owing to separation of the photoconductor layer from the signal electrode layer.

The scope of the first series of testing included measurement of five conditions: negligible rate of change, increased rate of change, exponential rate of change, prolonged low-temperature exposure, and electrical measurements to differentiate between the effect of absolute temperature and rate of change of temperature. The initial tests were at a rate of 1.8°F/min, which was assumed to be slow enough that any failure could be attributed to only the low temperature. The low temperature limits used were −58, −148, −170 (flight transit temperature), −238, and −292°F (lunar night temperature). Twenty-three vidicons were used in this initial test. There were two catastrophic failures at −148°F. Four tubes evidenced slight crazing; three of the failures occurred at −292°F, one at −238°F.

After investigating the effect of absolute temperature, the effect of rate of change of temperature was examined at a rate of 3.6°F/min with the same lower limits. Five vidicons, previously successful at the 1.8°F rate, were used in this test. There were no failures of the photoconductor.

Testing was continued at an exponential rate in order to simulate the space and lunar environment. The tests were from room ambient at an initial rate of approximately 7°F/min to −292°F. The tests were performed with vidicons which had survived previous tests at this temperature at a 1.8°F/min rate of change. The same lower limits were used. Thirteen vidicons were used in this test, and there were no photoconductor failures.

To determine the effects of long exposure, vidicons which had survived previous testing were cooled at an exponential rate from room ambient to −292°F and soaked for periods of 3 and 18 hr in separate experiments. Four tubes were used, and there were no failures of the photoconductor.

The results of the above experiments to investigate the possibility and nature of gross failure, i.e., crazing or peeling of the photoconductor may be summarized as follows:

(1) Catastrophic failure of the photoconductor occurred at −148°F on 2 of the 27 tubes tested.

(2) Photoconductors that survived −148°F also survived at lower temperatures.

(3) Minor crazing was confined to the dark current references which may be considered areas of weakness in the older type of vidicons.

(4) Rapid rate of change of temperature or sustained soaking produced no observable effect.

In addition to determining gross failures of the photoconductor and tube structure, it was essential to evaluate the effect of low-temperature exposure on vidicon performance. Each tube was completely tested electrically

UNCLASSIFIED
CONFIDENTIAL

UNCLASSIFIED

before and after each cryogenic test. The following measurements were made: gas ratio, shading, distortion, sensitivity, video to dark ratio, erasure, 400-line center resolution, 400-line corner resolution, 600-line center resolution, cathode image, and test pattern.

The electrical measurements of vidicon performance during the cryogenic testing indicated a change and diminution. Three vidicons developed open cathodes after exposure to low temperature. Three vidicons developed grid shorts, and one vidicon developed a glass crack. Three tubes became gassy, and it is assumed they developed leaks, but the problem requires further study. In two cases it is assumed the idium seal failed because the tube pressure increased to about 10^{-2} torr. There are some indications the leak rate may be greater initially and then may subsequently decrease. In addition, some small changes in corner resolution were observed.

All of the above failures are attributed to shifting of the tube's structure. This is probably due to a combination of stress relief and differential expansion between the various parts of the tube. The materials used are 7052 glass, quartz, nickel, kovar, indium, gold, and copper. The amount of stress varies due to glassing operations, forming and bending, and spot welding.

Shifting of the beam due to relative movement of the cathode and G-1 grid may be demonstrated by imaging the cathode before and after exposure to low temperatures. The reseau marks provide a convenient reference. An example of shifting of the cathode image is shown in Fig. 39.

During the initial testing it was observed that the G-5 grid developed wrinkles. The wrinkling begins at the edge where the mesh is clamped to the support ring. The amount of wrinkling depends on the temperature, and becomes progressively more pronounced after exposure to lower temperatures. Repeated cycling or soaking has no effect. A typical example of wrinkling of the G-5 grid after exposure to low temperature is shown in Fig. 40. Preliminary measurements indicate wrinkling of the G-5 grid may contribute to shading. Wrinkling was observed in 18 of the vidicons subjected to cryogenic testing. After a few weeks storage at room ambient the wrinkles disappeared in approximately half of the vidicons. This is probably because of the construction which places the mesh in tension at room temperature and may be understood by considering this construction. The support ring is made from kovar which is a low expansion alloy, while the mesh is copper which has a higher coefficient of expansion. It is this differential in expansion that causes wrinkling with decreasing temperatures, i.e., the copper shrinks too slowly.

Following the initial series, a later test was performed to determine the temperature at which catastrophic failure of the photoconductor occurred. This was necessary because the first tests did not permit observation of the photoconductor during the test. This test was made in a new Statham chamber which has a heated observation

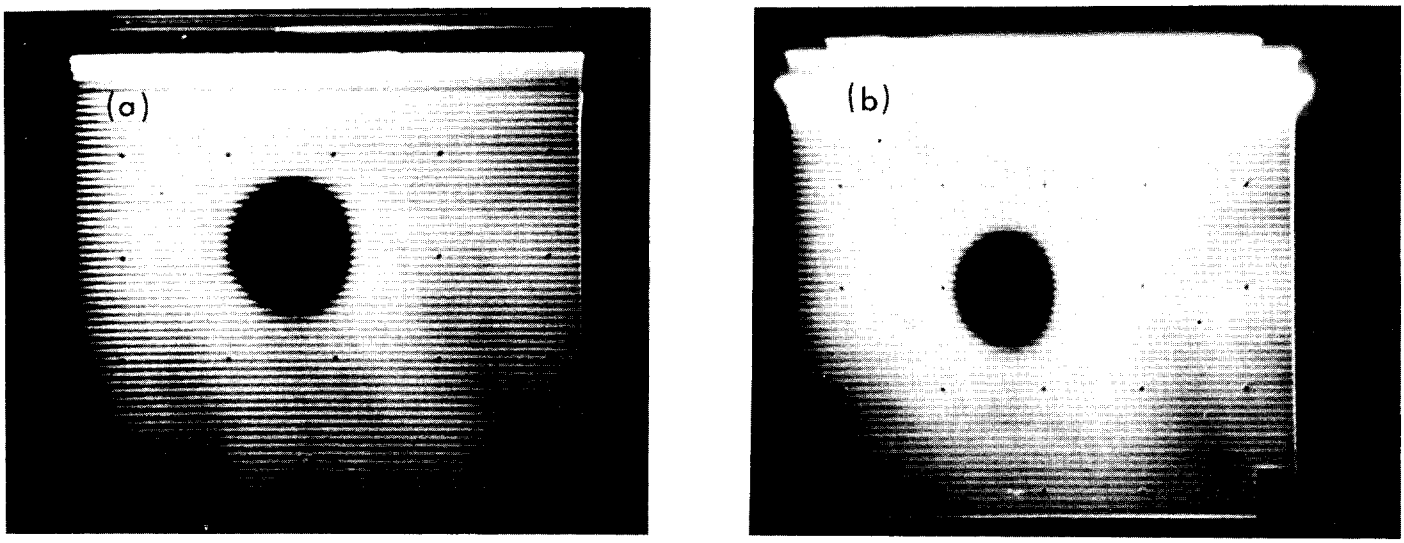

Fig. 39. Shifting of image cathode on an older type of vidicon because of exposure to −320°F for 18 hr: (a) initial cathode image; (b) after exposure to low temperature image of cathode has shifted to right

UNCLASSIFIED

UNCLASSIFIED

Fig. 40. Wrinkling of G-5 grid because of exposure to low temperatures

window through which it is possible to view the photoconductor during the test.

The photoconductor of the selected tube was a maroon color and almost opaque, and was selected because of its high failure probability. The tube was tested during calibration of the test chamber. The rate of descent was approximately 20°F/min. The photoconductor was observed to fail catastrophically; the entire surface crazed all at once at −100°F. The appearance of the surface is similar to previous failures, although there is more peeling than crazing.

b. Conclusions. The cryogenic testing will be continued to establish the reliability of each production run since it is believed the temperature ruggedness is determined solely by details of processing which are considered proprietary by the manufacturer. It is also likely that the relationship between temperature ruggedness and details of the processing are not known to the manufacturer and cannot be explicitly controlled. As a consequence, future tests will be performed carefully at slow rates and in steps as described above.

Changes in performance caused by shifting of the tube elements requires further evaluation. The relationship between resolution and shifting of the cathode is not known. Furthermore, the possibility of leaks developing as a consequence of exposure to low temperature is a serious problem. The reliability of the indium seal is suspect and will be investigated.

Further study of the factors that enable the photoconductor to withstand cryogenics is essential. Methods of depositing the film, configuration of the photoconductor, thickness, substrate surface, methods of cleaning the substrate, vacuum conditions, and contaminants should be considered. Wrinkling of the G-5 grid should be corrected. This will require some change in the processing by the manufacturer and probably an additional change of design to permit the use of more compatible materials.

Electrical measurements associated with the grid wrinkling suggest that wrinkling may contribute to shading. It is also possible that some shading is due to intrinsic properties of the photoconductor. These effects will become increasingly important with the need for greater resolution. The measurements are difficult to make, and further study will be made.

Additional tests in the Statham chambers should be made to confirm the results of the original test. These tests should be made at a slower rate and with improved lighting which will not heat the photoconductor. Also, an attempt will be made to photograph the failure with a high-speed camera while it is taking place.

O. Thermal Control

1. Flight Spacecraft Thermal Support

The following discussion summarizes the SC-1 solar-thermal-vacuum mission sequence tests, SC-1 launch operations support, and SC-2 solar-thermal-vacuum preparation.

a. SC-1 plugs-out solar-thermal-vacuum phase. An abbreviated plugs-out solar-thermal-vacuum mission sequence was performed on SC-1 January 21 and 22. In this phase, coast periods were contracted to shorten the total mission time to approximately 32 hr.

Most of the hardline access and special test equipment employed during earlier phases were removed. Compartments A and B hardline test harnesses were removed, and actual flight canisters were installed on the compartments. Data were transmitted and received through an RF link. The Canopus antireflection hood, TV-4 target shroud, and radar altimeter and doppler velocity sensor (RADVS) and altitude marking radar test waveguide

UNCLASSIFIED

UNCLASSIFIED

were also removed. Compartment B thermal switches 1 and 5 were damaged during the pretest preparation and were replaced.

All thermocouple instrumentation within compartments A and B was removed. Real-time thermocouple data were taken but were visually monitored only during critical mission phases such as eclipses and chilldown. At other times, the data were covered up and the real-time telemetry data were used to monitor temperatures during the mission in order to gain experience for spacecraft performance, analysis, and command operations during an actual flight.

Three solar intensity levels were used in the plugs-out solar-thermal-vacuum phase. A nominal (100% of a solar constant) was set during the first 12 hr followed by a 1-hr eclipse starting from nominal steady transit temperatures. At the conclusion of the eclipse, the intensity was changed to a high level (112% of a solar constant) and maintained for 12 hr. Another 47-min eclipse was performed at the conclusion of the high-intensity period, after which the intensity was lowered to 87% of a solar constant. This level was maintained for the subsequent 20 hr, except that a 30-min eclipse occurred during the 17th hr.

One purpose of the plugs-out phase was to determine if the hardline access and special test equipment degraded the environment enough to induce spacecraft temperature levels which are not representative. All temperature results in the plugs-out phase were close to those observed in previous phases except for the RADVS altimeter velocity and velocity sensor preamplifiers which were 15°F warmer than in previous tests in which the test waveguide was installed. This situation demonstrates that the test equipment permitted an extraneous heat loss not associated with the flight configuration. The resultant temperatures are well within RADVS start temperature requirements and are closer to pretest predictions than the temperatures observed with the waveguide installed.

b. SC-1 launch operations support. Thermal control personnel have been supporting the combined systems test at GD/C, San Diego, and launch operations preparations at AFETR. Specific tasks were preparation of a procedure for determining temperature anomalies during performance verification tests and coordination on the thermal aspects of a solar panel test in which the panel is illuminated with a simulated solar source. Thermal control personnel will also monitor and evaluate temperature telemetry during the joint flight acceptance composite tests and the actual systems readiness test and countdown preceding launch. The normal 40-min hold in the countdown 5 min before launch will allow evaluation of all temperature parameters to determine if they are in an acceptance range to permit the launch.

The final wrapping of the spacecraft will be reviewed prior to propellant loading to minimize the possibility of damage to thermal surfaces from propellant spillage. A final prelaunch thermal inspection will be made in order to provide direction for the final cleanup and touchup of thermal surfaces.

c. SC-2 solar-thermal-vacuum test preparations. The shadow shroud above TV camera 3 has been raised to allow the camera to move more freely. The design has been reviewed to ensure that the new placement yields satisfactory shadow definition. An additional LN_2 cooled shadow shroud system allows the antenna polar panel positioner axis drive motor to be qualified during solar-thermal-vacuum testing and at temperature levels anticipated during the terminal maneuver. The shroud system will reduce temperatures below those possible with the existing configuration. The installation will allow normal movement of the antenna-polar panel positioner during the terminal and posttouchdown positioning maneuvers.

Thermocouples have been assigned to areas of interest, and their nomenclature has been established. After appropriate rework, the SC-1 thermocouple cables will be used on SC-2. Knowledge obtained from SC-1 solar-thermal-vacuum tests has permitted reduction of the number of spacecraft thermocouples on SC-2.

2. A-21 Model Subsystem Thermal Analysis and Design

a. Vernier propulsion system propellant tanks. A study has been made of maximum temperatures and temperature responses in the oxidizer tank area to determine if the A-21 spacecraft should be protected against damage from overpressure and subsequent rupture of oxidizer tanks after touchdown. The data will indicate whether a propellant dump system is required.

The time of landing on the lunar surface effects temperature rise rate and the maximum temperature of the oxidizer tank. Therefore, employing the boundary conditions and parameters that influence heat transfer to the tank, three different landing times (or solar angles) were investigated to determine the severest thermal response and maximum temperature of a tank containing various

UNCLASSIFIED

UNCLASSIFIED

amounts of oxidizer. The investigation showed that, for the nominal worst case and maximum worst case, touchdown at $\alpha = 297$ deg (53 hr past sunrise) and $\alpha = 320$ deg (99 hr past sunrise) produced maximum tank temperatures and severest thermal responses, respectively.

The maximum tank temperatures for the nominal and maximum cases (touchdown at 297 deg) are predicted to be 218 and 250°F, respectively. These temperatures are experienced approximately 145 hr after touchdown in the first case and 140 hr after touchdown in the second case. These results will not represent temperatures on the A-24 tanks since these tanks, for equivalent oxidizer loads, will run warmer than the A-21 tanks.

b. Propellant lines. In an attempt to increase the durability of the thermal control surface finish on the lines, replacement of vapor deposited aluminum by polished aluminum on the propellant lines is being considered. This change will tend to increase the temperature on illuminated line segments. A study is in progress to determine the adequacy of the Sun shade on line 1 and whether shades will be necessary on lines 2 and 3.

c. Main retrorocket engine. A new method for evaluating propellant bulk temperature in the A-21 main retrorocket engine, based on the actual mass distribution of the propellant, has been devised and computerized. Transient bulk temperatures were computed from test data and compared with flight sensor data to provide a basis for computing bulk temperatures from flight sensor data. No empirical relationship was found, but some general tendencies were found to be common to both bulk temperature and flight sensor plots.

d. Roll actuator redesign. The roll actuator is being redesigned for SC-5 and following spacecraft. The pin puller has been moved from the bottom to the top of the roll actuator, and the rotation angle has been increased from ±6 to ±2 deg. The thermal control coatings on the roll actuator will be reevaluated because of the change in the pin puller location. The larger rotation angle of the engine increases the convection heating on the crushable block and altitude marking radar dish heat shields adjacent to landing gear leg 1. These heat shields will be reevaluated to assure their withstanding increased convection heating.

e. RADVS. The computer-programmed thermal model of the A-21 receiver-transmitter assemblies is now in operation. The model, synthesized from point-to-point antenna temperatures derived from test, is an analytical tool now capable of predicting antenna temperature distribution in response to all transit thermal environments, natural and spacecraft induced. The mathematical model and its thermal parameters have been documented.

f. Antenna-solar panel positioner. The transient thermal response of the A-21 antenna-solar panel positioner as a function of touchdown site is being investigated. The study is an extension of a previous analysis which determined the response at a limited number of touchdown sites.

3. A-24 Model Subsystem Thermal Analysis and Design

a. Main retrorocket engine. The A-24 main retrorocket engine design is basically an extension of the A-21 configuration. The principal change, in a thermal sense, arises from the increased propellant and cavity geometry, case material, and collar/nozzle attachment. The thermal design will be similar to A-21, requiring only determination of the propellant temperature gradient at ignition for A-24. An intensive correlation analysis is being made in which selected thermal parameters in the model used to predict A-21 engine gradients will be modified to optimize the accuracy with which the operational computer programmed model predicts preignition propellant temperatures. At the conclusion of this plase, synthesized values of external blanket temperature distribution derived from system thermal tests in conjunction with revised values of insulation blanket apparent thermal conductivity will be substituted into the model.

b. Soil mechanics/surface sampler instrument. A preliminary analysis of the temperature of the soil mechanics/surface sampler instrument accelerometer-strain gage amplifiers on the lunar surface showed that the amplifier temperature was dominated by the lower spaceframe temperature during most of the lunar day. At or near lunar noon, the lower spaceframe temperature is expected to be 280°F maximum, a value derived from a simulated lunar noon thermal test of an MT-1 spacecraft sector. Therefore, at lunar noon the amplifier temperature also may be 280°F, exceeding the maximum specified temperature of 257°F. The maximum temperature can be reduced to 220 or 240°F, however, by inserting a low thermal conductance interface at the attachment between the amplifier and the bracket.

Similarly, minimum expected amplifier temperatures may be below the −65°F operational limit owing to local shadowing of the instrument and lunar surface at off-noon

UNCLASSIFIED

UNCLASSIFIED

solar angles. These results are part of an assessment study directed toward relocating the soil mechanics/surface sampler amplifier from its externally mounted configuration into compartment B.

c. Inertial measurement unit — touchdown dynamics instrumentation subsystem. A detailed external thermal environment has been defined for the inertial measuring unit. The primary difference from the previous definition is in the degree to which the external spacecraft elements have been considered. These data are being incorporated into the unit thermal design analysis.

4. S-10 Vehicle Test Program

a. Phase I. Phase I (hot cone) testing on the S-10 was completed after 36 hr of solar thermal vacuum environment. After transit coast mode equilibrium conditions had been established, the cone heating modes were initiated. These modes consisted of heating simulated engine cones (Fig. 41) to 1300 and 1600°F for 4-min periods, followed by a 1900°F mode for 6 min on engines 1 and 3. Electrical arcing problems experienced on engine cone 2 prevented completion of the 6-min run, which was terminated after approximately 2.5 min.

The data, which are being analyzed and tabulated, will be submitted for structures evaluation. No significant visible vehicle damage was apparent, and preliminary indications are that existing engine cone heating protection devices are adequate.

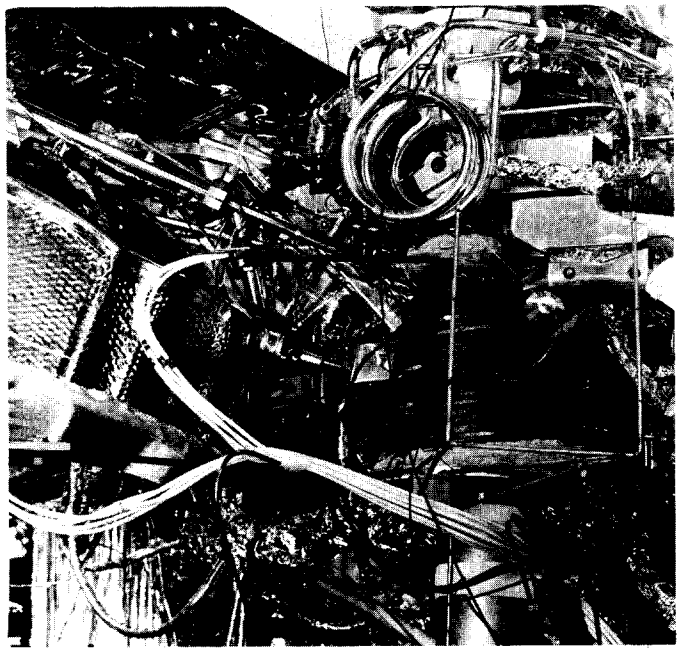

Fig. 41. Hot cone simulator

b. Phase II. Phase II testing was completed after approximately 95 hr of solar thermal vacuum environment. Phase II test environments, in the order of occurrence, are as follows:

(1) 63 hr of pure Xe spectrum at 93% solar constant (based on HAC radiometer 7120).

(2) 9 hr of 25% Hg-Xe and 75% pure Xe at 93% solar constant (based on HAC radiometer 7120).

(3) 40-min solar eclipse condition.

(4) 19 hr of pure Xe spectrum at 80% solar constant (based on HAC radiometer 7120).

(5) 3 hr of pure Xe spectrum at 93% solar constant to establish nominal solar constant initial conditions for eclipse.

(6) 2-hr and 24-min solar eclipse condition.

The change in solar spectrum from pure Xe to 25% Hg-Xe and 75% pure Xe was made to observe the effect on the various subsystems since the later spectrum is believed to be a better one for simulating the Johnson Sun on the white painted surfaces. The spectral change caused a temperature increase of approximately 5°F on the helium tank, vernier engines, and illuminated spaceframe tubing. An increase of approximately 10°F was noted on the top of the nitrogen tank, the flight control baseplate, and the propellant line shade at engine 1. No temperature change was observed on the compartment system Vycor glass radiators.

The purpose of the 2-hr 24-min solar eclipse environment was to obtain data on the effects of extended eclipse on the verier propulsion system.

The results of the phase II test are being analyzed. Based on the limited analysis completed thus far, the following observations have been made on some of the key subsystems:

(1) Compartments A and B ran approximately 5°F warmer than during JPL tests at the same power level; however, the solar intensity was 5% higher at the compartment radiator level than at the test plane. Each compartment also ran approximately 10°F warmer than in SC-1 tests at the same solar intensity and assumed the same power dissipation. No explanation of this anomaly is yet available.

UNCLASSIFIED

UNCLASSIFIED

(2) During phase II testing, the S-10 nitrogen tank regulator temperature was 12°F warmer than that of the SC-1 vehicle. The warmest portions of the S-10 tank ran at least 20°F warmer than the same points on the SC-1 tank. However, the S-10 nitrogen tank ran 20°F cooler in the JPL tests than in the HAC tests. The only significant difference between JPL and HAC tests was the change in retrorocket blanket to the new stitched blanket design; however, it has not been concluded whether that change was the cause of the temperature differences.

(3) The helium tank was repainted between HAC phases I and II to conform to the SC-2 paint pattern. With this pattern, the bottom of the tank ran approximately 20°F warmer than the SC-1, and the valve assembly ran approximately 10°F warmer than in SC-1 tests. The warmest point on the tank ran approximately 45°F warmer than the SC-1. During the phase I test when it had a paint pattern identical to SC-1, the S-10 helium tank ran approximately the same temperature as the SC-1.

(4) The auxiliary battery ran approximately 8°F warmer in the S-10 than in the SC-1 tests at the same solar intensity.

(5) No significant difference appeared to exist between the S-10 and SC-1 data for the RADVS system.

(6) During HAC phases I and II, the heated portions of the S-10 propellant lines behaved similarly to the SC-1. During S-10 testing at JPL, some propellant lines ran cold when the heaters remained on without cycling. It was found that some instrumentation harnesses had been laced to the lines and the thermostats such that they could have affected the system's temperature control capability. The potential problem was eliminated prior to HAC phase I testing, and the temperature control of propellant lines was according to expectations thereafter.

(7) The altitude marking radar heater duty cycle during HAC phase I testing was approximately 60%. During phase II testing, a retrorocket engine nozzle cooling shroud was employed to cool the nozzle from approximately −130°F in phase I to approximately −200°F, and the heater duty cycle increased to about 75%.

c. Phase III. The S-10 phase II (leg in Sun) testing (Fig. 42) consisted of approximately 23 hr of solar thermal vacuum environment at 100% solar constant, followed by a 1 hr 35 min solar eclipse and approximately 16 hr of testing at 87% solar constant.

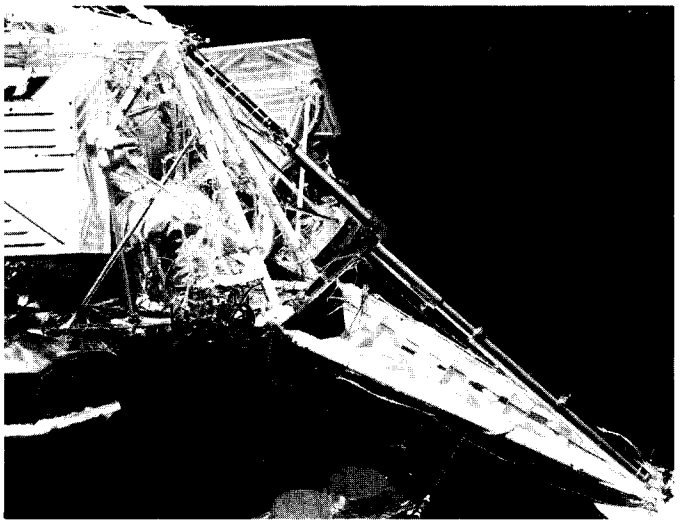

Fig. 42. Leg in Sun test

The leg temperatures were approximately 70 ±10°F, and shock absorber temperatures were approximately 80 ±10°F during the 93% solar constant run. The critical area of the shock absorber dropped to the minimum operating temperature of 20°F after 50 min of solar eclipse condition. These data agree well with predictions. Test data indicate that the shock absorber is relatively insensitive to leg plate temperature; however, the roll jet on leg 1 is well coupled thermally to the leg.

These conclusions are based on preliminary data analysis. A detailed analysis is under way.

5. Thermal Finishes

Evaluation of alternate white organic thermal control coatings has been completed. Four coatings with potentially greater resistance to ultraviolet light than the currently used HP4-144 (3M Co. White Velvet coating 202-A10) were tested for solar absorptance and infrared emittance before and after ultraviolet exposure. Exposure was at 1X solar intensity for 100 hr using a General Electric B-H6 lamp. Values representing averages of several specimens of each coating are given in Table 22. All of the coatings evidenced satisfactory adhesion to properly cleaned and/or primed aluminum.

Additional data obtained during the evaluation of repair techniques for HP4-135 inorganic white thermal

UNCLASSIFIED

UNCLASSIFIED

Table 22. Thermal coating ultraviolet exposure test values

Coating	Solar acceptance, α_s		$\Delta\alpha$	Infrared emittance, ϵ	
	Initial	After ultraviolet (100 SEH)		Initial	After ultraviolet (100 SEH)
HP4-144 3M White Velvet 202-A10 baked 1½ hr at 260°F	0.23	0.29	0.06	0.91[a]	0.91[a]
PDL 1-3072 Americal Cyanamid Acrylic Copolymer-TiO_2 baked 1½ hr at 250°F	0.22	0.25	0.03	0.85	0.87
PDL 1-3073 American Cyanamid Acrylic Copolymer-ZnO baked 1½ hr at 250°F	0.23	0.25	0.02	0.88	0.89
PDL 1-3074 American Cynamid Polyvinyl-Butyral baked 1½ hr at 260°F	0.22	0.24	0.02	0.82	0.82
S13 IITRI Silicone Elastomer-ZnO baked 24 hr at 260°F	0.22	0.22	0	0.90	0.92

[a]Data obtained from previous test.

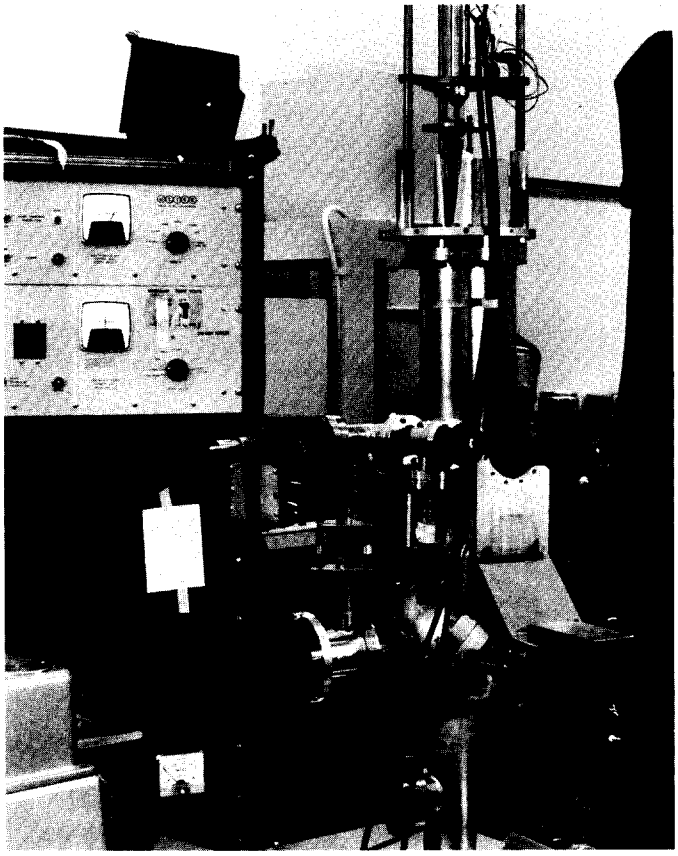

Fig. 43. Vacuum integrating sphere

control coating showed that final curing temperatures of 150 and 75°F (standard cure is 260°F) did not adversely affect the ultraviolet resistance of the reapplied coating. These low-temperature cures will facilitate repair of inorganic coatings on the spacecraft since baking at 260°F is not required for adhesion to most surfaces.

The HAC vacuum integrating sphere (Fig. 43) was placed in operation, and initial testing was performed. The equipment is capable of irradiating specimens with ultraviolet light and measuring the thermal radiative properties while still in vacuum. Exposure of S-13 the white silicone coating (cured 24 hr at 260°F) to approximately 1 day of ultraviolet from a B-H6 lamp produced a $\Delta\alpha \cong 0.03$, as measured under vacuum. Maximum damage occurred in the wavelengths greater than 1.0 μ. All damage bleached out instantaneously on exposure of the coating to air (i.e., solar absorptance returned to original value).

P. Engineering Mechanics

1. Summary

All shock absorbers made from 13V-11Cr-3A1 titanium have been delivered. A test to demonstrate that the shipping container is adequate to protect personnel in the event of a shock absorber explosion during shipment or storage is to be made. Type approval test on the A-24 shock absorber is scheduled to be completed by October

UNCLASSIFIED

UNCLASSIFIED

1966. The test will permit use of units of this design as early as spacecraft SC-3.

Analyses continue for a shock absorber utilizing crushable honeycomb rather than hydraulic principles to dissipate energy; results indicate no stability loss of performance at touchdown. A brief study has shown that elastic effects of vehicle response (e.g., antenna/solar panel positioner (A-SPP) motion) has minimal effect on vehicle stability at touchdown.

Tests continue on crushable blocks, using a different method to apply lateral loads. Results indicate a higher lateral strength capability than predicted previously. Three drops have been completed for S-15. Two significant problems developed which have been corrected. For the first two drops the coefficient of friction was too low and was corrected by bonding rubber to the bottom of the footpads. There were also instrumentation problems, which have been corrected by a series of mechanical, on-site calibration procedures.

The retrorocket engine CG shift test has been completed on S-9; results indicate the total shift is well within allowable limits. A test was added to the S-9 sequence to measure structural deflection in the area of the separation sensing and arming device for boosting acceleration. Using these data, it is expected that boost acceleration will contribute 0.036-in. deflection to the switch plunger.

2. Shock Absorber Procurement

A shipping container evaluation test specification has been written by HAC. This evaluation program on the container includes vibration, drop, and explosion tests in which a flight type shock absorber is deliberately ruptured in a manner to simulate a failure at maximum temperature expected in shipment.

Results of the shock absorber type approval tests are expected to be submitted to the type approval test review committee.

Component development testing of shock absorber 238927 is complete, except for the electric squib lock. Fabrication of the major components of the flight shock absorbers has begun. All detail drawings have been released and the stress analysis completed. Calculated weight of the new unit is 4.75 $\pm$0.10 lb without instrumentation. The delivery schedule has been altered so that complete type approval test results will be available by October. This will qualify the shock absorber for use on the SC-3 launch.

National Water Lift submitted the flight approval test (FAT) specification to HAC in March. Type approval test of the new type shock absorbers is expected to start in July.

3. Touchdown Dynamics

a. Shock absorber deviation evaluation. During type approval tests of the 264300 type shock absorber, a lack of Viton O-ring seal resilience at low temperature resulted in deviations from specification in both compression and extension damping, as shown in Fig. 44. Studies revealed that shock absorbers having these specification deviations exhibited acceptable vehicle stability, loads, and rebound. These deviations are restricted to SC-1 and SC-2 shock absorber design and are documented in the National Water Lift Co's failure analysis report No. 10127.

b. Crushable shock absorber. A computer program has been written to facilitate the investigation of the crushable shock absorber concept. This new program was used to establish a preliminary stability boundary for the A-24 vehicle having a shock absorber which deflects under a constant crushing force of 6000 lb. The resulting boundary is shown in Fig. 45.

The stability appears to be adequate in relation to specification requirements of a 7-ft/sec lateral velocity capability. More extensive investigation of this concept is under way.

c. Effect of vehicle flexibility on landing stability. A study was conducted to determine the effect of mast elastic response on vehicle landing stability. For a drop condition of 16 ft/sec longitudinal velocity, -7.5 cps lateral velocity (Fig. 46), the mast elastic energy has been calculated to be 24.2 ft-lb. This energy level, if it were all converted into toppling energy, could move the stability boundary 0.65 ft/sec in either the stable or nonstable direction. On the basis of these results, it is considered that the effect of vehicle flexibility on stability is not sufficient to warrant a continued high level effort; hence further work will be on a low priority basis.

d. Consideration of shock strut rebound action. A portion of the spring energy stored in the shock strut during compression is returned to the spacecraft during shock strut extension. Fig. 47 shows typical force-deflection curves of the SC-1 and SC-5 type shock absorber springs

UNCLASSIFIED

UNCLASSIFIED

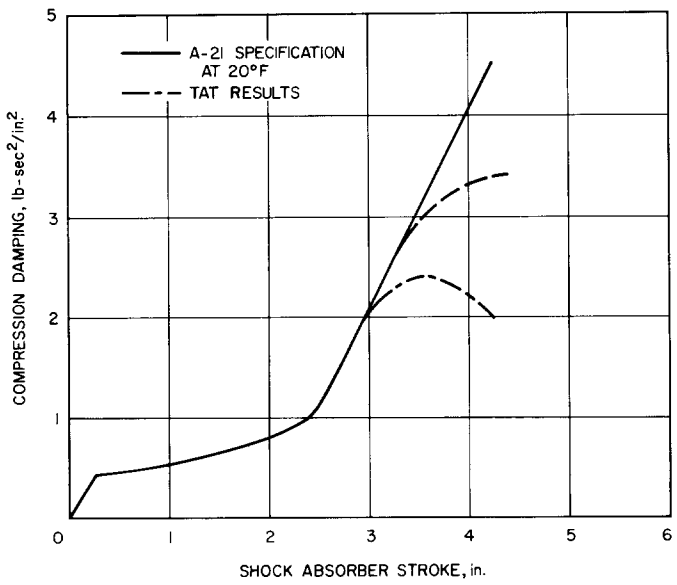

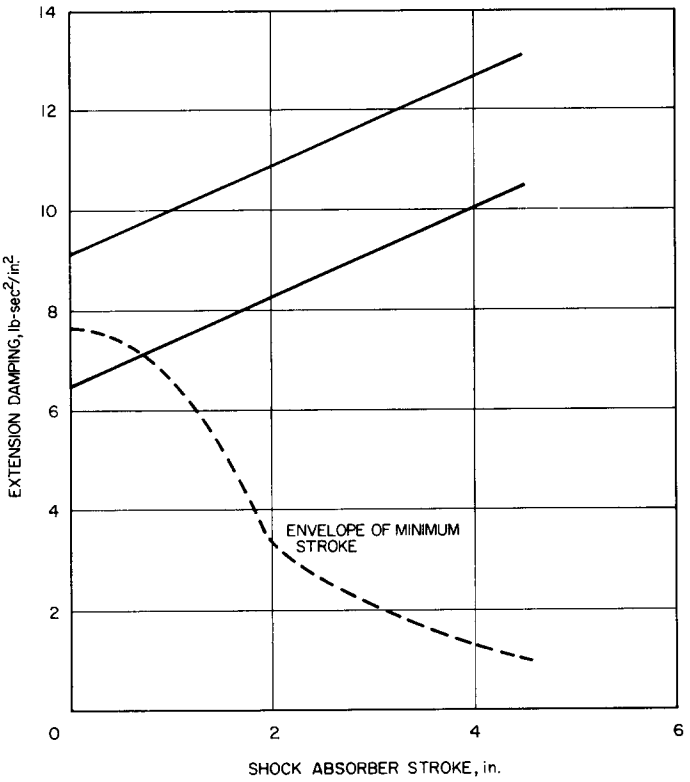

Fig. 44. Shock absorber compression and extension damping type approval test results at 20°F

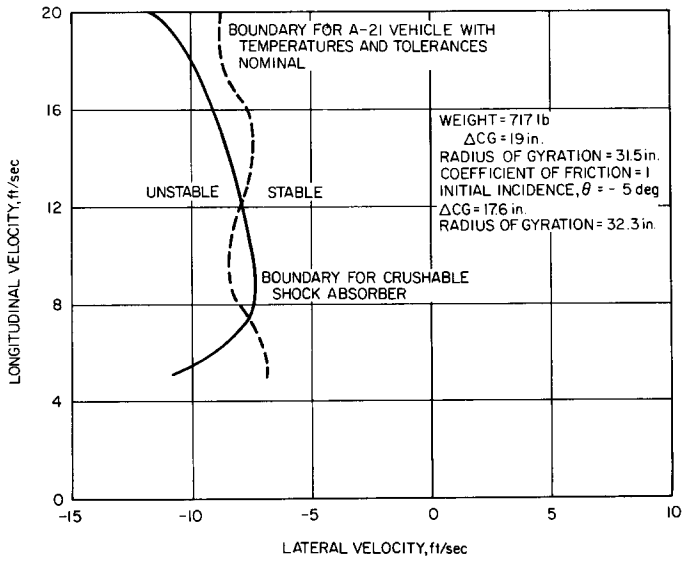
BOUNDARY FOR A-21 VEHICLE WITH TEMPERATURES AND TOLERANCES NOMINAL
WEIGHT = 717 lb
ΔCG = 19 in.
RADIUS OF GYRATION = 31.5 in.
COEFFICIENT OF FRICTION = 1
INITIAL INCIDENCE, θ = - 5 deg
ΔCG = 17.6 in.
RADIUS OF GYRATION = 32.3 in.
UNSTABLE
STABLE
BOUNDARY FOR CRUSHABLE SHOCK ABSORBER
LONGITUDINAL VELOCITY, ft/sec
LATERAL VELOCITY, ft/sec

Fig. 45. Preliminary stability boundary for crushable shock absorber

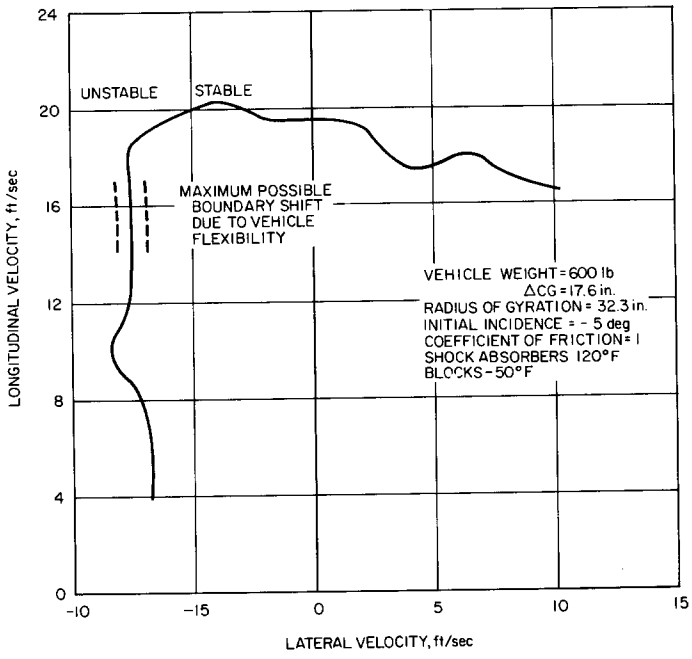
UNSTABLE
STABLE
MAXIMUM POSSIBLE BOUNDARY SHIFT DUE TO VEHICLE FLEXIBILITY
VEHICLE WEIGHT = 600 lb
ΔCG = 17.6 in.
RADIUS OF GYRATION = 32.3 in.
INITIAL INCIDENCE = - 5 deg
COEFFICIENT OF FRICTION = 1
SHOCK ABSORBERS 120°F
BLOCKS - 50°F
LONGITUDINAL VELOCITY, ft/sec
LATERAL VELOCITY, ft/sec

Fig. 46. Effect of vehicle flexibility on landing stability

UNCLASSIFIED

UNCLASSIFIED

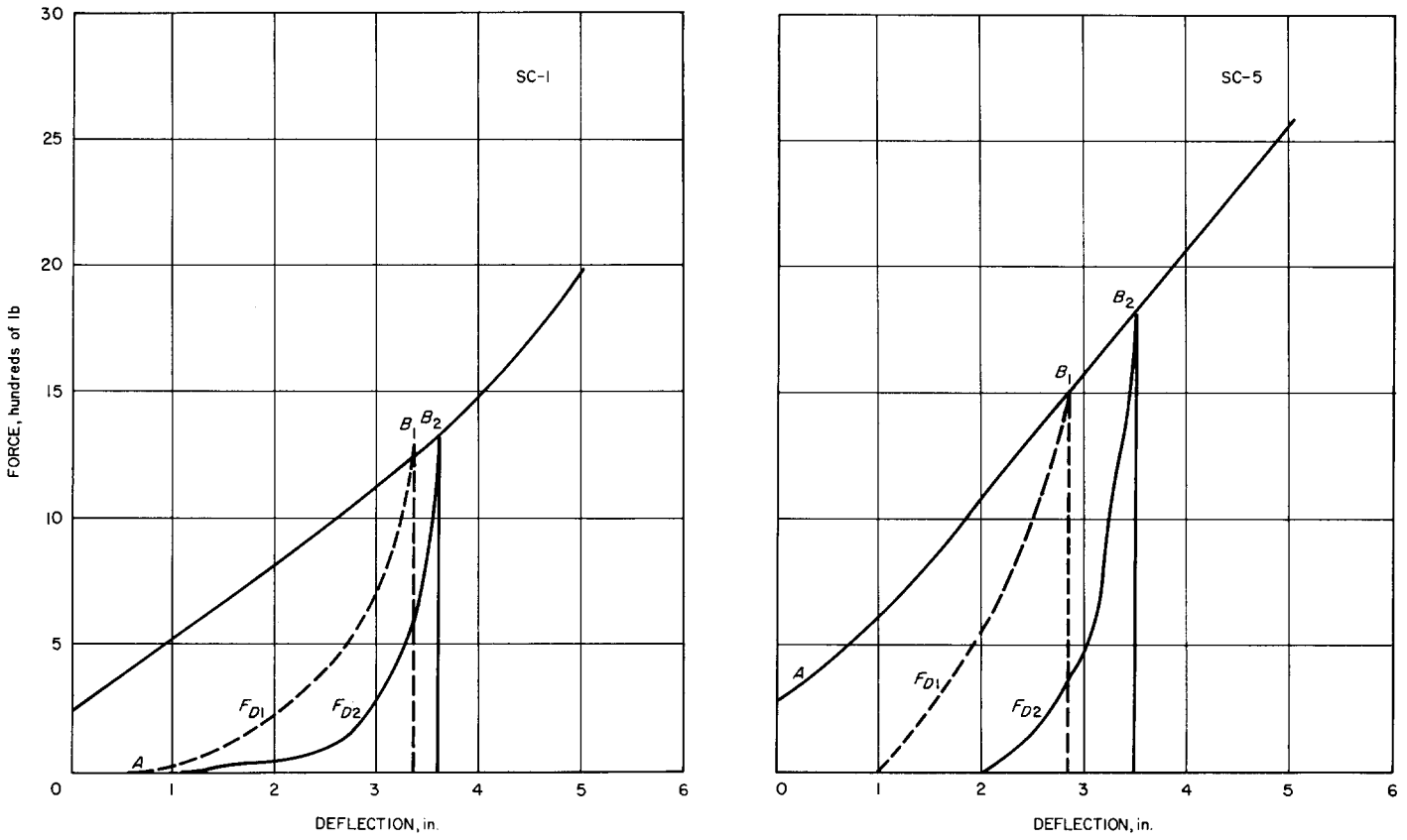

	SC-1	SC-5
TEMPERATURE, °F	70	70
SPRING CONSTANT, k, lb/in.	285	380
AREA, ft-lb	329	450
PRELOAD, lb	235	285
AREA UNDER CURVES, ft-lb		
B_1A	205	234
B_2A	232	303
F_{D1}	54	77
F_{D2}	40	60

Fig. 47. Nominal spring force versus deflection for SC-1 and SC-5 type shock absorbers

UNCLASSIFIED

UNCLASSIFIED CONFIDENTIAL

for the following initial landing conditions, case B in Fig. 48:

Initial longitudinal velocity, $x(0) = 20$ ft/sec

Initial lateral velocity, $z(0) = -4.0$ ft/sec

Friction coefficient, $\mu = 0$

Single leg uphill

Table 23 shows, for various landings, the energy required for compression, the magnitude of the energy returned, and the energy returned at a percent of compression energy. The landing initial conditions are defined in Fig. 48. Table 23 shows that the magnitude of energy returned by each of the double legs on a nonvertical landing with double legs downhill is almost constant, the average being 41.3 ft-lb for the SC-1 type vehicle and 61.3 ft-lb for the SC-5 type vehicle.

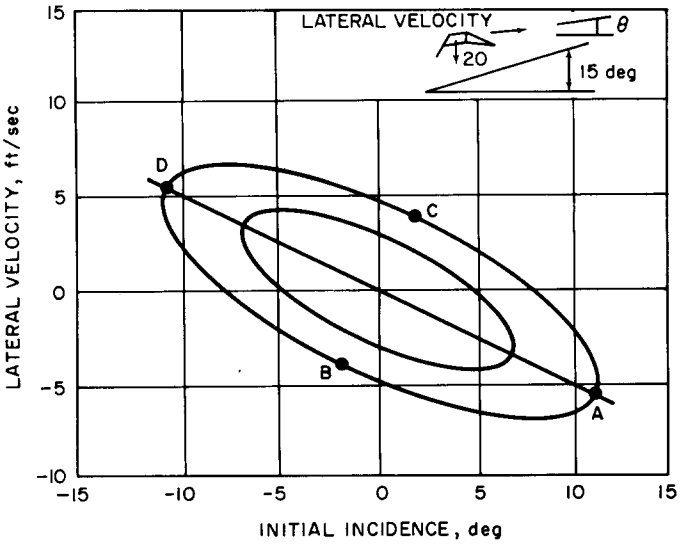

Fig. 48. Initial conditions for various landing types

In the case of abutment stability with the downhill double legs striking an abutment (the most critical case because of a smaller moment arm), the effect of the uphill single leg can normally be ignored because it will not remain on the surface for an appreciable length of time. In this case, the energy which is returned after compression due to impacting the abutment of the downhill shock struts may be a critical factor affecting stability. The effect of rebound energy is presently being studied using the simple model shown in Fig. 49, with current vehicle shock strut parameters defining spring and damping action.

4. Dynamic Tests

a. Crushable block tests. Tests have been conducted to determine the crushable properties of body blocks under combined axial and lateral loading. While the blocks were being axially crushed, a lateral load was applied at the base through a surface covered with rubber matting. Previous tests conducted in a similar manner used a ¼-in. semicircular collar to apply the lateral load. The use of the collar resulted in lower lateral forces than are

Table 23. Shock strut rebound energy

Landing type	SC-1						SC-5					
	Compression energy, ft-lb		Energy returned, ft-lb		% energy returned		Compression energy, ft-lb		Energy returned, ft-lb		% energy returned	
	Single leg	Double leg	Single leg	Double leg	Single leg	Double leg	Single leg	Double leg	Single leg	Double leg	Single leg	Double leg
A[a]	247	237	52	42	21.0	17.8	310	303	77	62	24.8	20.4
B[a]	205	232	54	40	26.3	17.2	234	303	77	60	32.9	19.8
C[a]	242	241	54	41	22.3	17.0	256	310	74	60	28.9	19.4
D[a]	247	241	66	42	26.7	17.4	264	326	81	63	30.6	19.3
Vertical landing velocity												
25 ft/sec	282	282	43	43	15.3	15.3	330	330	75	75	22.8	22.8
20 ft/sec	255	255	41	41	16.1	16.1	303	303	66	66	21.8	21.8

[a] Fig. 48.

UNCLASSIFIED CONFIDENTIAL

UNCLASSIFIED

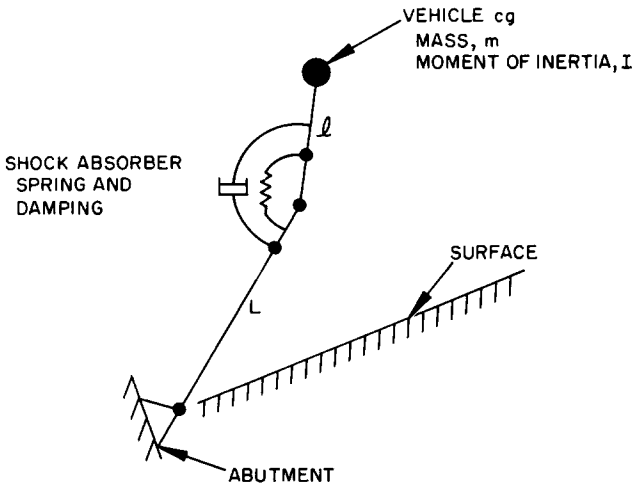

Fig. 49. Mathematical model for rebound energy effect on stability

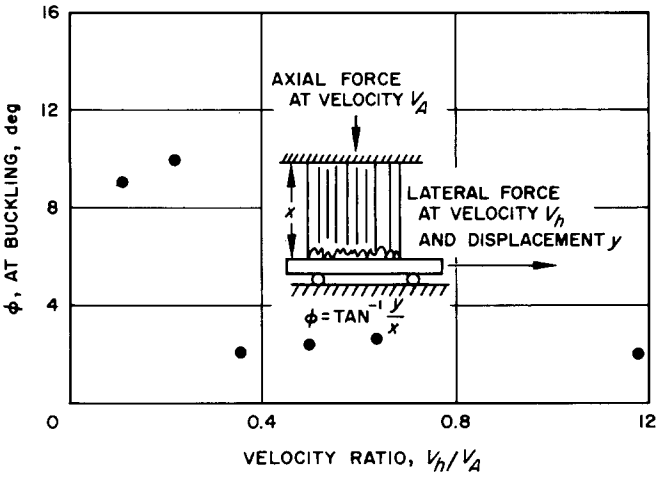

Fig. 51. Initial buckling conditions of crushable body blocks

reported here due to local deformation of the crushable material; i.e., use of the rubber matting applies the lateral load uniformly over the base of the block. Fig. 50 shows the maximum lateral forces measured while varying the ratio of lateral to axial velocity (the previous results using the ¼-in. collar are also shown for reference). Buckling of the blocks occurred in all cases. Fig. 51 shows angles representing the axial and lateral displacements when buckling occurred. Reduction of axial crushing force, as a result of the block buckling, varied from approximately 10 to 30%. The energy dissipated laterally varied from 3 to 11 ft-lb.

Additional tests were made using blocks that had been used for the T-21 drop tests and which, because of slight buckling, were canted to small angles. In these tests only an axial force was applied, and the base of the block was allowed to displace laterally on a free trolley. It was found that with blocks canted at angles between 4 and 10 deg the axial force was reduced from 1 to 25% of its maximum crushing force. Fig. 52 shows the axial force as a function of lateral displacement for a block canted at an initial angle of 6 deg.

b. S-15 drop tests. The first drop of the S-15 stability program was completed February 11, and the second was made February 21. Results indicated that a higher value of friction coefficient was necessary to obtain predictable and optimum test results. Unit friction tests were therefore conducted to verify the friction coefficient for drops 1 and 2 and to determine if neoprene rubber sheet

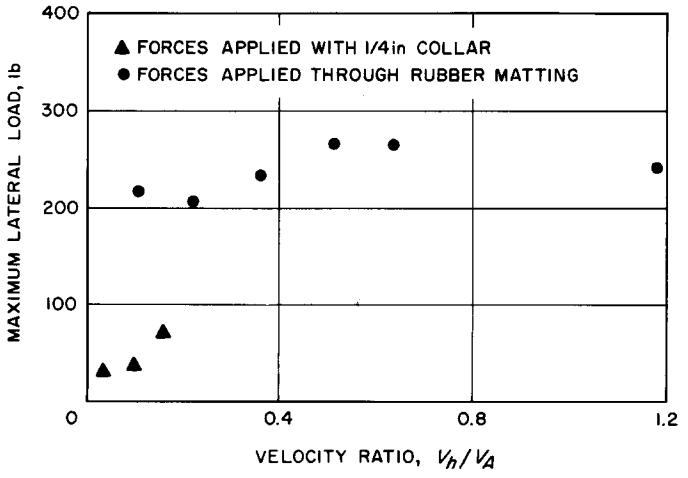

Fig. 50. Lateral force capability of crushable body blocks

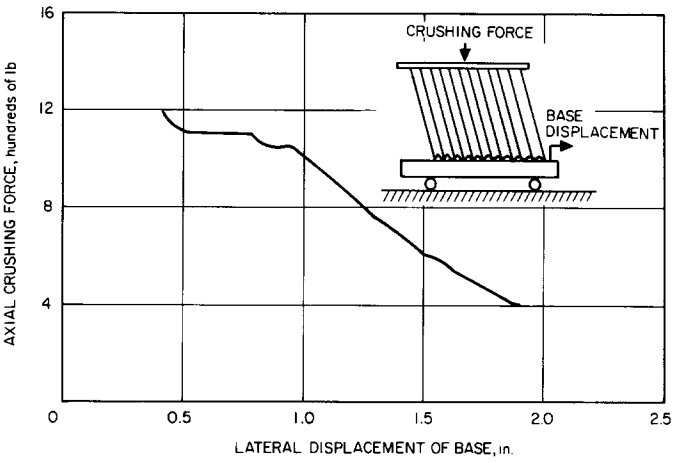

Fig. 52. Variation of body block crushing displacement

UNCLASSIFIED

UNCLASSIFIED
CONFIDENTIAL

bonded to the vehicle footpads would sufficiently increase the friction coefficient. From the unit tests it was determined that the friction coefficient for tests 1 and 2 was approximately 0.5 and that by bonding the neoprene rubber to the footpads a friction coefficient as high as 1.0 could be obtained.

A repeat of the second drop was made using the rubber covered footpads. Preliminary review of the data and motion picture coverage showed that the maximum vehicle pitch attitude was approximately 45 deg. This is a marginally stable condition, indicating that the friction coefficient has been sufficiently increased. Instrumentation modifications and a data review are currently being made together with a reassessment of the drop conditions.

5. Flight Instrumentation

a. Accelerometer amplifiers. Accelerometer amplifier assemblies for SC-1 through SC-7 are complete.

b. Strain gage amplifier. Strain gage amplifier assemblies for SC-4 have been completed. In the last program redirection, the strain gage installation was extended through SC-7. An order has been placed for additional amplifiers, and they are expected late in June. Assembly on SC-5 and up will be started in July.

c. Leg position potentiometers. The leg position potentiometer, identified by HAC component specification 988684, was initially qualified at 10^{-8} torr vacuum conditions. Because other space applications of this type of potentiometer have recently shown cold welding effects at 10^{-9} torr, it was decided to check 988684 at higher vacuums. To date, two potentiometers have been tested at 10^{-10} torr, and no detrimental cold welding has occurred. Two more will be tested as additional evidence that the present potentiometer can be satisfactorily used.

One of the two potentiometers tested had a molybdenum disulfide coating applied to the winding to aid in preventing cold weld. Since significant welding did not occur, neither of the second two potentiometers are to be coated. Also, since the worst welding temperature environment occurs at high temperature, the tests are conducted at 135°C only.

6. Static Tests

a. S-9 static test. A static test of structural type approval test vehicle S-9 was conducted to demonstrate the capability of the *Surveyor* spacecraft to meet those functional requirements of detail specification 224510E—*Surveyor* system functional requirements, that place limitations on permissible spaceframe structural deformations.

The spacecraft was mounted on three supports located in a horizontal plane and directly beneath the three retroengine support points. Loading designed to simulate the effects of retroengine deceleration on the spaceframe deflection was applied by means of dead weights suspended in such a manner that their lines of action passed through the centers of gravity of all major components, totaling 36, whose compact shape permitted single-point load application. Two additional components—omnidirectional antenna A and the A/SPP positioner—are loaded at three points each to represent their lateral extension realistically. The total weight of these 28 components was 626 lb, or 88% of the spacecraft (less retroengine) at retroengine burnout.

Lateral movement of the spacecraft CG caused by deceleration loads was determined from the measured lateral deflections of 18 of the major components, 12 of which, either because of their shape or the configuration of their supporting structure, were subject to significant excursions. The other 6 components were, in addition, checked for alignment since this is critical to the performance of the spacecraft. The weight of the 12 components constitutes 85% of the spacecraft weight (less retrorocket engine) at burnout.

Loading proceeded in the following increments: 1, 3, 6, 9, and 12 *g*. The total load applied at 12 *g* amounted to 7515 lb (where 1 *g* represents the dead weight of the A-21 spacecraft at retroengine burnout). Unloading took place in the reverse order. Deflection readings were recorded at each increment.

The instrumentation used to monitor deflections consisted of 94 dial indicators and 28 deflection beams mounted on rigid framework remote laboratory columns. The spacecraft support system consisted of three 6-ft vertical columns mounted rigidly on a 2-in. thick steel plate on a concrete floor. Ball bearing supports were provided to allow unimpeded lateral expansion or contraction of the spaceframe under load.

The following additional tests were performed in conjunction with the main S-9 CG shift test:

(1) *Vernier engine support bracket deflection test.* In this test the spring constant of the vernier engine support system under simulated thrust loading was

UNCLASSIFIED
CONFIDENTIAL

UNCLASSIFIED
CONFIDENTIAL

determined. A load acting along the engine centerline was applied by means of cables in increments of 25% from zero to full thrust. Rotational as well as translational deflections were monitored by five dial indicators per engine.

(2) *Altitude marking radar antenna deflection test.* In this test the effect of boost loads on the permanent displacement of the attitude marking radar antenna mounting was evaluated.

The following are preliminary test results.

Figs. 53 and 54 portray graphically the direction and magnitude of the spacecraft—retrorocket engine CG excursion during retrorocket deceleration. The directional nonlinearity observed in Fig. 53 at the first load increment is felt to be due to slip or "bottoming out" of mechanical joints in the substructure. Extrapolating the test data, as shown in Fig. 54, the resultant CG displacement of 12 g applied in a zero-g field is 0.0447 in. Adding an additional displacement calculated from predicted

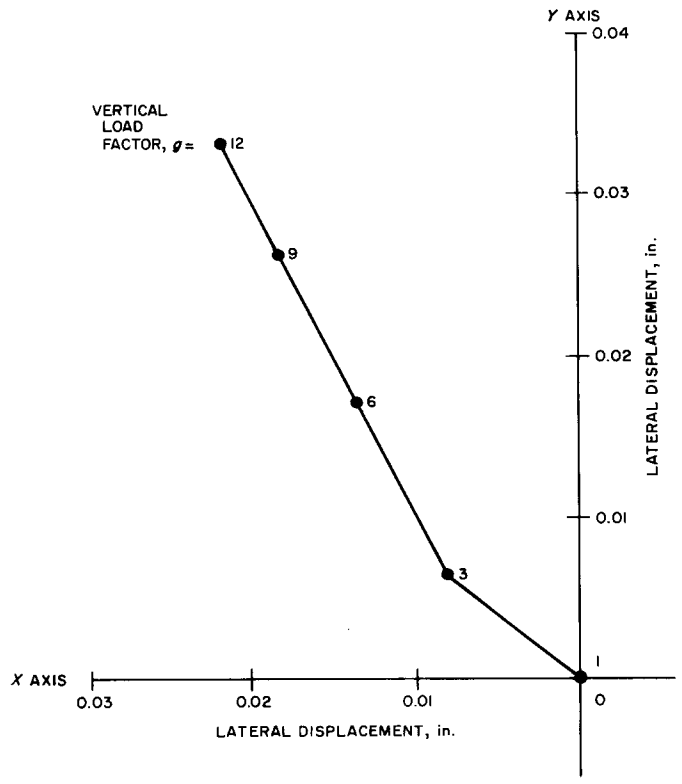

Fig. 53. CG shift with respect to retrorocket engine centerline

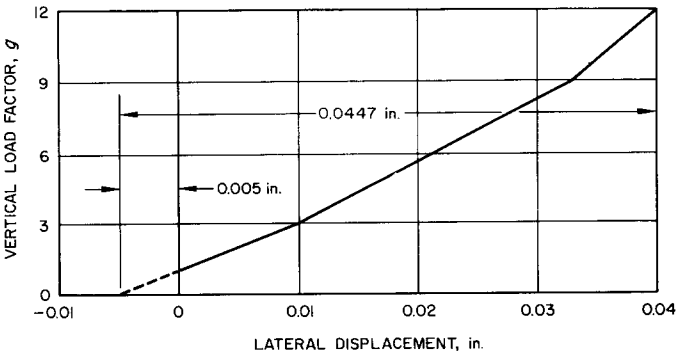

Fig. 54. S-9 CG displacement with respect to retrorocket engine centerline

spaceframe thermal gradients conservatively assumed acting in the same direction gives:

Predicted A-21

Δ(12-g load) = 0.0447 in.

Δ(thermal) = 0.0023 in.

ΔTotal = 0.0470 in.

Specification allowable

Δ = 0.070 in.

Deflections of the flight control sensor group measured during the S-9 static test are presented in Table 24 and Fig. 55. The orientation of the angles α and β is shown in Fig. 56, using the left-hand rule. The rotation of the flight control sensor group allowed by the system specification is 0.2 deg during retrorocket engine burning.

Table 24. Rotation of flight control sensor group with respect to spacecraft roll axis versus g-loading

g-Loading	Actual rotation, deg		
	α	β	Total
1	0	0	0
3	0.086	0.017	0.087
6	0.241	0.034	0.243
9	0.401	0.063	0.401
12	0.556	0.074	0.562
9	0.401	0.046	0.403
6	0.264	0.023	0.265
3	0.115	0.011	0.115
1	0.023	0	0.023

CONFIDENTIAL
UNCLASSIFIED

UNCLASSIFIED

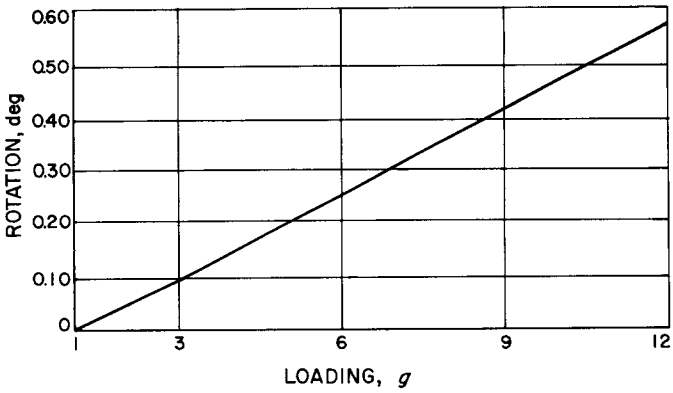

Fig. 55. Total rotation of flight control sensor group versus g-loading

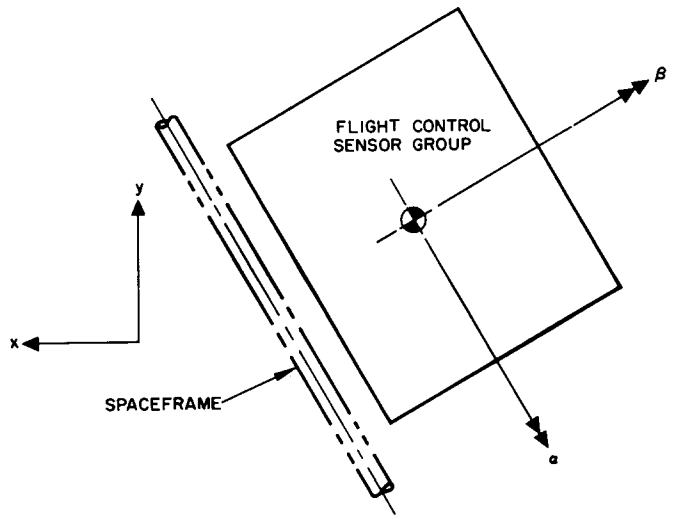

Fig. 56. Orientation of flight control sensor group rotations

These deflection data will be used in the preflight programming of A-21 missions.

Rotation of the vernier engine centerline for a simulated thrust of 100 lb was measured. The resultant angles of rotation of the engine centerline with respect to the spacecraft roll axis per 100 lb of thrust were as follows:

Vernier engine 1	0.46 deg
Vernier engine 2	0.48 deg
Vernier engine 3	0.46 deg

Specification allowable = 0.50-deg maximum.

b. S-9 Centaur *adapter deflection test.* A test designed to determine the vertical deflections of corresponding separation sensing and arming device attach surfaces on the *Surveyor* S-9 spaceframe and the *Centaur* adapter, with respect to one another under simulated boost conditions, was performed March 5. The *Centaur* adapter was rigidly supported on a 2-in. thick horizontal steel plate. The spacecraft was attached to the adapter in accordance with flight installation procedures. Loads representing the boost conditions were applied to major spacecraft components by means of dead weights so suspended as to act through the CG's of the respective components, and to the retroengine by means of a hydraulic jack acting through a truss evenly distributing the load to the three retro support skirt attach hinges.

Vertical deflections of the separation sensing and arming device at attach surfaces were measured by means of three dial gages whose support brackets were clamped to the top surface of the adapter at the locations of the three separation switch pedestals. The stems of the dial gages were aligned with the axes of the separation switch plungers and bore against aluminum plates installed in place of the separation switches (Fig. 57).

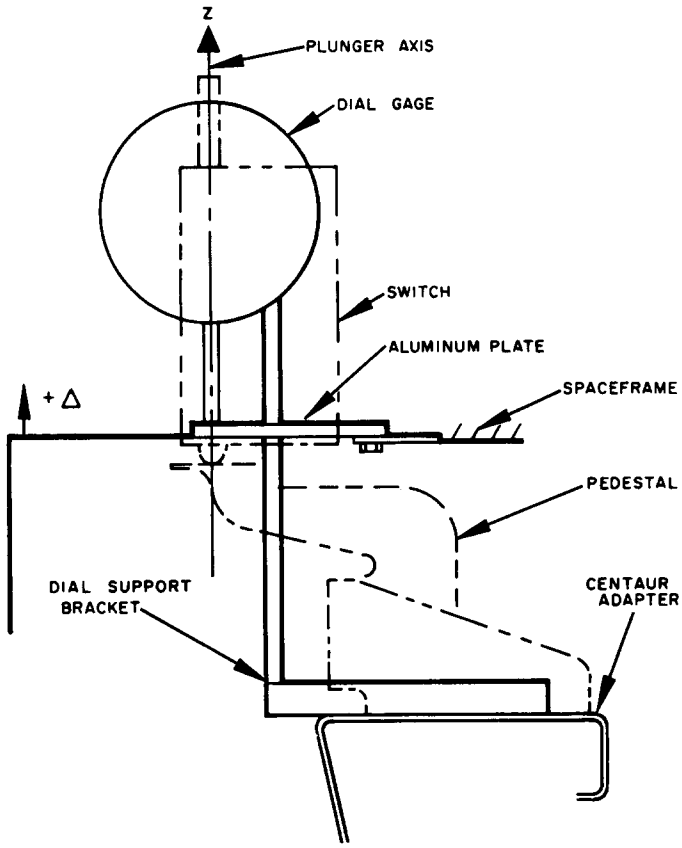

Fig. 57. Dial indicator diagram

UNCLASSIFIED

UNCLASSIFIED

Loads were applied in increments representing 1, 3, and 6 *g*. Two complete loading cycles were performed, and the dials recorded during loading and unloading operations.

The measured deflections of the three separation sensing and arming device supports, with respect to the corresponding pedestal mounts on the *Centaur* adapter, are shown graphically in Fig. 58.

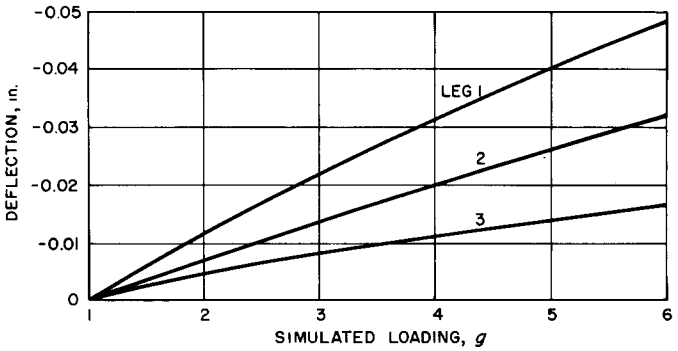

Fig. 58. Deflection of switch support with respect to adapter pedestal mount

Two loading operations were performed to a maximum of 6 *g* simulated *Atlas–Centaur* boost acceleration. The largest deflection (−0.0483 in.) was recorded at the separation sensing and arming device located near leg 2. Deflections are caused by a bending moment and a torque resulting from the concentrated retroengine support reaction acting at each of the three retroengine adapters. The retroengine used in S-9 was located in the maximum lateral eccentric position permissible in the spacecraft with centerline coordinates of

$$X = -0.117 \text{ in.}$$

$$Y = -0.892 \text{ in.}$$

This eccentric location results in large differences in the magnitude of local moments acting on each of the three adapters. Hence, large differences will be noted in the deflections measured at legs 1, 2, and 3.

The predicted location of the retroengine in A-21 is

$$X = +0.02 \text{ in.}$$

$$Y = -0.21 \text{ in.}$$

Extrapolation of the S-9 test data results in a predicted maximum deflection of the A-21 spacecraft relative to the *Centaur* adapter at leg 2 of −0.036 in.

Q. Telecommunications

1. Critical Data Recorder Antenna Subsystem Design[7]

a. Introduction. The critical data recorder (CDR) is, in effect, a small spacecraft designed to be carried aboard the larger *Surveyor* spacecraft. The prime mission objective of the CDR is to provide touchdown diagnostic data about the *Surveyor* spacecraft upon lunar landing, in case the *Surveyor* telecommunications system fails. A secondary mission objective of the CDR is to provide some data on the nature of the lunar surface in the event of a nominal or catastrophic lunar landing.

The antenna subsystem of the CDR encompasses antenna, RF transmission lines, and the RF properties of the impact limiting material and thermal control coverings.

b. Design constraints. The following is a list of the system design constraints that affect the antenna subsystem design:

(1) Orientation of the CDR with respect to the Earth is not provided.

(2) Antenna pattern coverage to include the Earth is required for a nominal landing and up to a 10,000 Earth *g* impact applied to the antenna mounting surface.

(3) Only one-way communications from CDR to Earth shall be provided.

(4) The total CDR system weight shall be limited to 15 lbs. The CDR capsule shall be limited to 12 lbs, with 3 lbs allocated to external system weight.

(5) The subsystem design shall be predicated on existing or immediately developable hardware.

c. Design considerations. A single, fixed antenna cannot provide one sense of polarized radiation into every direction in space (Ref. 18). Because of the small package size, the CDR capsule cannot contain a complex gravity oriented antenna system. Also, since the communications is one way (transmit only), this constraint rules out active phasing of an array of antennas. Therefore, two antennas having hemispheric patterns, pointing essentially in opposite directions are required to direct some radiation of acceptable polarization to the Earth.

[7]Prepared by JPL Technical Section 336.

UNCLASSIFIED

Since the *Surveyor* spacecraft will block or shadow radiation in some directions from one antenna on the CDR, the two antennas must be affixed to the spacecraft in positions that will yield acceptable radiation to the Earth in the blocked direction. However, in the event of a catastrophic landing, the CDR capsule will more than likely separate from the spacecraft. In this case, the CDR itself will require a minimum of two antennas back to back in order to provide minimal nonoriented pattern coverage.

Thus, the antenna system would require a minimum of three antennas. Two high impact antennas would be required on the CDR Capsule, and one lightweight antenna would be required on the *Surveyor*. The single antenna would be mounted opposite the CDR to provide pattern coverage in the blocked direction in the case of a nominal landing (wherein the CDR remains attached to the *Surveyor*).

The three antennas must not be operated simultaneously, or their mutually directed radiation may interfere destructively in certain directions. Hence, sequential RF switching must be provided to isolate and excite the antennas. The three-antenna system allows for no redundancy to system elements that are closest to the point of impact at 10,000 *g*. In addition, the three-antenna system minimum antenna gain occurs nominally at a look angle of 90 deg away from the boresight (which is 0 deg or the peak gain direction of one of the CDR capsule antennas).

Adding more antennas to the CDR capsule would provide some redundancy and also increase the nominal minimum gain level. That is, the worst case look angle (measured from the peak gain axis of the antenna) can be decreased from 90 deg by installing more than three antennas on the capsule. Fig. 59 is a plot of the worst case look angle from boresight for an array of η antennas.

Pursuing this design consideration, the maximum number of antennas on the capsule would be determined by weight considerations and the decreasing amount of time on each antenna for a fixed total transmission time. The possibility of having several antennas mounted closely together on a small size package raises the question of mutual coupling between antennas. That is, the internal sequential switch could provide infinite isolation between antenna excitation lines, but more than one antenna could radiate at one time if they were excited by external mutual coupling from the one antenna excited from the RF switch. Also, the mutual coupling or parasitic radiation problem could be aggravated by any trapped

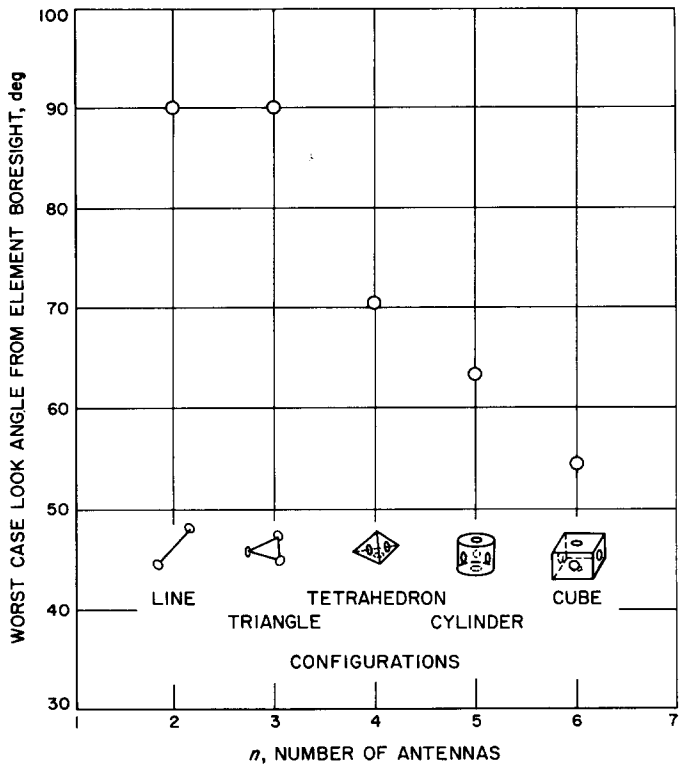

Fig. 59. Worst case look angle from element boresight for η-element array

radiation modes in the radome, which is shared by all the capsule antennas.

In addition, the radome of impact absorbing material and thermal control covering would be mounted directly against the capsule antennas. It is difficult to predict the radome transmission loss and antenna pattern spoiling due to refraction, since most of the theory governing dielectric interfaces is predicated on incident plane wave conditions. That is, normal theory could predict the radome degradation if the radome was in the far field of the capsule antenna.

An experimental investigation was begun to answer these questions.

d. Experimental investigation. The cavity backed spiral antenna was selected for investigation. This antenna has hemisphere-plus pattern coverage, is circularly polarized and has a small volume suitable for the CDR capsule. Impact tests of a mechanically strengthened version of the antenna had shown it to be capable of surviving high-g impact (9,000 *g*'s), when applied to the antenna mounting surface.

UNCLASSIFIED

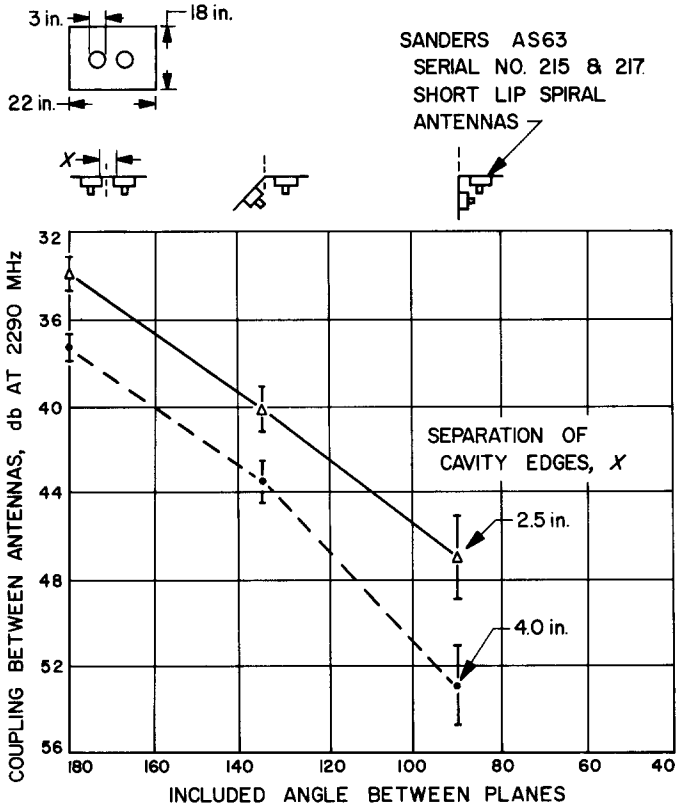

Fig. 60. Isolation between cavity backed spiral antennas

The first experimental investigation was to determine the amount of coupling between two closely mounted antennas. Fig. 60 is a graph of the measured isolation between two antennas for separation between cavity edges of 2.5 and 4.0 in. at various included angles between the planes of the antenna mountings. The isolation is very good, due to the fact that the antenna currents are confined to the radiating spiral arms of the antenna. Thus, in a radial direction from the center of the antenna the current magnitude decreases rather rapidly.

The next experiment was to measure the normal incidence transmission loss through the components of the radome. The measurement set-up is shown in Fig. 61. The nominal radome was to consist of a 1-in. thick piece of grain oriented balsa wood overlain with 0.020-in. thick fiberglass as a load spreader. The final elements to the radome would be either layers of unaluminized mylar or nonconductive thermal control paint. Measurements of the normal incidence loss were made by noting the power transferred between antennas without the radome sample and then with the radome sample, placing it flush against one of the antennas. Measurements were made at the CDR assigned frequency of 2290.185 MHz. The radome elements were tested singly and in combination. For all measurements the power differences were less than 0.3 db.

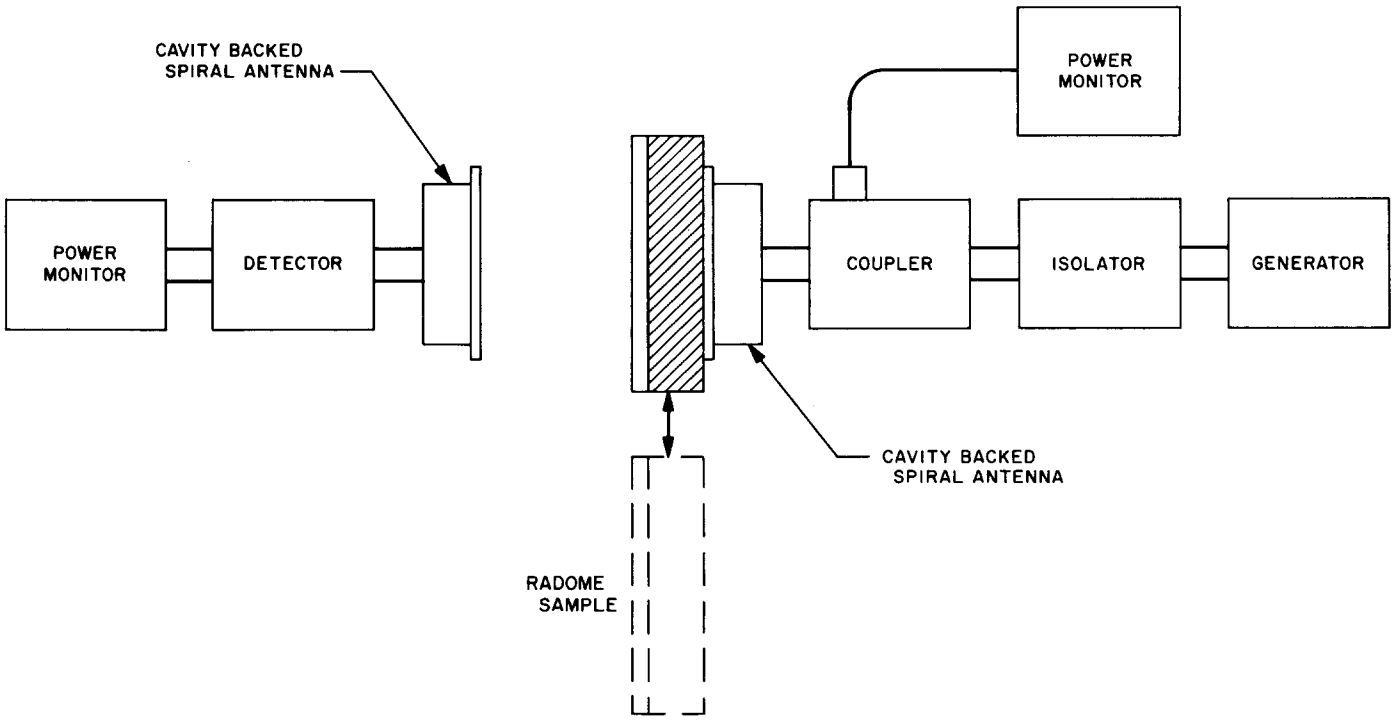

Fig. 61. Equipment setup for radome measurements

UNCLASSIFIED

UNCLASSIFIED

The next experimental investigation used a 6-antenna model of the CDR capsule with a 1-in. balsa cover, Fig. 62, in order to assess the antenna pattern performance. First patterns were recorded of the basic antenna alone, Fig. 63, and then patterns were made of the capsule with and without balsa to determine the radome pattern spoiling and also the effect of the capsule configuration. Fig. 64 shows the pattern of an antenna installed in the CDR model with and without the balsa wood radome.

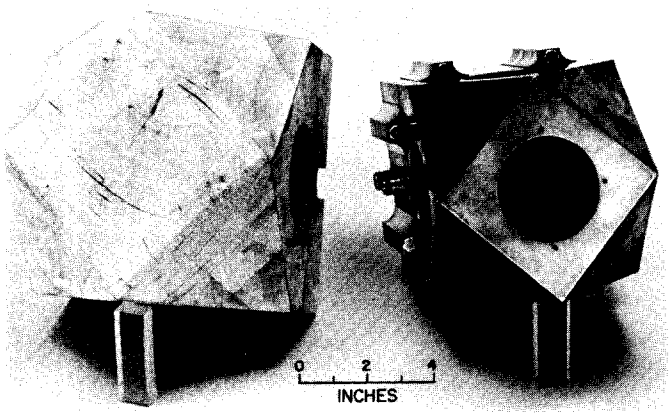

Fig. 62. Six antenna CDR model

Placing the antenna in the CDR model increases the gain because of the larger ground plane, while the balsa wood loss and refraction tends to decrease the gain. The ground plane effect predominates such that the normal antenna gain is increased on the peak of the beam from +4.6 to +5.5 db, while at 55 deg from the peak of the beam the gain is decreased from +1 to 0 db relative to right circular isotropic values.

Measurements of isolation between antennas on the balsa covered model confirmed the data in Fig. 60 for 90 deg. Pattern degradation due to multiple radiating antennas would thus be essentially a function of the RF switch isolation. For example, if at the worst case look angle of 54.6 deg for one of six antennas and if the two adjacent antennas were isolated by only 30 db of switch isolation, then the worst case interference phase combination could decrease the excited antennas gain by approximately 0.7 db.

Antenna patterns were also recorded for the four-antenna capsule model shown in Fig. 65. The worst case

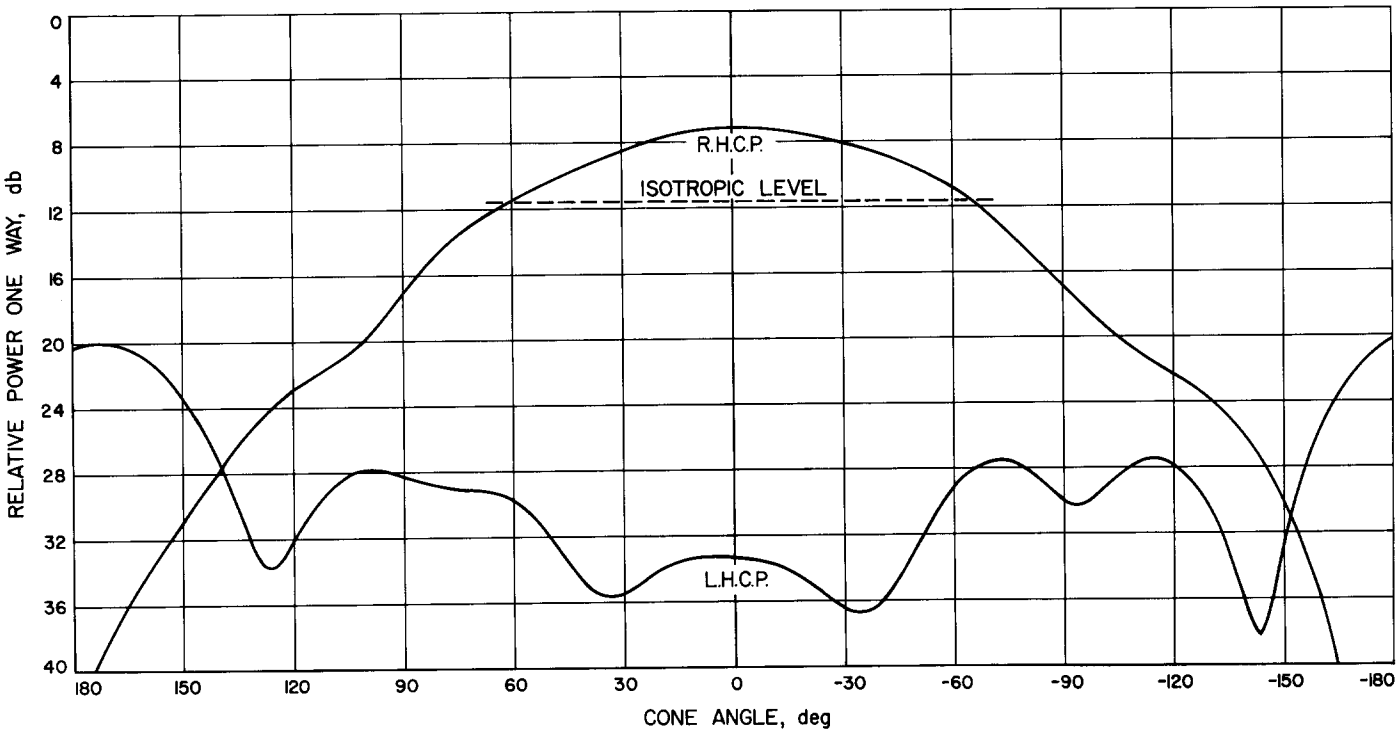

Fig. 63. Basic CDR antenna unmounted

UNCLASSIFIED

UNCLASSIFIED
CONFIDENTIAL

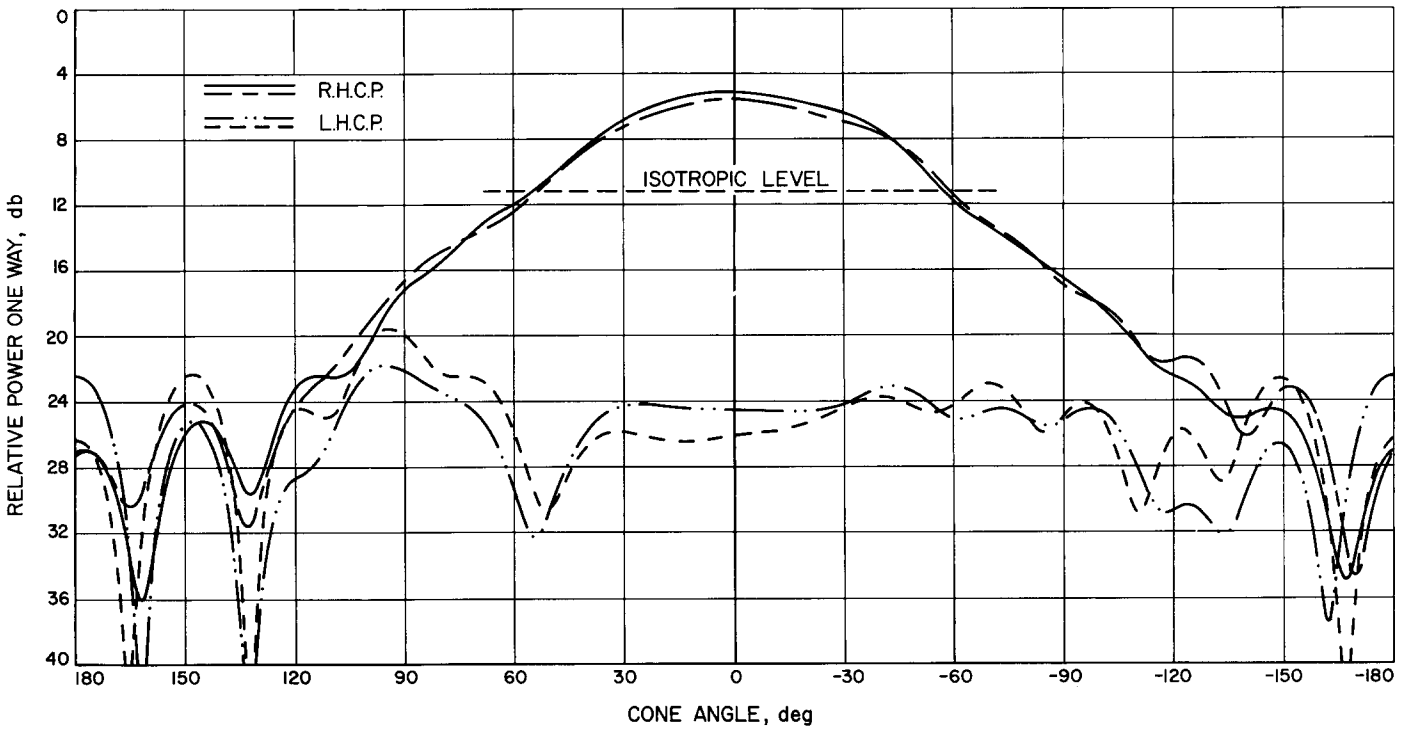

Fig. 64. CDR model with and without radome

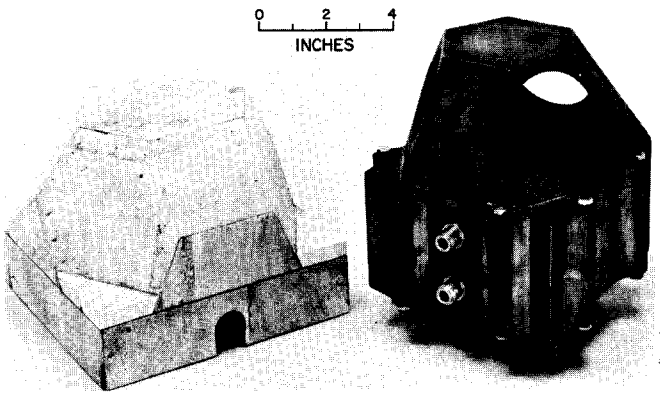

Fig. 65. Four antenna CDR model

look angle gain provided by this model was 2.5 db lower than the six-antenna model.

The final experimental investigation consisted of impact testing a sample of semiflexible coaxial cable and connectors, Fig. 66. The sample was 0.141 in. OD solid copper outer conductor, teflon dielectric, copperweld center conductor, Omnispectra Inc. (O.S.M.) cable. The gold plated stainless steel connectors were soft soldered to the cable.

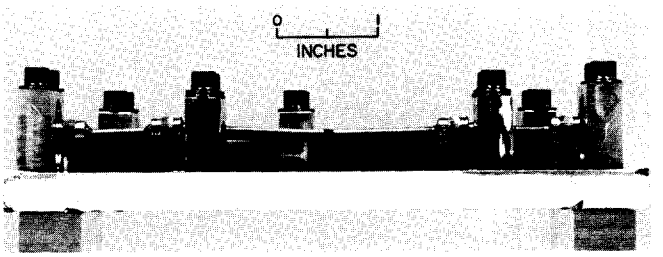

Fig. 66. O.S.M. cable impact test fixture

Fig. 67 is a graph of the system voltage standing wave ratio at 2290.185 MHz before and after impact at 5, 8, and 10,000 *g*'s. Although the assembly was still operational electrically, cracks had appeared in the solder after 8000 *g*'s. However, slight modifications such as hard solder or a different conductor material should strengthen the cable sufficiently.

e. Recommended design. The final recommended design was partly based on the data shown in Fig. 68 and on system weight considerations. In view of the unknown magnitude of the possible propagation loss contributions from multipath, blockage, and burial, it is desirable to build up as much communications margin as possible. One way to do this is to increase the number of antennas,

UNCLASSIFIED
CONFIDENTIAL

UNCLASSIFIED

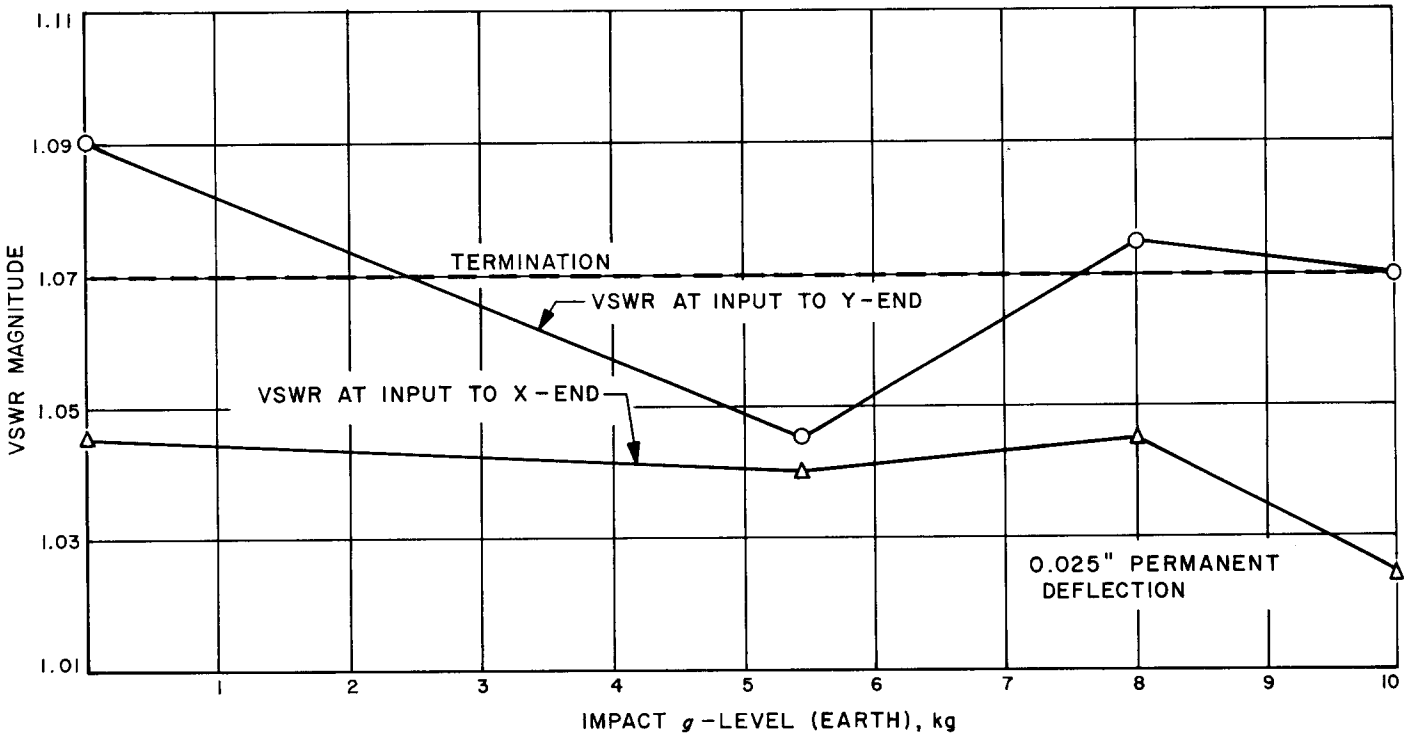

Fig. 67. VSWR of Omnispectra, Inc O.S.M. 0.141-in. OD solid copper outer conductor cable and connectors at 2300 MHz — impact normal to axis of cable run

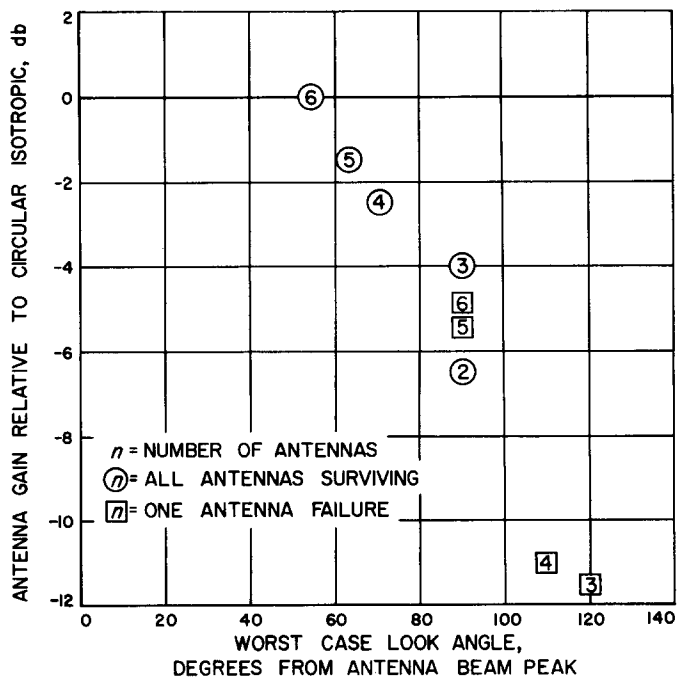

Fig. 68. η-antenna capsule performance

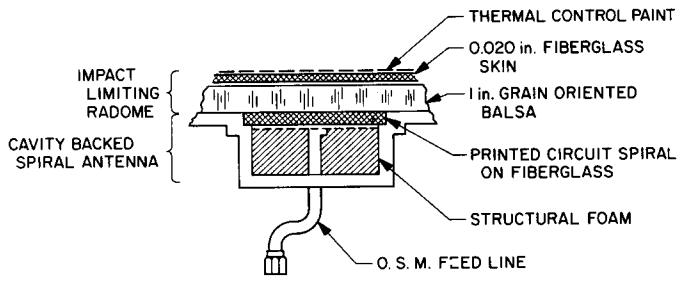

Fig. 69. Proposed CDR capsule antenna

thus increasing the worst case look angle gain. However, this increase must be kept within the allowable weight limitation. Fig. 10 also shows the effect of losing one antenna. Thus, for the CDR capsule, six antennas are recommended with one additional spacecraft mounted antenna to provide coverage in the blocked region in case of a nominal landing.

A cross section of a proposed capsule antenna is shown in Fig. 69. The cavity would be constructed integral to

UNCLASSIFIED

UNCLASSIFIED

the CDR chassis. The proposed RF transmission lines, internal to the CDR capsule from the switch to the antennas, are to be of gold plated stainless steel conductors with screw threaded connectors. All cable connections outside the CDR should be designed so that in the event of high velocity impact, the cable connections would break off at the capsule. This condition is required to prevent a length of flexible cable from wrapping itself about the CDR capsule and covering the antennas.

The proposed elements of the radome should be quite satisfactory for RF transmission.

References

1. Jaffe, L. D., *Surveyor Project Lunar Scientific Model*, Project Document No. 54, Jet Propulsion Laboratory, Pasadena, August 3, 1965.
2. *Surveyor* Model A-21A Design and Performance Notes, Hughes Aircraft Company, SSD 5424, September 15, 1965.
3. Richard, R. J., *Earth-Moon Trajectories*, 1965-70, Technical Report 32-503 (Revision 1), Jet Propulsion Laboratory, Pasadena, November 15, 1965.
4. "*Surveyor* Spacecraft Bimonthly Progress Summary," Hughes Aircraft Company, Space Systems Division, SSD 4306R, mid-April through mid-June 1964.
5. "*Surveyor* Spacecraft Bimonthly Progress Summary," Hughes Aircraft Company, Space System Division, SSD 5163R, mid-February through mid-April 1965.
6. Roberts, L., "Action of a Hypersonic Jet on a Dust Layer," Institute of Aerospace Sciences, Paper No. 63-50, presented at the 31st Annual Meeting, New York, 1963.
7. Edwards, R. H., *Interaction of the Surveyor Vernier Rocket with the Surface of the Moon*, Interdepartmental Correspondence to J. M. Bozajian, Document Number 4162.1/34, Hughes Aircraft Co., El Segundo, California, April 12, 1961.
8. Schaaf, S. H., *High Speed Aerodynamics and Jet Propulsion*, Vol. III, Section H, ed. by H. W. Emmons, Princeton University Press, Princeton, New Jersey, p. 694, 1958.
9. Stitt, L. E., Interaction of Highly Underexpanded Jets with Simulated Lunar Surfaces, National Aeronautics and Space Administration, TN D-1095, December 1961.
10. Spady, A. A., Jr., *An Exploratory Investigation of Jet Blast Effects on a Dust Covered Surface at Low Ambient Pressure*, National Aeronautics and Space Administration, TN D-1017, February 1962.
11. Land, N. S., and Clark, L. V., *Experimental Investigation of Jet Impingement on Surfaces of Fine Particles in a Vacuum Environment*, National Aeronautics and Space Administration, TN D-2633, February 1965.
12. Marte, J. E., and Fox, N. L., *An Experimental Study of the Flow Field Produced by Three Hypersonic Jets Impinging on a Surface in a Vacuum Environment*, Technical Memorandum No. 33-231, Jet Propulsion Laboratory, Pasadena, California, July 30, 1965.

UNCLASSIFIED